mgr Salwador Cyranowski

„The role of chitinase-3-like protein 1 in the pathobiology of gliomas”

Rozprawa na stopień doktora nauk medycznych i nauk o zdrowiu w dyscyplinie nauki medyczne

Promotor: prof. dr hab. Bożena Kamińska-Kaczmarek

Pracownia Neurobiologii Molekularnej, Instytut Biologii Doświadczalnej im. M. Nenckiego Polskiej Akademii Nauk w Warszawie

Studium Medycyny Molekularnej, Wydział Lekarski, Warszawski Uniwersytet Medyczny

Obrona rozprawy doktorskiej przed Radą Dyscypliny Nauk Medycznych Warszawskiego Uniwersytetu Medycznego

Warszawa, 2023 r.

Słowa kluczowe: glejaki, glejak wielopostaciowy, CHI3L1, chitinase-3-like protein 1, edycja genomu, inwazyjność, neowaskularyzacja

Badania, których wyniki zostały zawarte w niniejszej rozprawie finansowane były przez: Narodowe Centrum Nauki: nr grantu 2020/39/B/NZ4/02683.

Podziękowania

Swoje szczególne podziękowania kieruję do **Pani Profesor dr hab. Bożeny Kamińskiej-Kaczmarek** za wprowadzenie mnie w naukę o glejakach, opiekę nad moją pracą doktorską, umożliwienie wykonania badań w prowadzonej przez siebie Pracowni Neurobiologii Molekularnej Instytutu Nenckiego PAN oraz pomoc w tworzeniu niniejszej pracy.

Ogromne podziękowania kieruję do **Koleżanek i Kolegów z wyżej wspomnianej Pracowni oraz Instytutu**, w szczególności w stronę dr Juliana Swatlera, dr Aleksandry Ellert-Miklaszewskiej, dr hab. Bartosza Wojtasia, dr Katarzyny Poleszak, dr hab. Małgorzaty Zawadzkiej i dr Mitrajita Ghosh, za istotne w przygotowaniu niniejszej pracy wsparcie merytoryczne i duchowe, intelektualny sparing stymulujący do myślenia oraz humor i ciekawą znajomość.

Chciałbym również podziękować **wszystkim Członkom Pracowni Neurobiologii Molekularnej**, w szczególności dr Adrii Jaume-Canalda, dr Karolinie Stępniak, dr Chinchu Jayaprakash, dr Annie Malik, Paulinie Szadkowskiej, lek. wet. Marii Pasierbińskiej, Karolowi Jackowi, Paulinie Kamińskiej, Monice Dźwigońskiej, Paulinie Pilanc-Kudlek oraz dr Kamilowi Wojnickiemu i lek. Szymonowi Baluszkowi za tworzenie miłej atmosfery w pracy (którą nagminnie i z przekorą niszczyłem).

Bardzo serdecznie dziękuję **Koleżankom i Kolegom ze Studium Medycyny Molekularnej** Warszawskiego Uniwersytetu Medycznego (WUM), w szczególności dr Mateuszowi Gielacie i dr Sonii Dębek za wspólną naukę i wsparcie.

Dziękuję również **Koleżankom i Kolegom z kierunku lekarskiego WUM**: Zofii Głowniak, Mateuszowi Maciejewskiemu, Juli Grabowskiej, Oli Kaczmarek i Marceli Grzelak, bez których wsparcia nie udałoby mi się dotrwać do końca doktoratu w połączeniu ze studiami na kierunku lekarskim.

Najserdeczniej dziękuję swoim **Przyjaciołom** Oldze Bracichowicz i Marcinowi Nowakowskiemu oraz Oli i Tomkowi Krzywańskim oraz **Rodzeństwu** Beniaminowi i Konstancji za wierne kibicowanie, cierpliwość i wyrozumiałość dla mojego ciasnego grafiku.

Dziękuję również wszystkim pozostałym, którzy byli ze mną i wspierali mnie w trakcie doktoratu.

Najmocniejsze podziękowania kieruję w stronę swoich **Rodziców**, **Marioli i Roberta Cyranowskich**, przede wszystkim za umożliwienie mi edukacji i warunków do rozwoju, bez których nie byłoby mnie tu, gdzie dziś jestem. Im, niniejszym, dedykuję tę rozprawę.

Table of contents

Abbreviations

5-ALA — 5-aminolevulinic acid
AC-like — astrocyte-like
AD — Alzheimer's disease
ADAM — the disintegrin and metalloproteinase
ADAMTS — ADAM with thrombospondin motifs
Akt — a serine/threonine protein kinase encoded by the oncogene in the transforming retrovirus isolated from the thymoma cell line AKT-8
AMCase — acidic mammalian chitinase
APC — antigen presentation cells
AQP4 — aquaporin 4
BBB — blood-brain barrier
BrdU — bromodeoxyuridine
C/EBP — CCAAT-enhancer-binding proteins
CCL — C-C chemokine
CHI3L1 — chitinase 3-like protein 1
CHI3L5 — retina-specific chitinase-like protein
CHIT1 — chitotriosidase
CNS — central nervous system
CRISPR — Clustered Regularly Interspaced Short Palindromic Repeats
CSF — cerebrospinal fluid
CTLA-4 — cytotoxic T-lymphocyte associated protein 4
DA — diffusive astrocytoma
DAPI — 4′,6- Diamidino-2-Phenylindole
DEG — differentially expressed genes
DNA - deoxyribonuclease acid
DTT — dithiothreitol
ECM — extracellular matrix
ELISA — enzyme-linked immunosorbent assay
EMT — epithelial-to-mesenchymal transition
EPR — enhanced permeability and retention
FAK — focal adhesion kinase
FBS — fetal bovine serum
FPKM — fragment per kilobase million
Gal-3 — galectin-3
GAM — the glioma-associated microglia and macrophages
GAPDH — glyceraldehyde-3-phosphate dehydrogenase
GBM — glioblastoma
GCM — glioma-conditioned medium
GCS — glioma stem cells
GFAP — glial fibrillary acidic protein
GFP — green fluorescence protein
HB-EGF — Heparin-binding EGF-like growth factor
HUVEC — human umbilical vein cord
IBA1 — ionized calcium-binding adapter molecule 1
ICOS — Inducible T-cell costimulatory
IL13Rα2 — interleukin-13 receptor subunit alpha-2
ISF — interstitial fluid
IVC — ventilated home cages individually
KO — knock-out
LAG3 — Lymphocyte Activating 3
MAPK/Erk — mitogen activated protein kinase ERK
MES-like — mesenchymal-like
MHC — major histocompatibility complex
MMP-1 — matrix metalloproteinase 1
MMP-14 — MT1-MMP (membrane type 1-matrix metalloproteinase
MMP-2 — matrix metalloproteinase 2
MMP-9 — matrix metalloproteinase 9
mRNA — messenger RNA
NHA — normal human astrocyte
NPC-like — neural progenitor cell-like
OPC-like — oligodendrocyte like
OvCHIT1 — oviduct-specific chitinase-like protein 1
PA — pilocytic astrocytoma
PBS — phosphate-buffered saline
PD-1/2 — programmed cell death 1/2
PD-L1/2 — programmed cell death ligand 1/2
PFA — paraformaldehyde
PGE2 — prostaglandin E2
PMSF — phenylmethylsulfonyl fluoride
qPCR — quantitative real-time PCR
RFP — red fluorescence protein
RNA — ribonucleic acid
RT — reverse transcription
scRNAseq — single-cell RNA-sequencing
SD — standard deviation
SPP1 — Secreted Phosphoprotein 1, osteopontin
TAMs — tumor-associated microglia and macrophages
TBS — Tris-buffered saline
TCGA — The Cancer Genome Atlas
TGF-β — transforming growth factor beta
THBS1 — thrombospondin 1
TIM3 — T cell immunoglobulin and mucin domain-containing protein 3
TME — tumor microenvironment
TMEM219 — transmembrane protein 219
TNF-α — tumor necrosis factor α
VEGF — vascular endothelial growth factor
vWF — von Willebrand factor
WHO — World Health Organization
WT — wild-type

Streszczenie

CHI3L1 to wydzielane, nieenzymatyczne glikozylowane białko, która wiąże się z białkami, proteoglikanami i polisacharydami obecnymi na powierzchni komórek i w macierzy pozakomórkowej. Oddziaływania CHI3L1 z licznymi cząsteczkami utrudniają zrozumienie funkcji tego białka. Podczas gdy wiele badań wskazuje na zwiększenie ekspresji mRNA/białka CHI3L1 w różnych nowotworach, jego rola w procesie nowotworzenia i progresji nowotworu pozostaje niejasna.

Przeprowadzono kompleksową analizę ekspresji CHI3L1 w glejakach w wielu publicznych zbiorach danych, w tym w TCGA (The Cancer Genome Atlas) oraz w danych transkryptomicznych z pojedynczych komórek (scRNAseq), aby określić komórkowe źródło ekspresji CHI3L1 w glejakach. Najwyższy poziom mRNA/białka CHI3L1 wykryto w glejaku wielopostaciowym (GBM), wysoce agresywnym pierwotnym guzie mózgu. Wyciszenie ekspresji CHI3L1 w ludzkich komórkach glejaka U87-MG znacząco wpłynęło na profil transkrypcyjny oraz inwazyjność tych komórek *in vitro* i silnie zmniejszyło wzrost guzów wewnątrzczaszkowych U87-MG u myszy z niedoborami odporności swoistej. Co interesujące, wyciszenie ekspresji CHI3L1 w komórkach glejaka spowodowało normalizację unaczynienia guzów oraz zmniejszenie nacieku mieloidalnych komórek odpornościowych do mikrośrodowiska guza. Wykazano, że komórki pozbawione CHI3L1 miały zmniejszoną ekspresję/aktywność metaloproteinazy 2 (MMP-2), co wiązało się ze zmniejszoną inwazyjnością guzów oraz obniżoną ekspresję osteopontyny (SPP1), istotnego czynnika promującego gromadzenie się komórek mieloidalnych w złośliwych glejakach. Wyniki przedstawione w rozprawie wskazują, że CHI3L1 jest kluczowym czynnikiem w progresji złośliwych glejaków, regulującym ważne procesy wpływające na agresywność guzów. Terapie celowane zmniejszające ekspresję lub aktywność CHI3L1 mogą stanowić obiecującą, nową strategię leczenia pacjentów z glejakiem wielopostaciowym.

Abstract

Chitinase-3-like protein 1 (CHI3L1) is a secreted, non-enzymatic glycoprotein that binds proteins and carbohydrates, and interacts with cell-surface and extracellular-matrix proteins, proteoglycans, and polysaccharides. Multiple interacting partners of CHI3L1 make the dissection of its functions challenging. While many studies reported an upregulation of CHI3L1 mRNA/protein in various tumors, its exact roles in tumorigenesis remain elusive. We performed a comprehensive analysis of *CHI3L1* expression in multiple public datasets including TCGA (The Cancer Genome Atlas) and single-cell RNAseq datasets to determine the cellular source of *CHI3L1* expression in gliomas. The highest CHI3L1 mRNA/protein levels were detected in glioblastoma (GBM), a highly malignant and diffusive brain tumor. We demonstrate that CHI3L1 knockout in human U87-MG glioma cells grossly affects transcriptional profile and *in vitro* invasiveness of these cells, and strongly reduces the growth of intracranial U87-MG tumors in athymic mice. Remarkably, CHI3L1 knockout in glioma cells resulted in normalization of tumor vasculature and diminished infiltration of glioma-associated myeloid cells. Mechanistically, CHI3L1 depleted cells had reduced MMP2 expression/activity, which was associated with reduced invasion, and downregulated osteopontin (SPP1), a crucial factor driving the myeloid cell accumulation in GBM. Altogether, the presented work demonstrates that CHI3L1 is a key player in GBM progression, and its targeting represents a novel strategy in therapy of GBM patients.

1. Introduction

1.1 The functions of chitinase-3-like protein 1 in physiology and cancer

1.1.1 The biochemical properties and interacting partners of CHI3L1

Chitinase-3-like protein 1 (CHI3L1, also known as YKL-40) is a secreted 40 kDa glycoprotein that belongs to the glycoside hydrolase family 18. This family includes enzymatically active chitinases such as chitotriosidase (CHIT1), acidic mammalian chitinase (AMCase), retina-specific chitinase-like protein (CHI3L5), and oviduct-specific chitinase-like protein 1 (OvCHIT1), as well as non-enzymatic chitinase-like proteins (CLPs) or chi-lectins such as CHI3L1. CHI3L1 contains a functional glycoside-binding domain and has been shown to bind multiple carbohydrates including chitin, heparin, heparan sulfate and hyaluronic acid[1]. Since chitin is a structural protein of many lower organisms, including arthropods in mammalian diet, inhalable dust mites, arthropod and nematode parasites, and pathogenic fungi, mammalian chitinases and chitinase-like proteins are considered to have evolved as defense mechanisms of the innate immune system[2,3].

The loss of enzymatic activity has been reported as a recent evolutionary event, pointing towards the evolution of chitin-binding proteins from active anti-pathogen functions towards modulators of inflammatory responses, inflammation resolution and tissue remodeling following an inflammatory response[2,3]. Since CHI3L1 has been reported to also bind protein ligands in mammals, it is considered a cytokine and growth factor, however a specific receptor has not been identified. The ability of CHI3L1 to bind both proteins and carbohydrates permits potential interactions with a wide spectrum of cell-surface and extracellular matrix proteins, proteoglycans, and polysaccharides. Several interacting partners of CHI3L1 play multi-facet roles in physiology and disease, making the CHI3L1 signaling network extremely complex[1].

CHI3L1 has been reported to interact with numerous proteins: interleukin-13 receptor subunit alpha-2 (IL13Rα2)[4,5], transmembrane protein 219 (TMEM219)[4], galectin-3 (Gal-3)[6], and CD44[7]. The binding of CHI3L1 to IL-13Rα2 is dependent on the CD and chitin binding motif of CHI3L1 and the extracellular domain of IL-13Rα2 but does not require IL-13Rα2 N-glycosylation[8]. The depletion of TMEM219 or IL-

13Rα2 decreased CHI3L1-stimulated HB-EGF (Heparin-binding EGF-like growth factor) production by epithelial cells and activation MAPK/Erk (mitogen activated protein kinase ERK) and Akt (a serine/threonine protein kinase encoded by the oncogene in the transforming retrovirus isolated from the thymoma cell line AKT-8) in macrophages. Null mutations of TMEM219 or IL-13Rα2 abolished the inhibitory ability of CHI3L1 in oxidant-induced apoptosis and lung injury, and support for melanoma metastasis[4]. In gastric cancer CHI3L1 binding to CD44v3 activates Erk, Akt, and β-catenin signaling, therefore enhances cancer cell metastasis[7].

CHI3L1-IL-13Rα2 interactions induce Wnt/β-catenin pathways that are involved in the regulation of tumor metastasis and allergic reaction. CHI3L1 binds to IL-13Rα2 and through this interaction regulates oxidant injury, apoptosis, pyroptosis, inflammasome activation, pathogen responses, melanoma metastasis, and signaling via TGF-β (transforming growth factor beta)[9].

The interactions of CHI3L1 with CD44v3/IL13Rα2 complex induce Erk1/2, Wnt/β-catenin and Akt signaling pathways that participate in promoting epithelial-to-mesenchymal transition (EMT) in gastric cancer cells[5,7]. The interactions of CHI3L1 and type I collagen have been reported to regulate collagen fibril formation[10]. Detailed studies showed that chitohexaose and hyaluronan preferentially bind to CHI3L1 over collagen, with the negatively charged hyaluronan as the preferred physiological ligand. Collagen binds to two sites in CHI3L1 and this binding may play a role in fibril formation[11]. Collagen fibrils and their nets are major components of the extracellular matrix providing physical support for cells but also determining cellular behavior and tissue functioning in the majority of mammalian tissues[12,13].

A summary of binding partners of CHI3L1 and downstream signaling evoked by their interaction is depicted in Figure 1.1.

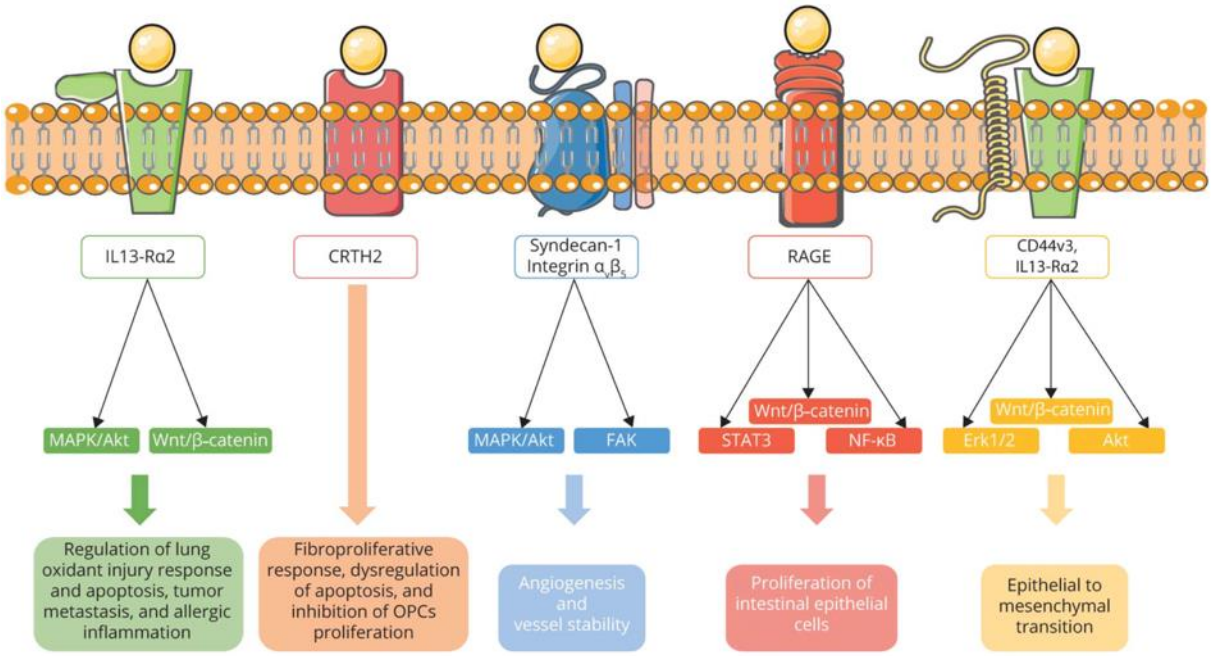

Figure 1.1. The interaction of CHI3L1 with selected protein ligands and the downstream signaling pathways relevant to cancer initiation and progression. Adapted from Pinteac et al.[5] Abbreviations: CRTH2, chemoattractant receptor homologous molecule expressed on Th2 cells; FAK, focal adhesion kinase; NFκB, nuclear factor of kappa B cells; RAGE, receptor for advanced glycation end products.

Moreover, a role of CHI3L1 in angiogenesis was demonstrated. CHI3L1 binds to syndecan-1 and integrin αVβ5 to signal through FAK (focal adhesion kinase) and MAPK/Akt pathways to promote angiogenesis[14]. CHI3L1 up-regulates VEGF (vascular endothelial growth factor) expression in glioma U87-MG and SNB-75 cells, and both proteins synergistically promote endothelial cell angiogenesis *in vitro*. CHI3L1 acts via a membrane receptor syndecan-1 and integrin αvβ5 and triggers a signaling cascade through FAK to ERK-1 and ERK-2, leading to elevated VEGF and enhanced angiogenesis. Blockade of CHI3L1 activity or expression decreased tumor growth, angiogenesis in animals implanted subcutaneously with human glioma cells[15].

Due to multiple functions CHI3L1 has been implicated in the remodeling of connective tissues, wound healing, inflammation resolution processes, alternative macrophage activation, and angiogenesis[1,16].

1.1.2 The regulation of CHI3L1 expression in macrophages

CHI3L1 expression is cell type-restricted. For example, in contrast to many other myeloid cell markers, CHI3L1 expression is absent in human monocytes and strongly induced during their maturation to macrophages. Molecular analyses by primer extension and S1 nuclease protection assays revealed the presence of two transcriptional initiation sites, located 82 and 126 bp upstream of the ATG start codon in the human *CHI3L1* promoter[17]. A promoter fragment (1.3 kb) in the 5' flanking region contains consensus binding sequences for many transcription factors, and direct binding of Sp1, PU.1, Sp3, USF, AML-1, and C/EBP factors has been detected in gel shift assays. Mutational analysis of the promoter pointed to the role of Sp1 as the dominant regulator of CHI3L1 expression in macrophages[18].

1.1.3 The expression of CHI3L1 in brain pathologies

CHI3L1 plays an important role in brain inflammation. Its presence in the cerebrospinal fluid (CSF) is a biomarker of neuroinflammation as it increases with aging, in neurodegenerative dementia and early in Alzheimer's disease (AD)[19–21]. CHI3L1 is often reported as a reliable prognostic and/or diagnostic biomarker in neurodegenerative diseases[22–24], neuroinflammation[25–29] and ischemic pathologies[30]. Epidemiologic studies showed that a variant in the human *CHI3L1* gene, which results in a reduced presence of CHI3L1 in the CSF, is associated with slower AD progression. *Chi3l1* deletion in mice did not affect astrocyte activation but moderately promoted microglia activation. In a mouse model of AD, *Chi3l1* deletion reduced amyloid plaque burden and increased CD68 (the myeloid cell marker) expression. The results suggested that CHI3L1 may suppress phagocytic activation of glial cells and promote amyloid accumulation. Consequently, *Chi3l1* knockdown increased phagocytosis of the β-amyloid peptide by astrocytes and microglia in vitro. Interestingly, basal and inflammation induced expression of *Chi3l1* was regulated by the circadian clock and deletion of BMAL1 or CLOCK/NPAS2 (the clock proteins) strongly suppresses basal *Chi3l1* expression, while deletion of the negative clock regulators PER1/PER2 increased *Chi3l1* expression[31].

CHI3L1 has been reported to have a direct neurotoxic effect towards mouse primary cultured neurons[32], however, it seems to play a neuro-protective role in stroke. In a mouse model of stroke, the depletion of CH3L1 decreased M2-like (cytoprotective) microglia polarization and resulted in increased neuronal cell death[33]. This suggests that CHI3L1 might prevent neuronal cell death in ischemic brain injuries.

1.1.4 The expression of CHI3L1 in cancer

CHI3L1 has emerged in 1990s as a biochemical marker of joint injury, rheumatoid arthritis[34–36], asthma and intestinal inflammation[37–41]. It was quickly followed by reports showing elevated blood serum levels of CHI3L1 in cancer patients[42–46], opening the second of the two research areas (next to inflammation) that CHI3L1 has been mostly investigated in: cancer.

Figure 1.2A shows a bar plot of *CHI3L1* expression in 32 cancer types and corresponding healthy tissues from GEPIA database[47] (RNAseq data).

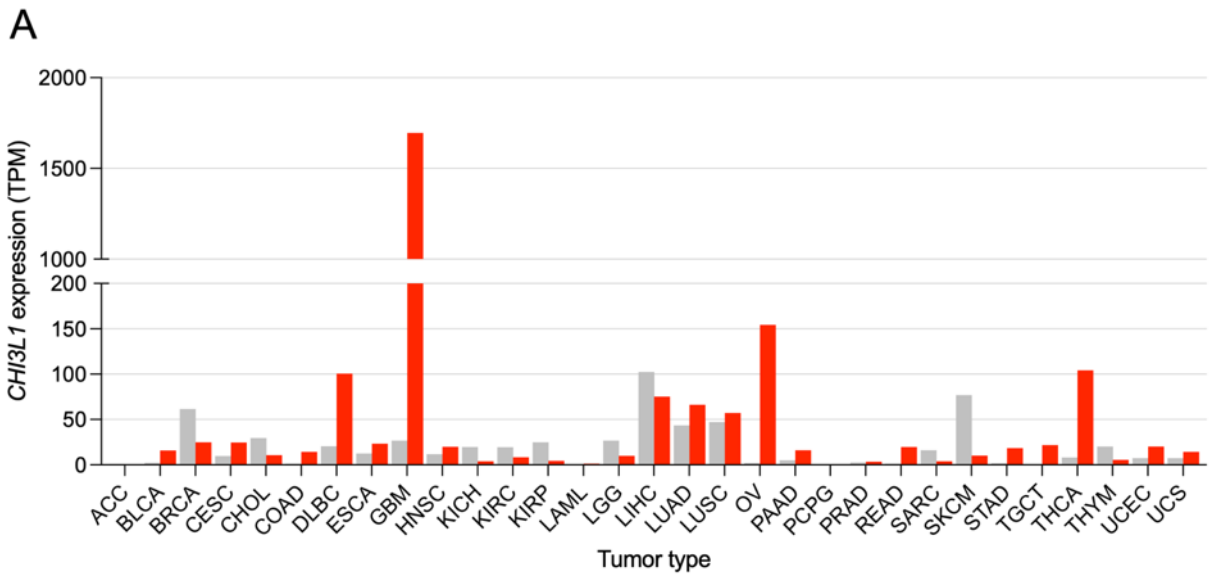

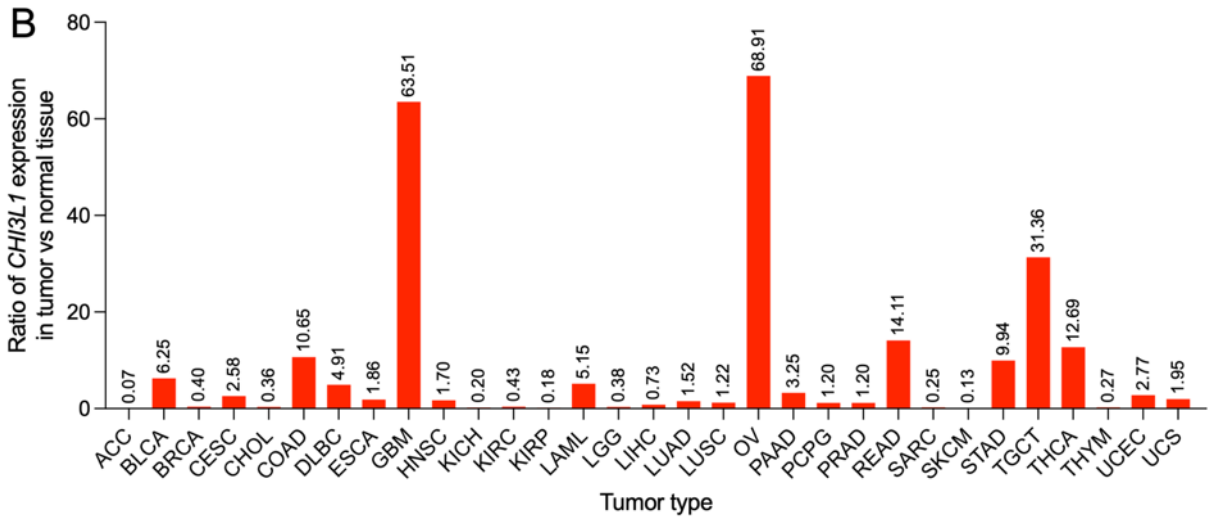

Figure 1.2. Expression of *CHI3L1* in various tumor types. A. Bar plot of the *CHI3L1* expression profile across various tumor samples and paired normal tissues from the GEPIA database[47]. TPM, transcripts per million. B. Ratio of *CHI3L1* expression in tumor versus normal tissue. Data from the GEPIA database. ACC adrenocortical carcinoma, BLCC bladder Urothelial Carcinoma, BRCA breast invasive carcinoma, CESC cervical squamous cell carcinoma and endocervical adenocarcinoma, CHOL cholangiocarcinoma, COAD colon adenocarcinoma, DLBC lymphoid neoplasm diffuse large b-cell lymphoma, ESCA esophageal carcinoma, GBM glioblastoma, HNSC head and neck squamous cell carcinoma, KICH kidney chromophobe, KIRC kidney renal clear cell carcinoma, KIRP kidney renal papillary cell carcinoma, LAML acute myeloid leukemia, LGG brain lower grade glioma, LIHC liver hepatocellular carcinoma, LUAD lung adenocarcinoma, LUSC lung squamous cell carcinoma, MESO mesothelioma, OV ovarian serous cystadenocarcinoma, PAAD pancreatic adenocarcinoma, PCPG pheochromocytoma and paraganglioma, PRAD prostate adenocarcinoma, READ rectum adenocarcinoma, SARC sarcoma, SKCM skin cutaneous melanoma, STAD stomach adenocarcinoma, TGCT testicular germ cell tumors, THCA thyroid carcinoma, THYM thymoma, UCEC uterine corpus endometrial Carcinoma, UCS uterine carcinosarcoma, UVM uveal melanoma.

Out of 32 neoplasms included in the GEPIA database, 12 (38%) are characterized with at least 2-fold overexpression of *CHI3L1* compared to a healthy tissue (Fig. 1.2B). Among these malignancies, glioblastoma (GBM), the most lethal primary brain tumor, is characterized with the highest overexpression of *CHI3L1*. In terms of tumor vs. healthy tissue ratio of *CHI3L1* expression, GBM is surpassed only by ovarian cancer.

The principal cellular source of CHI3L1 are chondrocytes and synovial cells[48], neutrophils[49], activated macrophages[50] and cancer cells, including cancer stem cells.

Therefore, CHI3L1 mRNA/protein levels are elevated in diseases characterized by chronic inflammation and tissue remodeling and many human cancers[16]. Increased serum levels of CHI3L1 correlate with malignancy, poor prognosis, and shorter overall survival in breast, colon, prostate, ovary, thyroid, lung, liver and brain cancers[10].

CHI3L1 has been documented to play a role in every step of tumorigenesis: initiation, promotion, progression, and metastasis. In a mouse model of lung cancer, tumor nodules were significantly reduced in *Chi3l1*$^{-/-}$ mice and CHI3L1 was shown to destabilize and decrease the level of p53, a well-established tumor suppressor protein, in lung cancer cells[51]. The same phenomenon was observed in colon cancer cells[52], further pertaining to the role of CHI3L1 in the initiation of tumorigenesis.

CHI3L1 has been reported to promote cancer cell proliferation in a model of hepatocellular carcinoma[53] and was found to be elevated in highly proliferative epithelium of MOLF/EiJ mice[54]. Moreover, CHI3L1 promotes macrophage recruitment and angiogenesis in colorectal cancer[55] and glioblastoma[56]. The depletion of CHI3L1 in HER2-enriched breast cancer cells resulted in reduced migration and invasion as well as reduced ability to induce angiogenesis in an *in vitro* assay[57]

CHI3L1 inhibits the degradation of type I collagen and hyaluronic acid by inhibiting the proteolytic activity of metalloproteinase 1 (MMP-1)[12], but at the same time induces other metalloproteinases such as MMP-9[58]. Therefore, by impacting the levels of MMPs, it influences cell adhesion and migration, tissue remodeling, fibrosis, and potentially tumorigenesis. Macrophage-derived CHI3L1 has been reported to promote gastric and breast cancer cell metastasis via IL13Rα2-MAPK-MMP axis[59]. A pharmacological blockade of CHI3L1 with a small molecule inhibitor was shown to diminish melanoma and lung cancer metastasis by blocking IL-13Rα2-mediated JNK-AP-1 signals[60]. CHI3L1 has also been shown to promote proliferation, migration and metastasis of gastric carcinoma cells via CD44-β-catenin-Erk/Akt signaling[7].

Evasion of the immune response is one a hallmark of cancer, and programmed cell death 1 (PD-1) and PD-1 ligand 1 (PD-L1) are major immunomodulators of immunosuppression. CHI3L1 regulated the expression of immune inhibitors such as PD-L1 (programmed cell death ligand 1), PD-L2, PD-1, LAG3 (Lymphocyte Activating 3), and TIM3 (T cell immunoglobulin and mucin domain-containing protein 3) which

contributed to melanoma progression and lymphatic spread. Antibodies against CHI3L1 or PD-1 had antitumor effects in lung metastasis mouse models and T cell-tumor co-cultures. Bispecific antibodies that simultaneously target CHI3L1 and PD-1 had synergistic cytotoxic effects in tumor models[61]. CHI3L1 inhibited the expression of ICOS (Inducible T-cell costimulatory), ICOSL and CD28 but stimulated CTLA-4 (cytotoxic T-lymphocyte associated protein 4) and the B7 proteins in a melanoma lung metastasis model. Individual or combined treatment with anti-CTLA-4 and anti-CHI3L1 antibodies had antitumor effects in melanoma lung metastasis which represents a promising therapeutic strategy in lung metastasis[61].

1.2 Glioblastoma – basic facts

1.2.1 Gliomas – classification and epidemiology

Gliomas are neoplasms that originate from the neural stem cells or progenitor cells of the central nervous system (CNS). Malignant tumors constitute one-third of all primary brain tumors and occur at the yearly incidence rate of 7 per 100 000[62]. Gliomas encompass a broad category of diverse tumors originally classified based on their microscopic similarity to the precursor cells of glial lineages – the putative cells of glioma origin. The histopathological glioma classification relied on the morphological resemblance of the neoplastic cells to healthy brain cells, assigning tumors with astrocytic features as astrocytomas and oligodendroglial features as oligodendrogliomas[63]. The classification of CNS tumors by the World Health Organization (WHO) published in 2016, revised this approach and included molecular markers in addition to the histological characterization[64]. Based on the growth pattern and genotype diffuse gliomas have been grouped together and further defined with both histological and molecular characteristics. This classification has been updated in 2021, including more sophisticated molecular diagnostic methods such as global disturbances of genome methylation and/or methylation status of and specific genes[65].

The diffuse gliomas are characterized by a highly infiltrative growth pattern resulting in the migration of neoplastic cells within the brain parenchyma, which impedes their surgical resection or elimination by focused radiotherapy. In adults, the diffuse gliomas constitute 80% of all malignant gliomas and encompass adult IDH1-

mutant astrocytomas, oligodendroglioma, pediatric gliomas, and IDH1-wildtype glioblastomas (GBM). The non-diffuse gliomas with more apparent tumor borders encompass pilocytic astrocytomas and ependymomas[65].

Despite decades of research, the therapeutic options for malignant gliomas are very limited, which is reflected by high mortality rates. The most aggressive glioma type – GBM, which constitutes more than a half of all gliomas, is primarily diagnosed at an older age (median of 65 years), and shows the worst median survival of 15 months[62,66]. WHO 2016 grade II and III gliomas are associated with better survival – 5-7 years in grade II, 2-3 years in grade III, and are more frequently diagnosed in younger patients (median 34 and 39 years, respectively)[62,67]. The therapeutic intervention is largely restricted to surgical resection and chemo- and/or radiotherapy. Multiple therapies have been tested in clinical studies, yielding a very limited improvement of patient outcomes[68].

1.2.2 The hallmarks of glioblastoma pathology

1.2.3 The invasiveness of GBM into brain parenchyma

A major characteristic of diffuse gliomas (such as glioblastoma) is their capacity to extensively infiltrate the brain parenchyma. Malignant cells tend to grow along the paths of least resistance such as blood vessels, white matter tracts and the leptomeningeal space (also called subarachnoid space). The extensive malignant cell invasion results in tumor expansions that reach deep into the brain parenchyma leading to destruction and dysfunction of the surrounding brain tissue[69]. This growth pattern represents a major challenge in clinical management as it precludes complete surgical resection. The outgrowing tumor extensions can be difficult to distinguish from the healthy tissue during surgery, which might lead to incomplete resection and accelerated recurrence of the disease. There are methods available that facilitate the removal of the tumor extensions e.g., the fluorescence-guidance with 5-aminolevulinic acid (5-ALA) under ultraviolet light[70]. The complete resection is desirable, but it is not free of significant clinical complications such as cognitive impairment, vision loss, paresis, etc. depending on the location of the tumor in the brain and the proximity to vital, neurologically competent areas that must be sacrificed to remove the malignancy.

Thus, the prevention of the extensive growth pattern of diffusive gliomas is highly desirable in the first place.

The extracellular matrix (ECM) of the brain parenchyma differs in terms of composition and rigidity from other organs because it is relatively poor in collagens[71] but rich in tenascin-C, thrombospondin 1 (THBS1), hyaluronan, glycosaminoglycans and various proteoglycans such as versican and CNS-specific brevican and neurocan[72,73]. Collagen is present in the brain mainly in the perivascular ECM along with other molecules such as laminin, fibronectin, vitronectin, entacin and heparan sulfate[72] (as shown in Fig. 1.3). An increase in the expression of collagen-coding genes, especially *COL3A1*, *COL4A1* and *COL5A2*, is associated with a malignant growth in the brain as the tumor utilized collagen scaffolding to pave its invasion[71].

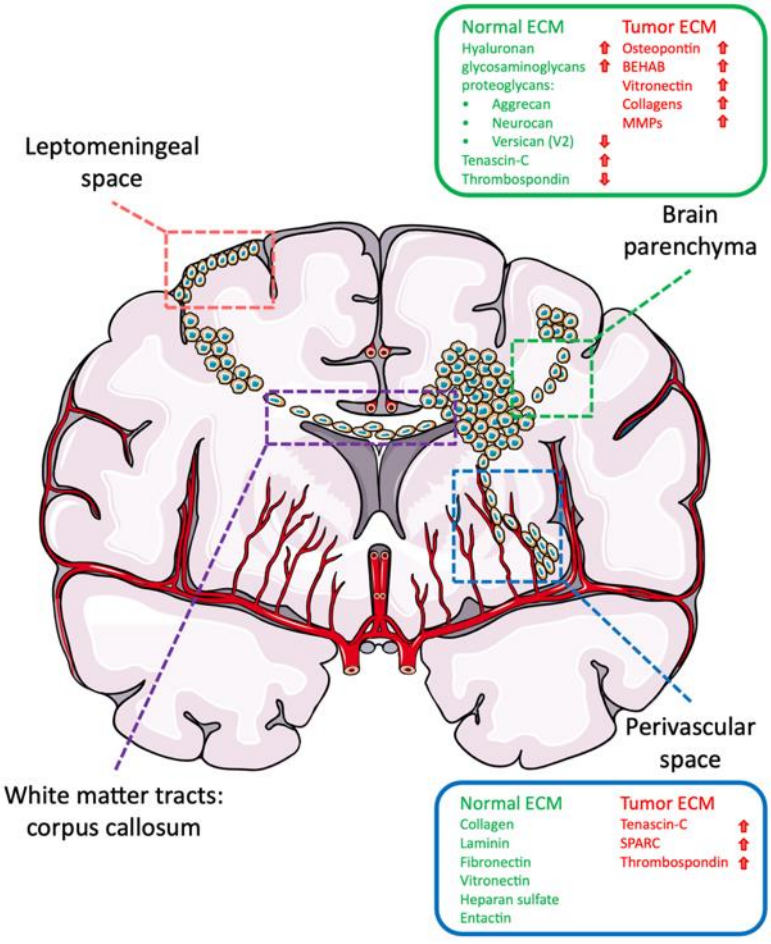

Figure 1.3. Main routes of invasion of diffusive gliomas and site-specific changes of the ECM caused by growing tumor. Adapted from de Gooijer et al. 2016[72].

In order to invade surrounding tissue, diffuse gliomas use several protein degrading enzymes, most importantly matrix metalloproteinases (MMPs), members of the disintegrin and metalloproteinase (ADAM) family, and ADAMs with thrombospondin motifs (ADAMTS) proteins[69]. The secreted MMP-2 and MMP-9 as well as MT1-MMP (membrane type 1-matrix metalloproteinase, also known as MMP-14) play important roles in GBM invasion and their expression is correlated with tumor grade[74,75]. This is confirmed in public databases showing an upregulation of these MMPs at the mRNA level compared to normal brain. All three MMPs also show the highest expression in GBM compared to other glioma types like astrocytoma and oligodendroglioma[76].

Tumor-associated microglia and macrophages (TAMs) express MT1-MMP, which is involved in ECM remodeling and invasion. MT1-MMP supports glioma cell invasion by the proteolytic cleavage of the glioma cell-derived pro-MMP-2 into its active form[77]. The metalloproteinases ADAMs and ADAMTSs affect cell adhesion through integrin interactions via their disintegrin domain[78]. Particularly ADAMTS-4/5 are upregulated in GBM surgical samples and show confined expression in astroglial and GBM cells. ADAMTS-5 may also promote invasion through a cleavage of the brain-specific ECM proteoglycan brevican. ADAM-17 may affect GBM invasion through its function as a sheddase (shedding off ectodomains of membrane proteins) for activation of EGFR ligands such as tumor necrosis factor α (TNF-α) and TGF-α[78].

1.2.4 The role of myeloid cell infiltration and tumor microenvironment

Malignant gliomas, including glioblastoma, are considered immunologically inert tumors characterized by a highly immunosuppressive microenvironment and low potential for activation of the acute inflammatory and anti-tumor responses. This is partly attributed to the CNS being an immunologically distinct (or privileged) site. The CNS is shielded from the peripheral circulation by the blood-brain barrier, there are no obvious connections with the lymphatic system and there is low expression of major histocompatibility complex (MHC) proteins by the cells of the CNS[79]. Nevertheless, malignant gliomas are massively infiltrated by the immune cells that can constitute up to 30% of tumor mass[80]. The immune population is dominated by myeloid cells[81],

especially the brain-resident microglia, and monocytes/macrophages infiltrating from the periphery, whereas infiltration of activated T cells is rather low.

The immune landscape of malignant gliomas results from several mechanisms. Tumor cells secrete factors recruiting and modulating the function of certain immune populations, e.g., chemokines CCL (C-C chemokine) 2, CCL7 and CCL12 that attract monocytes, dendritic cells (DCs), natural killer (NK) cells, and T cells; chemokine CCL22 that recruit regulatory T cells; TGF-β that blocks cytotoxic T lymphocytes; prostaglandin E2 (PGE2) that downregulates the production of inflammatory Th1 cytokines, upregulates Th2 immunosuppressive cytokines and inhibits anti-tumor activity of NK cells[80,82,83]. In addition, eliciting the adaptive immune response is blocked due to e.g., ineffective presentation of tumor antigens to T cells by antigen presentation cells (APC), accumulation of T regulatory cells that produce interleukins 10 and 35 (IL-10, IL-35) and TGF-β which has an inhibitory effect on the response of the cytotoxic T lymphocytes[84]. The T cell infiltration to the brain is impeded by the T cells sequestration in the bone marrow during GBM development[85]. T cells that successfully migrated to the tumor mass are frequently hypo-responsive due to chronic antigen exposure, which is defined as T cell exhaustion. Exhausted T cells in GBMs upregulate many immune checkpoint proteins e.g., PD-1 which is overstimulated by the malignant cells expressing cognate ligand PD-L1 that binds to PD-1 and renders T cells inert or apoptotic[86].

The glioma microenvironment is rich in non-neoplastic cells including stromal, endothelial, and immune cells encompassing microglia, monocytes/macrophages, DCs, T cells, B cells, and NK cells. However, the glioma-associated microglia and macrophages (GAMs) constitute the most abundant population of immune cells in the glioma microenvironment[87]. Despite the accumulation of the immune system cells to the tumor-bearing brain parenchyma, GAMs do not counteract tumorigenesis, but rather promote tumor progression. High numbers of amoeboid, activated GAMs are associated with poor patient survival prognosis[88]. GAMs are recruited to the tumor niche and undergo tumor-directed education. As a result, GAMs contribute to tumor progression and evasion of the anti-tumor immune response via e.g., releasing immunosuppressive cytokines, inhibiting cytotoxic responses of NK cells, and blocking the activation of CD4+ T cells (reviewed in [89]).

1.2.5 The neovasculature of glioblastoma

Aberrant vasculature is a hallmark of glioblastoma pathology. Physiologically, angiogenesis is a highly regulated process and is essential for the adequate supply of nutrients and oxygen to the developing or healing tissues[90]. There are many players involved in the process, but the most important ones are endothelial cells, mural cells (smooth muscle cells and pericytes), soluble growth factors (such as VEGF, FGF, HIF-1α) and proteolytic enzymes such as MMPs that facilitate vessel sprouting[91]. In many cancers, but particularly in glioblastoma, this process is unbalanced and uncontrolled. There are many mechanisms that glioblastoma utilizes to orchestrate this process. First, GBM produces large quantities of pro-angiogenic factors such as VEGF that drive the neoangiogenesis. It also displaces mural cells from the existing blood vessels in a process known as vessel co-option[92]. Lastly, glioblastoma cells form non-endothelial, cancer-cell-lined microvascular channels in the process of vascular mimicry[93]. As a result, the tumor vessels are collapsed and disorganized, many of these vessels form a dense network of aberrant capillaries, the blood flow is turbulent and insufficient for an optimal perfusion of the tissue. This contributes to hypoxia, necrosis and immunosuppression, and creates a specific TME[94–97].

Importantly, the perivascular niche is also affected. Physiologically, blood vessels of the brain are lined with an endothelium that is permeable to molecules ranging from 0.1 nm (sodium ion) to 11.5 nm (immunoglobulin G) in diameter[98], and is tightly covered by pericytes and astrocytic endfeet. This physical and functional barrier, called blood-brain-barrier (BBB) allows for a strict control of substances entering the brain parenchyma. The space between the blood vessel and cells covering it (astrocytes, pericytes), known as the glymphatic system, serves as a buffer for cerebrospinal fluid (CSF) and interstitial fluid (ISF) exchange that facilitates an efficient clearance of solutes and waste from the brain[99]. The most prominent protein involved in the process is aquaporin 4 (AQP4), an astrocyte-specific water channel that is used to control the volume of the CSF and ISF. In glioblastoma, the astrocytes and pericytes are displaced from the BBB by malignant cells, which disrupts the function of the barrier and glymphatic system and results in a damaging “permeability and retention effect”[100].

Despite the BBB being disrupted and more permeable, the delivery of anti-tumor drugs to the tumor remains a key challenge in the treatment of GBM[101]. Anti-angiogenic treatment fails to bring about permanent de-vascularization; rather, normalized tumor vessels emerge from the neovascular tree (as shown in Fig. 1.4). Given the obstacles in the drug delivery to the site of GBM, the normalization of vasculature is desirable for an effective anti-tumor activity in GBM.

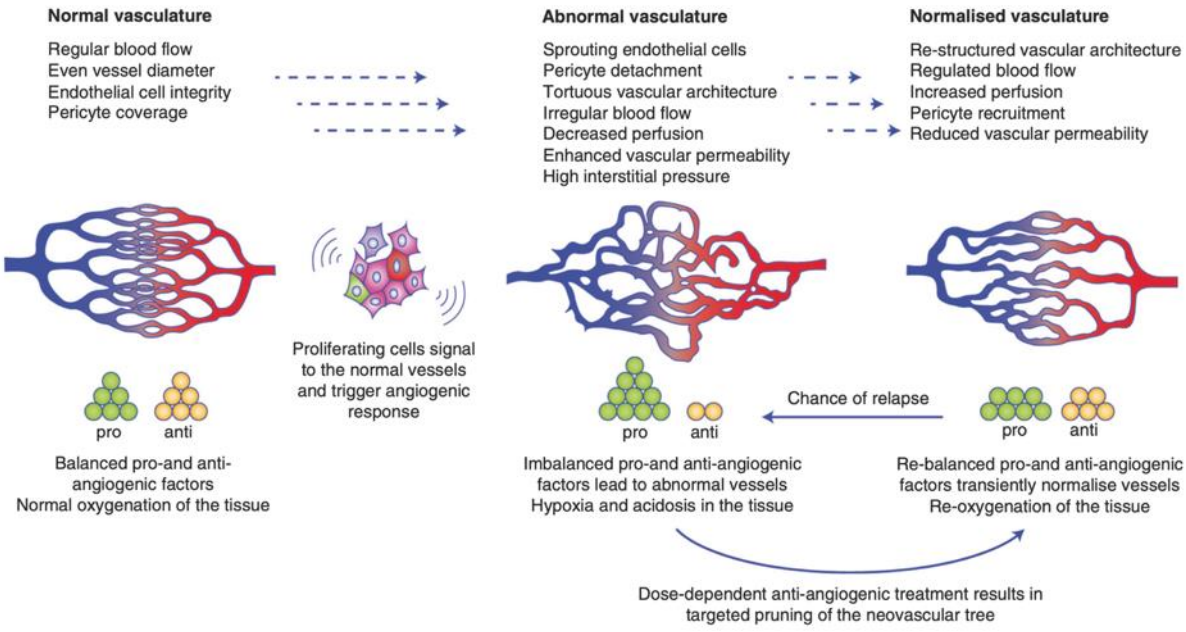

Figure 1.4. Schematic illustration of the vascular network in a physiological (normal), pathogenic (abnormal) and normalized state. In a normal network, there is a balance of pro- and anti-angiogenic factors. This balance is skewed towards pro-angiogenic factors in abnormal scenarios e.g., neoplastic growth. In the normalized vascular network, pro-angiogenic factors still outweigh the anti-angiogenic factors but the ratio of the two is smaller, which confers an increased functionality of the network for e.g., drug delivery to the site of the tumor. Adapted from Magnussen et al.[102]

1.2.6 The roles of CHI3L1 in glioblastoma

In the brain, *CHI3L1* is upregulated during inflammatory processes in neurological disorders, and its expression is abundant in reactive astrocytes and macrophages but not in microglia, brain resident myeloid cells[103,104]. The level of CHI3L1 protein is elevated in approximately 65% cases of glioblastoma (GBM), the most common and lethal primary brain tumor with a median survival of only 15

months[105,106]. *CHI3L1* expression in the Cancer Genome Atlas (TCGA) gliomas was identified as one of markers of the mesenchymal subtype of glioblastoma, the most malignant subtype of GBM[107]. CHI3L1 was undetectable by Western blotting in lower-grade gliomas (WHO 2021 grades 2 and 3) and normal brain tissue[108]. CHI3L1 serum levels were substantially elevated in numerous GBM patients and correlated with tumor grade and tumor burden[105]. Higher CHI3L1 expression was significantly associated with poorer radiation response, shorter time to progression and shorter overall survival[109]. Moreover, *CHI3L1* high expression is associated with activation of PI3K/AKT/mTOR signaling in GBM[56].

Transient suppression of CHI3L1 in U87-MG human glioma cells results in a decreased MMP-2 production and a lower gelatinolytic activity *in vitro*[110]. CHI3L1-Gal3-Gal3BP protein complexes have been reported to regulate infiltration and reprograming tumor-associated myeloid cells resulting in deficits of T cell–mediated immune responses in GBM progression[56].

CHI3L1 has been linked to angiogenesis as it affects endothelial tubulogenesis *in vitro* as potently as VEGF[111]. CHI3L1 increased VEGF expression by signaling through syndecan-1, integrin αVβ5 and phosphorylated FAK in human U87-MG glioma cells (represented schematically in Fig. 1.5)[14]. CHI3L1 levels were elevated and associated with elevated VEGF in subcutaneous but not in intracranial U87-MG and SNB-75 experimental gliomas[15]. CHI3L1 signaling was also implicated in GBM resistance to bevacizumab (the VEGF inhibitor and anti-angiogenic drug). The potential mechanisms involve vascular mimicry, production of angiogenic factors, modulation of pericyte coverage of blood vessels, increased invasiveness of GBM cells and mesenchymal transition[94]. The exact role of CHI3L1 in GBM progression is poorly understood or documented, especially in terms of the impact on GBM vasculature and invasiveness, but it has been increasingly implicated as a cytokine, growth factor and pro-angiogenic factor.

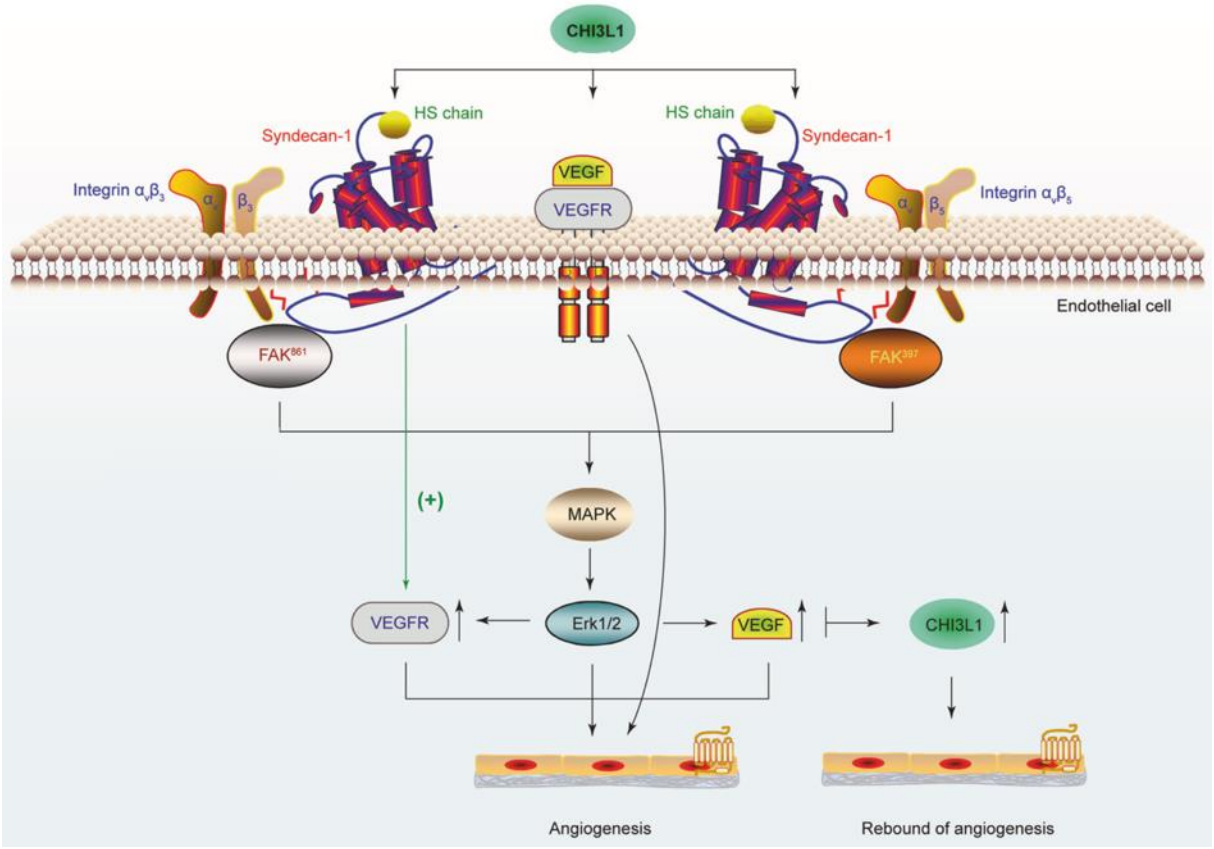

Figure 1.5. Schematic illustration of interacting partners of CHI3L1 and downstream signaling pathways associated with angiogenesis. CHI3L1 induces coordinated activation of Syn-1 and integrin αvβ5 to activate FAK397 and downstream signaling pathways, upregulating VEGF in U87-MG human glioma cells. Adapted from Zhao et al.[1]

2. Aims

Despite a wealth of information regarding expression and potential functions of CHI3L1, its role in glioma pathogenesis has not been fully elucidated. The current data implicate CHI3L1 in numerous pathological processes involving immune cells activation, tissue remodeling, wound healing, and angiogenesis. In neoplastic cells some of the CHI3L1 functions are hijacked and employed to support tumor invasion and progression.

The presented study aims at better description of CHI3L1 expression profiles in gliomas and elucidating its role in glioma progression using a relevant glioma model. The mechanisms through which CHI3L1 is involved in the glioma progression are to be disclosed.

The specific goals were the following:

1. To identify a cellular source of CHI3L1 in gliomas using public data repositories.
2. To obtain a genetically engineered cell line depleted of *CHI3L1* gene using CRISPR/Cas9 technology and characterize properties of gene edited cells.
3. To define transcriptomes of parental (WT) and CHI3L1 KO cells and identify key differentially expressed genes and pathways.
4. To evaluate the impact of CHI3L1 depletion in human glioma cells on growth of intracranial gliomas.
5. To identify mechanisms underpinning the effects of CHI3L1 depletion on tumor growth.

3. Materials and methods

3.1 Patient samples

Total RNA from two patient cohorts were analyzed in this study. The first cohort encompassed 76 glioma samples of various WHO grades (described in our previous study[112]) and analyzed using reverse-transcription quantitative PCR (RT-qPCR). Normal brain controls used as a reference for gene expression experiments were purchased from: Agilent 540005 (lot 0006127195, Female 66 years), Biochain R1234035-50 (lot B304105, Male 25 years), First Choice Human Brain Reference RNA AM6050 (lot 1207015, mix of RNA from male and female donors). The second cohort was 31 tumor samples collected and analyzed by RNA sequencing as described in our previous study[113]. Patients' permissions have been collected and these studies were approved by the Bioethics committees of the respective hospitals.

3.2 Human cell lines and cell culture

Human established glioblastoma cell lines LN229, U251, LN18, T98G, U87-MG, U87-MG-RFP (purchased from ATCC, American Type Cell Collection) and human primary glioblastoma cells WG4 and WG9 (established in the laboratory[114]) were cultured in 1 g/L glucose Dulbecco's modified Eagle's medium (DMEM) (Gibco, #11885084) supplemented with 10% fetal bovine serum (FBS) (Gibco, #16000044) and antibiotics (100 U/mL penicillin, 100 µg/mL streptomycin, Gibco, #10378016). Normal human astrocytes (NHA; purchased from Lonza, #CC-2565) were cultured in Clonetics media and dedicated reagents (Lonza, #CC-3187). Cells were cultured in a humidified atmosphere CO_2/air (5%/95%) at 37°C (incubator, Heraeus). Cells were passaged after reaching the confluence up to 10th passage from the initial seeding.

3.3 RNA extraction and reverse transcription quantitative PCR (RT-qPCR)

Cells (seeded and cultured for 48 h) were washed with PBS and collected using a cell scraper and centrifugation. Glioma and NHA cells were lysed using RLT buffer containing 1% (v/v) β-mercaptoethanol and total RNA was isolated using RNeasy Mini Kit (QIAGEN, #74104) according to the manufacturer's recommendations.

QIAshredder columns (Qiagen) and DNase digestion step were employed to facilitate cell lysis and the depletion of genomic DNA, respectively. RNA was eluted in 30 µL of high-purity nuclease free water and its quantity and quality were determined using NanoDrop 2000 spectrophotometer (ThermoFisher) and Agilent 2100 Bioanalyzer with RNA 6000 Nano Kit (Agilent). Samples were stored at -80°C. For reverse transcription (RT), the reaction mix contained RNA (0.5 µg), oligo(dT)20 (1 µL of 50 µM stock), dNTPs (1 µL of 10 mM stock), specific primers and sterile RNase-free water (up to 13 µL of total volume). This mix was incubated at 65°C for 5 min. Next, 5X First-Strand Buffer (4 µL), DTT (1 µL of 0.1 M stock), SuperScript III Reverse Transcriptase (200 U/µL; 0.5 µL, Invitrogen) and sterile RNase-free water (1.5 µL) was added followed by 1 h incubation at 50°C for cDNA synthesis, and 70°C for 15 min to inactivate the enzyme.

Quantitative real-time PCR (qPCR) was performed on 12.5 ng of cDNA in duplicates using SYBR Green detection reagents (Fast SYBR™ Green Master Mix, Applied Biosystems, #4385612) and the primers listed in Table 1.

Target	Sequence/reference
GAPDH	Forward 5′-AGGGCTGCTTTTAACTCTGGT-3′
	Reverse 5′-CCCCACTTGATTTTGGAGGGA-3′
18S	Forward 5′-CGGACATCTAAGGGCATCAACA-3′
	Reverse 5′-AACGAACGAGACTCTGGCATG-3
CHI3L1	BioRad, ref. ID: qHsaCED0044484
CHI3L1 (site ‘887’)	Forward 5’-CTGTTCTTGAGTGTGTTGAGCA-3’
	Reverse 5’-GCAACGATCACATCGACACC-3’
CHI3L1 (site ‘589’)	Forward 5’-GTATCCTACCCACTGGTTGCC-3’
	Reverse 5’-CGGAGCCACAGTCCATAGAATC-3’

Table 1. Sequences of oligonucleotides used as primers for RT-qPCRs.

The amplified product was normalized to the endogenous expression of glyceraldehyde-3-phosphate dehydrogenase mRNA (*GAPDH*) or 18S rRNA and represented as delta Ct values.

3.4 CRISPR/Cas9 genome editing

The CRISPR/Cas9 genome editing reagents were designed using manufacturer's online tool (Sigma). Single guide sgRNA molecules targeting two exons in *CHI3L1* gene were ordered: HS0000229887 (site '887') and HS0000230589 (site '589'). U87-MG-RFP human glioma cells (2×10^6) were electroporated with 0.5 µg pCMV-Cas9-GFP plasmid (Sigma, #CAS9GFPP) and 2 sgRNAs (150 pmol each) or control non-targeting sgRNA (sgCTR) in SE electroporation buffer (100 µL in a Nucleofector cuvette, Lonza, #V4XP-1024) using a Nucleofactor 4D X unit (Lonza, #AAF-1003X) according to manufacturer's instructions. After electroporation, cells were seeded on T150 flask in 20 mL standard culture media pre-incubated for 1 h in 37°C before seeding. Cells were then maintained under standard culture conditions for 24 h before sorting the CRISPR/Cas9-transfected population.

3.5 Fluorescence-activated cell sorting (FACS) and clonal selection

Cells were harvested using trypsin (0.25%, Gibco, #25200056), centrifuged for 5 min at 300 × *g* and resuspended in Stain Buffer (BD Pharmingen, #554656). Cells were sorted in a single-cell mode into five 96-wells flat-bottom culture plates into 100 µL of high glucose GlutaMAX™ DMEM (Gibco, #10566016) supplemented with 15% FBS (Gibco, #16000044) using BD FACSAria II cell sorter (BD Pharmingen). Gates for sorting were set for RFP-high and GFP-positive events (Fig. 3.1). Culture plates with sorted cells were incubated under standard cell culture conditions immediately after sorting. Next, media for single-cell clones were changed every 3 days for a conditioned medium which comprised of 50% 48 h-conditioned U87-MG medium (filtered through 20 µm strainer) containing essential growth factors and 50% fresh high glucose GlutaMAX™ DMEM supplemented with 15% FBS. This medium provided growth factors and optimal conditions for single clones to proliferate and establish a colony. When colonies were established, cells were detached using 0.5% trypsin and transferred to a 6-wells culture plate, allowed to grow to 85% confluency and passaged to achieve a large number of cells. Cells were collected, suspended in 1:9 DMSO to FBS and stored at -80°C or used for further experiments. All flow cytometry experiments were performed at the Laboratory of Cytometry, Nencki Institute of Experimental Biology, Warsaw, Poland.

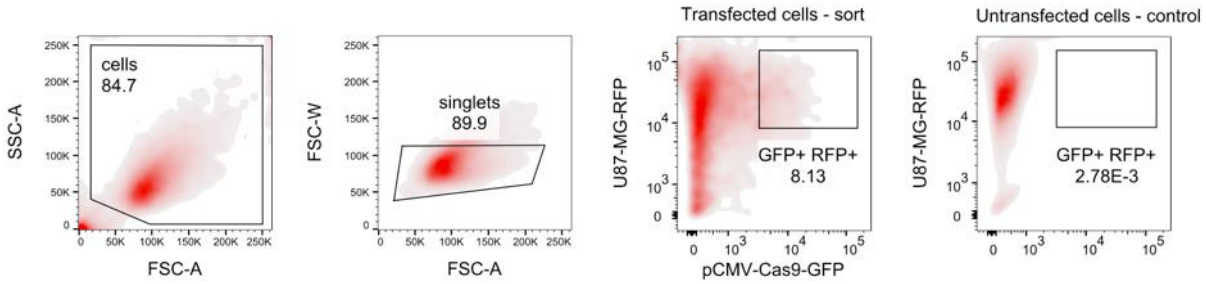

Figure 3.1. Gating strategy for the flow cytometric sorting of U87-MG-RFP successfully transfected with pCMV-Cas9-GFP plasmid.

3.6 Enzyme-linked immunosorbent assay (ELISA)

To select U87-MG KO clones with low CHI3L1 expression, cell culture supernatants were analyzed for the presence of the human protein using Human Chitinase 3-like 1 Quantikine ELISA Kit (R&D Systems, #DC3L10). Cell culture supernatants were centrifuged for 10 min at 300 × *g* before the assay to remove residual cells. Tests were performed according to manufacturer's protocol and measurements were acquired with a scanning multiwell spectrophotometer. Quantity of detected protein was normalized to a cell number or total protein content per sample.

3.7 Cell proliferation assays

The proliferation of cells was measured using two independent methods. For flow cytometry assay, 5×10^4, 2.5×10^4 or 1.25×10^4 cells were seeded onto a 12-wells culture plate and stained with a cytoplasmic dye eF450 (1:1000, eBioscience™ Cell Proliferation Dye eFluor™ 450, #65-0842-85). Batches of dyed cells were analyzed for the eF450 signal at day 3, 4 and 5 after addition of the dye using LSR Fortessa (BD Pharmingen) analyzer. Cells were also analyzed immediately after the incubation with the dye (day 0). For BrdU incorporation assay, 3×10^3 cells were seeded onto a 96-wells culture plate and allowed to grow for 48 h before the incubation with BrdU solution (1:1000, Cell Proliferation ELISA, BrdU (colorimetric), Roche, #11647229001) for 2 h. After the incubation, cells were processed according to manufacturer's protocol and the BrdU signal was measured using a scanning multiwell spectrophotometer. BrdU assays were performed in 6 technical replicates to ensure accurate read-out.

3.8 RNA sequencing and data analysis

RNA was isolated using the RNeasy kit (QIAGEN, #74104) and RNA quality/yield was verified using Bioanalyzer 2100 (Agilent Technologies, #G2939BA). mRNA libraries were prepared using KAPA Stranded mRNAseq Kit (Roche, #07962142001) according to the manufacturer's protocol (KR0960-v6.17). mRNAs were enriched from the starting material of 500 ng of total RNA using poly-T oligo-attached magnetic beads (Kapa Biosystems). Enriched mRNA was fragmented, then the first and the second strand of cDNA were synthesized. Subsequently, adapters were ligated, and loop structure of each adapter was cut by USER enzyme (NEB, #M5505S). Finally, the amplification of obtained dsDNA fragments that contained a specific adapter sequence was performed using NEB starters. Quality of final libraries was determined using Agilent Bioanalyzer High Sensitivity dsDNA Kit (Agilent Technologies, #5067-4626). Concentrations of the final libraries were measured using Quantus Fluorometer and QuantiFluor ONE Double Stranded DNA System (Promega, #E4871). Libraries were sequenced on HiSeq 1500 (Illumina) on the rapid run flow cell with a paired-end settings (2× 76 base pairs). The acquired fastq files were aligned to hg38 human reference genome with STAR program[115], and reads were counted to genes using feature Counts algorithm SUBREAD package[116]. Gene counts were normalized, and differential analysis was performed using the DESeq2[117]. Genes were considered differentially expressed (DEG) with FDR corrected p-value (padj) <0.05. REACTOME pathway analyses[118] were performed using R package clusterProfiler[119] to annotate the functions of differentially expressed mRNAs.

3.9 Housing of athymic (Foxn1$^{nu/nu}$) mice

The animal study was conducted according to the protocol approved by the First Local Ethics Committee in Warsaw, Poland (approval number 1123/2020). Experiments were performed on athymic male mice (Rj:ATHYM-Foxn1$^{nu/nu}$, Janvier Labs, #SM-ATH-M), housed in individually ventilated home cages (IVC), 2-5 mice per cage, in a pathogen free environment. Mice were fed with standard chow *ad libitum* and kept under standard day/night conditions. Upon arrival to the animal house facility from the breeder, animals were housed for at least 2 weeks as an adaptation period before the start of the procedure.

3.10 Intracranial glioma implantation

Ten weeks old male mice were anesthetized with isoflurane inhalant anesthesia (4–5% induction, 1–2% maintenance, 21% oxygen) using Isoflurane vaporizer (Temsega), and opioid analgesic Butorphanol (2 mg/kg, s.c.; OrionPharma). Mice were also injected with an anti-inflammatory drug Meloxicam (2 mg/kg, s.c.; Boehringer) and local analgesic Bupivacaine (5 mg/kg, s.c. at the site of incision; Polfa). Before starting the surgical procedure and during the surgery, the depth of anesthesia was verified by the lack of pedal reflex in the limb and breathing regularity. Choice of specific anesthetics was recommended by a veterinarian and approved by the First Local Ethics Committee in Warsaw, Poland. When mounted in the stereotactic instrument, Vidisic gel (2 mg/g Carbomerum, Bausch&Lomb) was placed on each of the animal's eyeball to prevent excessive drying of the conjunctiva. After performing a 1 cm longitudinal skin incision at the level of sagittal suture, 1 mm diameter hole was drilled with a micromotor drill (Stoelting Co.) 1 mm anterior and 2 mm lateral (to the right) to the bregma. WT or CHI3L1 KO U87-MG-RFP glioma cells (5×10^4 cells in 1 µl of DMEM) were implanted under aseptic conditions into the right striatum using 1 µL syringe with a 26-gauge needle in a stereotactic apparatus (Stoelting Co.) at speed 1 µL/3 min. Once the injection of cells finished, the needle was slowly retracted at the speed of 1 mm/min. The cranial bone loss was compensated for with surgical bone wax (SMI). Before implantations cells were checked for Mycoplasma contamination using a commercial PCR test. Cells were kept on ice throughout the procedure for no longer than 4 h. The incision area was sutured using silk non-absorbable sutures (Atramat, #CE1935-45 USP 5-0/EP1) by performing interrupted suture, topic analgesic was applied onto the site of suturing (Lignocainum cream containing 20 mg/g of lidocaine hydrochloridum). Mice were immediately placed into a clean cage and observed to confirm full recovery from anesthesia.

3.11 Magnetic resonance imaging

Heads of the animals were scanned with 7T BioSpec 70/30 MR system (Bruker) equipped with Avance III console and actively shielded gradient system B-GA 20S (amplitude 200 mT/m) with an integrated shim set up to 2nd order. A combination of transmit cylindrical radiofrequency volume coil (8.6 cm inner diameter, Bruker) and

head-mounted mouse dedicated receive-only array coil (2×2 elements, Bruker) was used. The animals were anesthetized with 1.5-2% isoflurane (Baxter) in oxygen and positioned prone with the head placed in the MR-compatible bed integrated with an anesthesia mask. Respiration and rectal temperature were monitored throughout the experiment with a MR-compatible small animal monitoring system (SA Instruments). All the imaging sessions started with a localizer protocol consisting of three orthogonal scout scans to accurately position the animal inside the magnet center. To evaluate volumes of the brain structures, structural transverse MR images covering the whole brain were acquired with T2-weighted TurboRARE (TR/TEeff = 7000/30 ms, RARE factor = 4, spatial resolution = 86 μm × 86 μm × 350 μm, 42 slices, no gaps, number of averages (NA) = 4, scan time ~ 23 min). The MRI evaluation was performed at the Laboratory of Small Animal Magnetic Resonance Imaging at the Mossakowski Medical Research Institute, Warsaw, Poland. MRI scans were then analyzed using Osirix DM DICOM Viewer software (v13.0.2.).

3.12 Collecting animal tissues and blood samples

On day 21 after glioma implantation, the animals were anesthetized with an i.p. injection of ketamine (160 mg/kg) and xylazine (20 mg/kg) and after the verification of the unresponsiveness to the noxious stimuli and absent reflexes, mice were transcardially perfused with an ice-cold PBS (Gibco, #18912014) and 4% paraformaldehyde (PFA, sigma, #158127) in PBS. Right before the perfusion, the right atrium of the heart was perforated and 500 μL venous blood was collected into 1.5 mL tubes without anticoagulants. Mice were sacrificed and brains removed and post-fixed for 48 h in 4% PFA in PBS at 4°C. Then, brains were placed in 30% sucrose in PBS at 4°C until sunk to the bottom of a tube. Subsequently, the brains were frozen in Tissue Freezing Medium (Leica, #14020108926) and serial 12 or 50 μm thick coronal sections were collected and stored at -80°C. Collected blood was kept for 2 h at room temperature to allow coagulation and then centrifuged for 10 min at 3.000 x *g*. After centrifugation, blood serum was carefully collected into 1.5 mL tubes, supplemented with proteinase inhibitor PMSF (phenylmethylsulfonyl fluoride, effective concentration 1 μM, Sigma, #P7626) and stored at -80°C. Sera collected from tumor-bearing mice were analyzed for human and mouse CHI3L1 using Human Chitinase 3-like 1

Quantikine ELISA Kit and Mouse Chitinase 3-like 1 Quantikine ELISA Kit (R&D Systems, #DC3L10 and #MC3L10, respectively). Tests were performed according to the manufacturer's protocol.

3.13 Fluorescence microscopy

Mouse brain cryosections of 12 or 50 µm thickness were used for immunostaining. For immunostaining of vWF, IBA1, AQP4, brain sections were thawed and dried for 2 h in room temperature and then rehydrated in PBS for 15 min. Next, sections were washed three times in 0.05 M TBS (Tris-buffered saline, Sigma, #T5912) and then incubated with 10% donkey serum with 0.1% Triton X-100 (Sigma, #X100) in TBS for 2 h at room temperature, then separately stained with primary antibodies: goat anti-Iba1 antibody (1:500; Abcam, #ab5076), rabbit anti-von Willebrand factor (1:1000; Agilent, #A008229-2), rabbit anti-aquaporin 4 (1:200, Abcam, #ab125049) for 24 h at 4°C followed by incubation with donkey anti-goat Alexa Fluor 488 (1:1000, Invitrogen, #A-11055), donkey anti-rabbit Alexa Fluor 488 (1:1000, Invitrogen) and donkey anti-rabbit Alexa Fluor 647 (1:1000, Invitrogen, #A-31573) for 2 h at RT. Primary antibody was omitted in a negative control. Sections were then washed and mounted with Vectashield Vibrance® Antifade Mounting Medium with DAPI (Vector Labs, #H-1800-2).

For GFAP, CD31and laminin staining, brain sections were thawed and dried for 5 min at 37°C temperature and then kept in chilled methanol in -20°C for 30 min. Next, sections were washed three times for 5 min each in PBST (0.1% Triton X-100 in PBS) and then blocked with 3% donkey serum in Blocking Buffer: 0.4% Triton X-100 in PBS for 2 h at room temperature, then separately stained with primary antibodies: rabbit anti-GFAP antibody (1:200; Dako, #Z033429-2), rat anti-CD31 antibody (1:100, Novus Biologicals, #NB600-1475), rabbit anti-laminin (1:50; Abcam, #ab11575), for 24 h at 4°C followed by incubation with donkey anti-rat or anti-rabbit Alexa Fluor 488 (1:500, Invitrogen, #A-21208 or #A-21206, respectively), for 2 h at RT. Primary antibody was omitted in a negative control. Sections were then washed three times in PBST for 5 min each, one time in PBS for 5 min, one time in ultrapure water for 5 min and mounted with Vectashield Vibrance® Antifade Mounting Medium with DAPI. Images were

captured on Zeiss Axio Imager M2 microscope. Image processing and quantification was performed using ImageJ software (NIH). The number of non-capillary vessels was quantified by excluding blood vessels of diameter below 10 µm as depicted in Figure 3.2.

A

Vessel type	Diameter (µm) in mouse
Aorta	535
Artery	150
Arteriole	18
Capillary	4
Venule	14
Vein	250

B

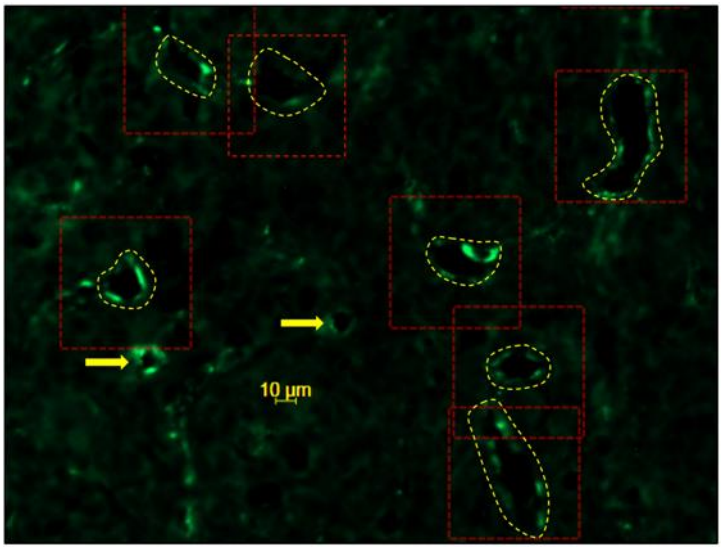

Figure 3.2. Quantification of non-capillary blood vessels in tumors sections stained for vWF. A. Diameter of blood vessels in mouse[120]. B. Blood vessels that appeared with diameter of above 10 µm (encircled with yellow dashed line) were calculated as non-capillary. Vessels with diameter below 10 µm (yellow arrows) were excluded from the analysis.

The microvessel density was calculated by measuring the area fraction taken up by the signal coming from vessels of diameter below 10 µm using Threshold, Analyze, Measure and Area fraction tools in ImageJ as shown in Figure 3.3.

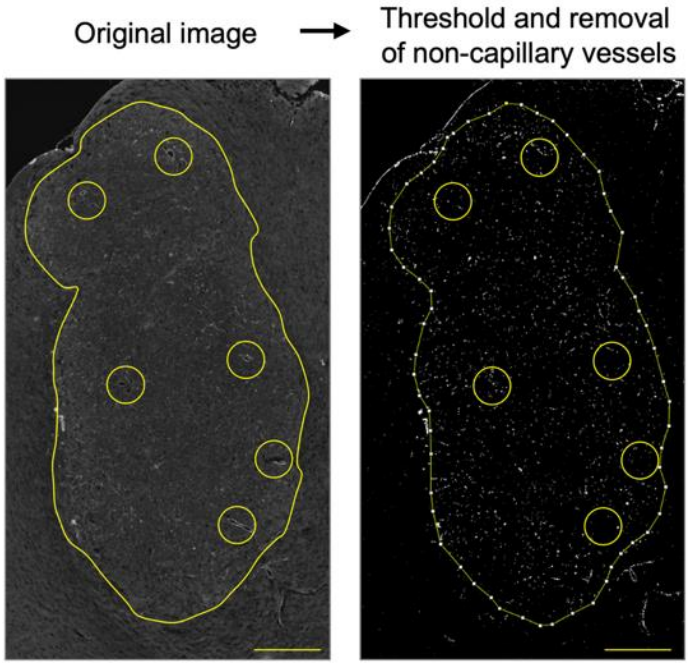

Figure 3.3. Quantification of microvessel density in tumor sections. Original images with vWF signal were transformed into masks using Threshold tool. Signal from non-capillary vessels (yellow circles) within the area corresponding to tumor (outlined in yellow) was removed. Remaining signal coming from the tumor was quantified using Analyze > Measure > Area fraction tool sequence. Scale bars represent 300 μm.

Immunopositive signals from Iba1, laminin, AQP4 and GFAP were quantified using Threshold, Analyze, Measure, Raw Integrated Density tools in ImageJ. Confocal images were taken using Zeiss LSM 780 or Zeiss LSM800 Airyscan microscope at the Laboratory of Imaging Tissue Structure and Function, Nencki Institute of Experimental Biology. The images shown in Figure 4.25 are 3D renderings of z stacks of sections stained for CD31: 639×639μm and at least 40 μm of z stack (z steps 3.5 μm). The vessels and tumor cells were rendered using surface rendering of Bitplane Imaris Image Analysis software.

3.14 Matrigel invasion assay

Cell culture inserts (8 μm pore size Costar, #3422) were coated with 1 mg/mL Growth Factor Reduced Matrigel Matrix (BD Biosciences, #354230) in DMEM, and dried at 37 °C for 5 h. U87-MG glioma cells (4×10^4) were seeded on matrigel-covered membrane in an upper compartment and then inserts were transferred to a 24-well plate with or without human SV40 microglial cells (HM SV40) in a lower compartment

(as shown in Fig. 3.4A). After 18 h, cells invading through the matrigel were fixed with 95% methanol and stained with DAPI (4′,6- Diamidino-2-Phenylindole; 0.01 mg/ml, Sigma, #D9542). The membranes from inserts were cut out and invading cells were visualized using fluorescence microscope (Leica DM4000B) and cell nuclei were counted from five independent fields/slide using ImageJ software as depicted in Figure 3.4B. The statistical significance was calculated using a chi-square test (*p<0.05, **p<0.01, ***p<0.001). OR stands for odds ratio.

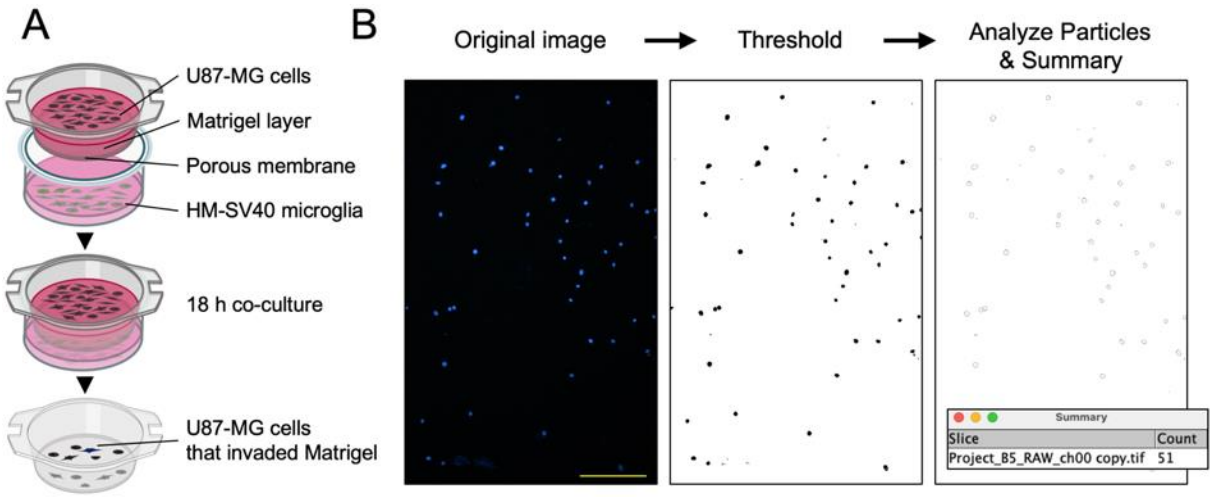

Figure 3.4. Matrigel invasion assay. A. Schematic representation of the experimental procedure. B. Quantification of matrigel invasion assay using the ImageJ software. Original fluorescence images with cell nuclei stained with DAPI were transformed into a black-and-white mask with Threshold tool, then particles corresponding to cell nuclei were outlined and quantified using Analyze Particle tool. Nuclei from five independent fields of view were counted. Scale bar represents 200 μm.

3.15 Gelatin zymography

U87-MG cells were seeded onto 24-wells plate at 5×10^5 cells per well in 1 mL DMEM supplemented with 10% fetal bovine serum (FBS) and antibiotics (100 U/mL penicillin, 100 μg/mL streptomycin). After 24 h, culture medium was discarded (to get rid of endogenous MMPs from blood serum) and replaced with a corresponding medium without FBS. Cells were incubated in FBS-free medium for 24 h and then, the culture medium was collected, centrifuged for 10 min at 300 × *g* to pellet floating cells and the cell-free medium was subjected to gelatin zymography. In brief, samples were diluted in 5× Laemmli buffer without dithiothreitol (DTT) and subsequently separated electrophoretically using 8% acrylamide–bisacrylamide (29:1, Sigma, #A3699) gels supplemented with 2 mg/mL porcine gelatin (Sigma, #9000-70-8), 380 mM TRIS–HCl

(pH 8.8, Roche, #10812846001), 0.1% SDS (Sigma, #L3771), 0.1% ammonium persulfate (Sigma, #A3678) and 0.6 µl/ml of TEMED (Sigma, #1.10732). Once electrophoresis was done, gels were rinsed twice with 2.5% Triton X-100 at RT before incubation in a renaturation buffer containing 50 mM TRIS–HCl pH 7.6, 10 mM CaCl2 (Sigma, #C1016), 1 µM ZnCl2 (Sigma, #39059), 1% Triton X-100 and 0.02% sodium azide (37°C, 100 rpm). After 24 h gels were stained with Coomasie brilliant blue, washed with PBS, and subjected to a densitometric analysis. Cell culture medium with FBS was used as a positive control as FBS contains gelatin-degrading enzymes.

3.16 Public data analysis

Analysis of public data was performed using R Statistical Software (version 4.2.2; R Foundation for Statistical Computing). RNAseq data (FPKMs) were downloaded from the Ivy Glioblastoma Atlas Project[121] and normalized RNAseq and protein data from The Brain Protein Atlas (BPA)[122,123]. Correlation of CHI31L1 mRNA and protein expression level was computed in the BPA dataset, using Kendall correlation and von Waerden test followed by post-hoc U-Mann-Whitney tests to determine differences between tumor regions. Exact Fisher tests was performed for overlap of genes, whose expression correlated with CHI3L1, and MESlike1 signature by Neftel et al.[124].

3.17 Statistical analysis

All biological experiments were performed on 3-5 independent cell passages. The results were expressed as means ± standard deviation (SD). P values were calculated using chi-square, two-tailed t test; one-way ANOVA or linear regression analysis followed by appropriate post-hoc test using GraphPad Prism v9 (GraphPad Software). Differences were considered statistically significant for P values <0.05.

3.18 Data availability

RNAseq data are available in the NIH GEO database with the accession number GSE231816.

4. Results

4.1 The determination of *CHI3L1* expression in gliomas of various WHO grades

The comprehensive evaluation of *CHI3L1* expression in in-house and public bulk and single-cell RNA seq datasets was performed. Using real-time quantitative PCR (RT-qPCR) *CHI3L1* mRNA was determined in glioma samples from 76 patients with juvenile pilocytic astrocytomas (PA, n=15), diffusive astrocytomas (DA, n=17) and glioblastomas (GBM, n=44). Normal human brain samples were used as a control (NB, n=3). *CHI3L1* was overexpressed in samples isolated from PA and GBM patients in comparison to normal brains (Fig. 4.1A). Next, *CHI3L1* expression was evaluated in RNA-sequencing dataset from a cohort of 31 patients diagnosed with PA (n=11), DA (n=7) and GBM (n=13). RNA from normal brain was used as a reference control (n=4). *CHI3L1* expression showed the same pattern, namely was overexpressed in PA and GBM samples in comparison to normal brain (Fig. 4.1B).

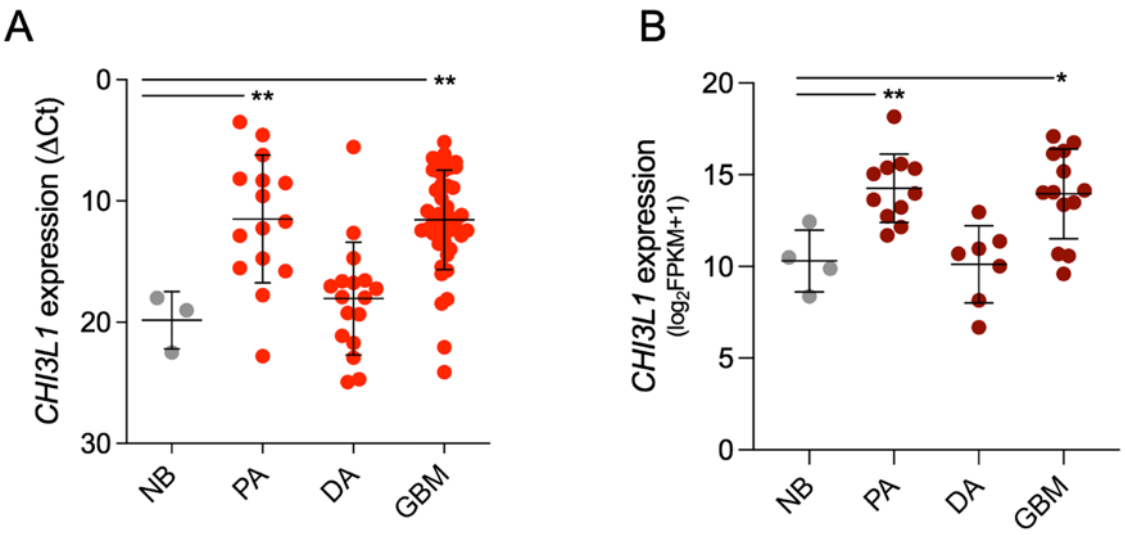

Figure 4.1.*CHI3L1* is overexpressed in glioblastomas and pilocytic astrocytomas. A. *CHI3L1* mRNA levels in patient-derived samples (cohort 1) determined using RT-qPCR), data is presented as mean±SD; NB, normal brain n=3; PA, pilocytic astrocytoma, n=15; DA, diffusive astrocytoma n=17; GBM, glioblastoma n=44. Statistical analysis by one-way ANOVA, Tukey's multiple comparison test, * P≤0.05, ** P≤0.01. B. *CHI3L1* levels in bulk-RNAseq gene expression datasets composed of 31 patient-derived samples (cohort 2); NB n=4, PA n=11, DA n=7, GBM n=13.

These data demonstrate overexpression of *CHI3L1* in GBM resected specimens, but also shows high expression of *CHI3L1* in PA tumors, which are described as benign, circumscribed, and non-invasive.

4.2 The determination of the cellular source of CHI3L1 in glioblastoma

In order to determine the cellular source of CHI3L1 in glioblastoma, a publicly available single-cell RNA-sequencing database of 28 *IDH1*-wt GBM tumors was explored (the Single Cell Portal, Broad Institute)[124]. This database distinguishes 4 types of cells in glioblastoma: malignant cells, macrophages, oligodendrocytes, and T cells. At single-cell resolution, *CHI3L1* was found to be expressed predominantly by malignant cells, with a lesser expression in glioma-associated macrophages (Fig. 4.2).

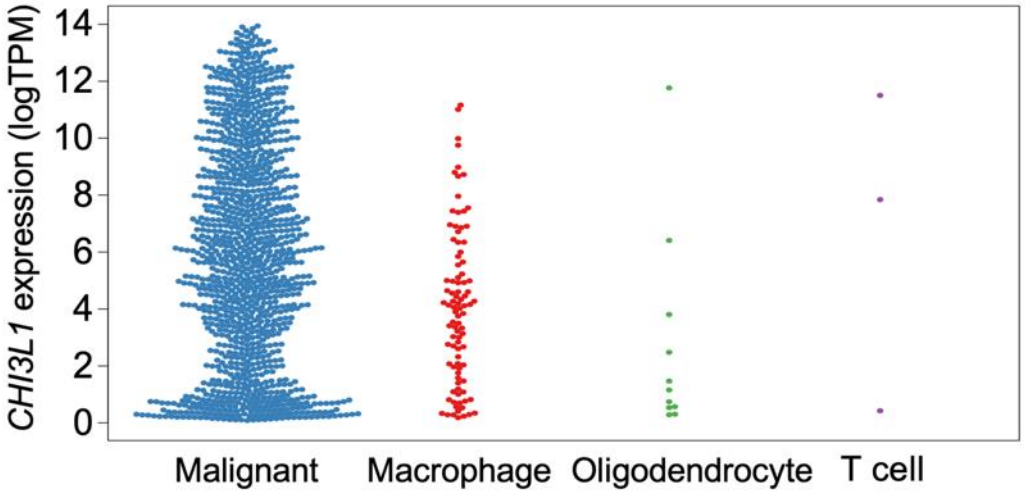

Figure 4.2. Malignant cells are the main source of *CHI3L1* mRNA in glioblastoma. Beeswarm plot of *CHI3L1* expression in malignant, stromal, and immune cells in GBMs.

The Single Cell Portal enables to explore the expression of the gene of interest within several cellular state signatures defined by Neftel *et al.*[124]: mesenchymal-like (MES-like1 and 2), astrocyte-like (AC-like), oligodendrocyte progenitor cell-like (OPC-like) and neuronal progenitor cell-like (NPC-like1 and 2). *CHI3L1* was expressed predominantly within the MES-like state of tumor cells (Fig. 4.3A). A linear regression analysis was performed, and the results show high positive correlation between *CHI3L1* expression and genes classified as MES-like1 (Fig. 4.3B). The genes listed in the MESlike1 signature were cross-checked with the proteins correlated with CHI3L1 in the Brain Protein Atlas database[122,123]. Out of 27 genes assigned to the MESlike1 signature, 25 correlated positively with CHI3L1 at a protein level in GBMs (Fig. 4.3C).

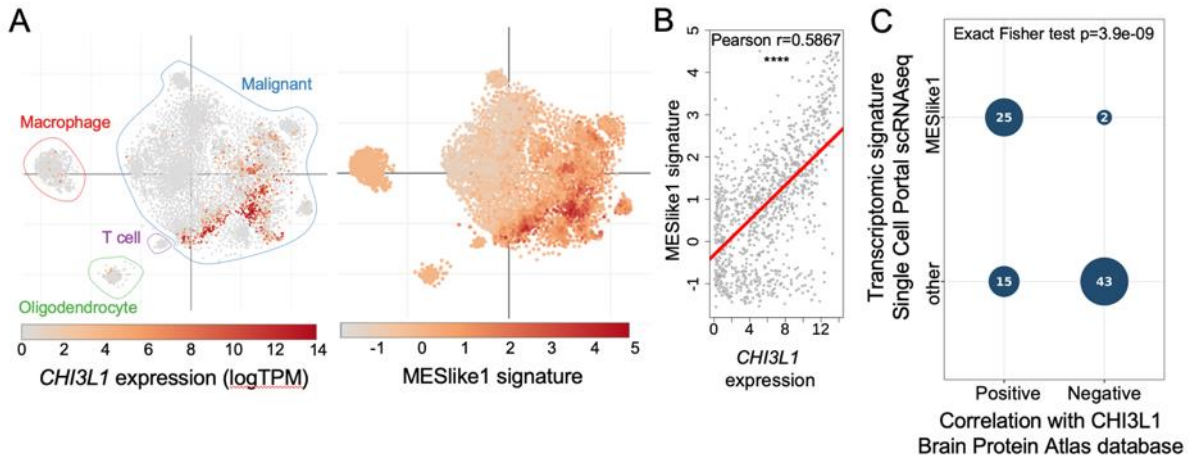

Figure 4.3.*CHI3L1* expression is positively correlated with the mesenchymal gene expression profile in human GBMs at single-cell resolution. A. Left: tSNE plot showing distribution of *CHI3L1* expression across GBMs at single-cell resolution. Right: tSNE plot representing MESlike1 signature in the dataset. **B**. Scatter plot representing a positive correlation between the mesenchymal signature and *CHI3L1* expression. Linear regression line in red. **** P ≤0.0001. **C.** Correlation analysis between genes associated with the mesenchymal signature in the Single Cell Portal and proteins correlating with CHI3L1 in the Brain Protein Atlas database. Exact Fisher test. Numbers in circles indicate the number of genes/proteins.

CHI3L1 expression was also found to correlate negatively with OPC-like and NPC-like1 signatures, which represent distinct cellular states of glioblastoma (Fig. 4.4)

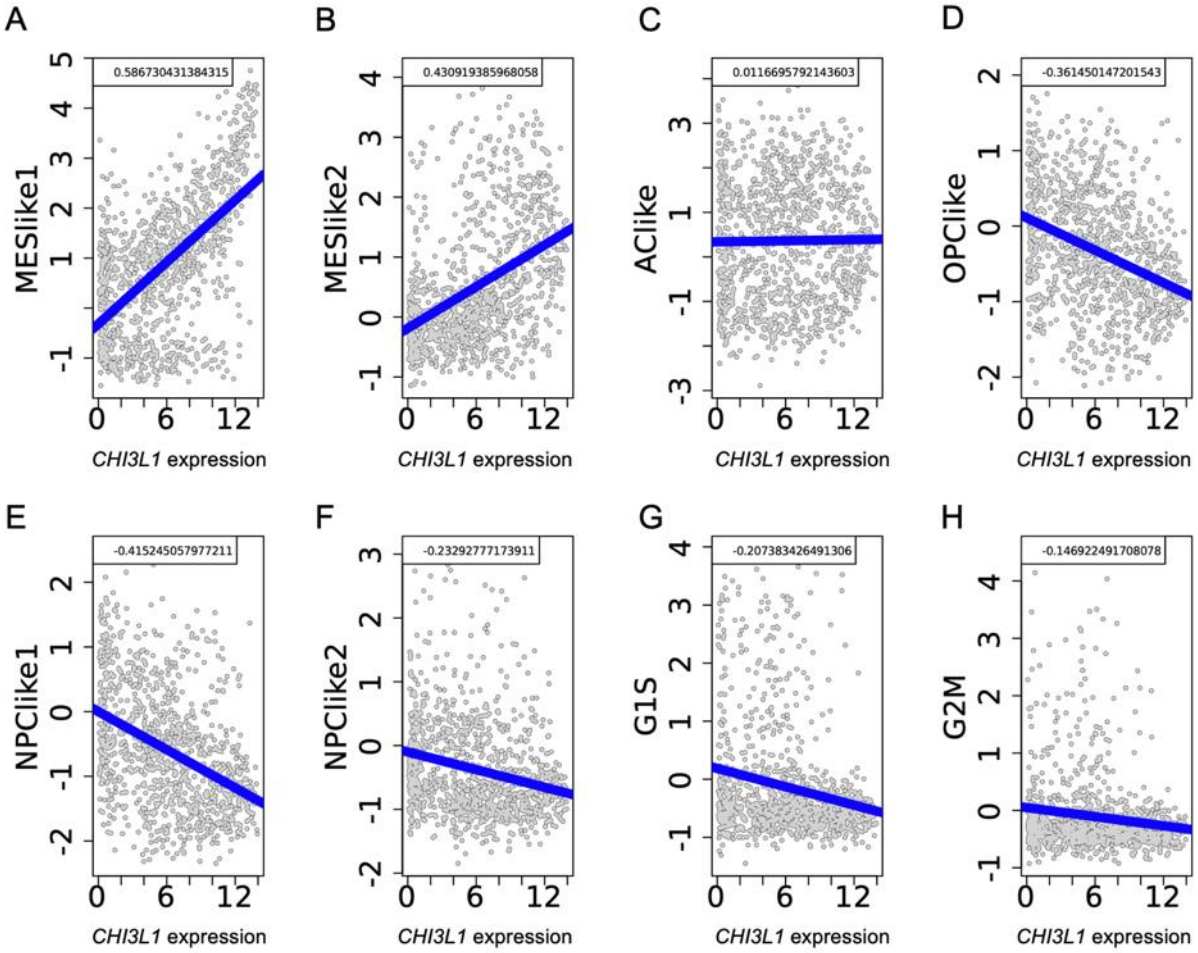

Figure 4.4. Correlation of CHI3L1 expression with various transcriptomic signatures in GBMs. A-H. Scatter plot representing a linear regression analysis between the various cellular state signatures defined in The Single Cell Portal and *CHI3L1* expression. Linear regression line in blue. Significance of all analyses at P ≤0.0001.

4.3 The expression of *CHI3L1* in human glioma cell lines

The expression of CHI3L1 mRNA was determined in several established human glioma cell lines (LN229, U251, LN18, T98G, U87-MG) and primary cells from patient-derived glioma samples (WG4 and WG9). Immortalized, non-transformed human astrocytes (NHA, normal human astrocytes) were used as a reference control. Majority of the tested cells had lower *CHI3L1* expression than NHA, U87-MG had the *CHI3L1* expression comparable to NHA, while WG9 primary cells exhibited higher *CHI3L1* levels in comparison to NHA (Fig. 4.5A). CHI3L1 concentration was measured by ELISA in glioma-conditioned medium (GCM) collected from LN229, U87-MG and WG9 cells. CHI3L1 was undetectable in the GCM of LN229, which was predicted based on very low transcript levels. The level of the protein was 3 times higher in U87-MG (mean

88 pg/mL) and around 50 times higher in WG9 cells (mean 1384 pg/mL) in comparison to NHA (mean 28 pg/mL) (Fig. 4.5B).

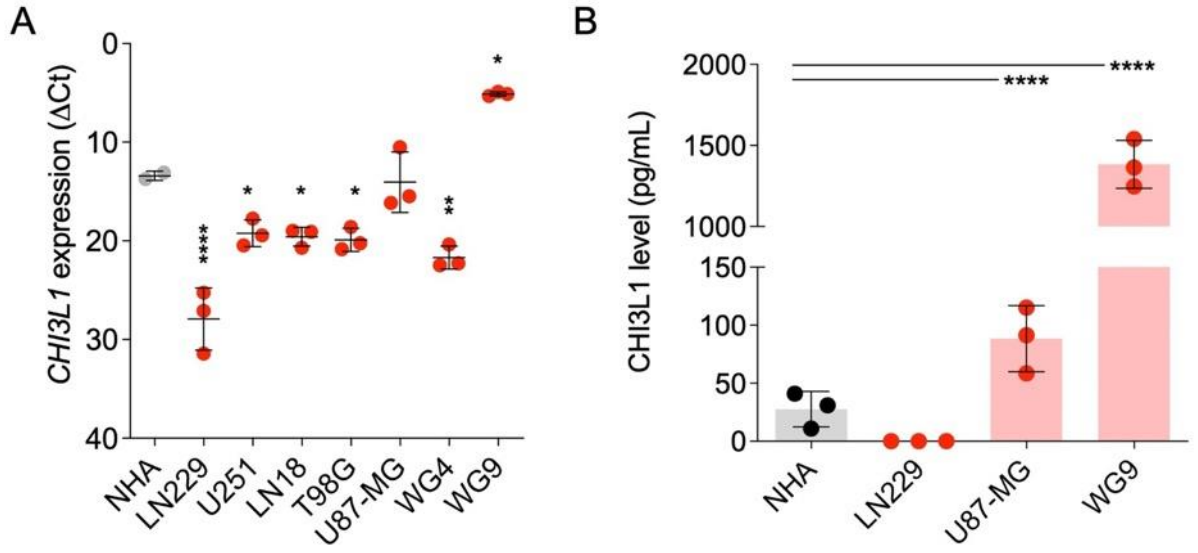

Figure 4.5. Accumulation of CHI3L1 in conditioned media from human U87-MG glioma cells and patient derived WG9 cells. Assessment of CHI3L1 expression at the mRNA (A) and protein (B) level in normal human astrocytes (NHA), five glioma cell lines (LN229, U251, LN18, T98G and U87-MG) and two GBM patient derived cell cultures (WG4, WG9). Mean ± SD is presented, one-way ANOVA. Tukey's multiple comparison test. * P≤0.05, ** P≤0.01, **** P≤0.0001.

The tested cell lines were evaluated for the effect of *CHI3L1* knock-out (KO) on cell viability using large-scale loss-of-function screening database (DepMap, Broad Institute)[125]. U87-MG were scored the highest among the tested cell lines on the CHI3L1 "gene effect" score, which is a measure of how cell viability is dependent on *CHI3L1* knock-out (Fig. 4.6).

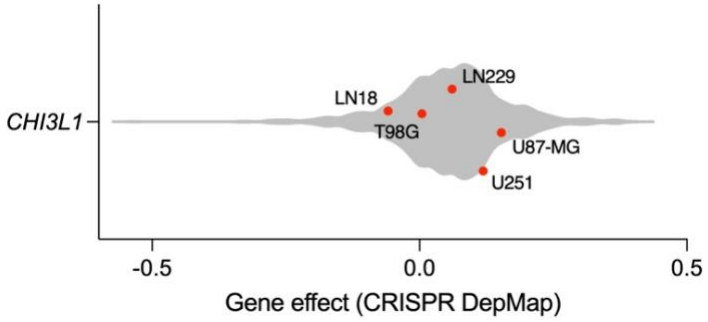

Figure 4.6. *CHI3L1* knock-out has a low effect on cell viability of U87-MG human glioma cells. Cancer Dependency Map (DepMap, Broad Institute) plot of "gene effect" of tested human glioma cell lines. The higher the gene effect, the lower the impact of CRISPR-mediated knock-out of CHI3L1 on the viability of the cells.

Based on these results, U87-MG cells were selected for CRISPR/Cas9 mediated knock-out of *CHI3L1*. The primary WG9 cell cultures grew relatively slow in vitro, which made it impossible to use them for silencing of *CHI3L1* even though these cells had highest level of CHI3L1 both at mRNA and protein level. Moreover, WG9 cells do not establish tumors in recipient mice (data unpublished).

4.4 The development of CHI3L1 KO cells using CRISPR/Cas9 genome editing

4.4.1 The selection of U87-MG-RFP sgCHI3L1 transfectants

To evaluate the effect of CHI3L1 depletion on glioma cells, CRISPR/Cas9 genome editing was applied to generate human glioblastoma cells depleted of CHI3L1 (KO) (Fig. 4.7).

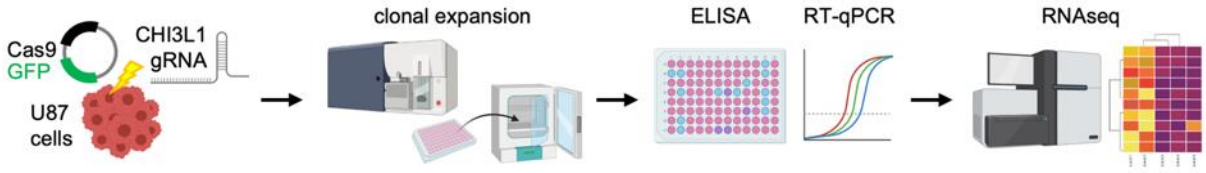

Figure 4.7. Experimental pipeline for developing *CHI3L1* knock-out in U87-MG-RFP (U87) human glioblastoma cells using CRISPR/Cas9 genome editing technique.

U87-MG-RFP cells were transfected with two CHI3L1-specific guide RNAs (sgRNA) and pCMV-Cas9-GFP plasmid using electroporation as described in Methods. Before sorting, the cells were seeded onto the culture flask and assessed for the presence GFP signal using fluorescence microscopy. Cells appearing as orange (indicated with arrows) in Figure 4.8 are the successfully transfected cells.

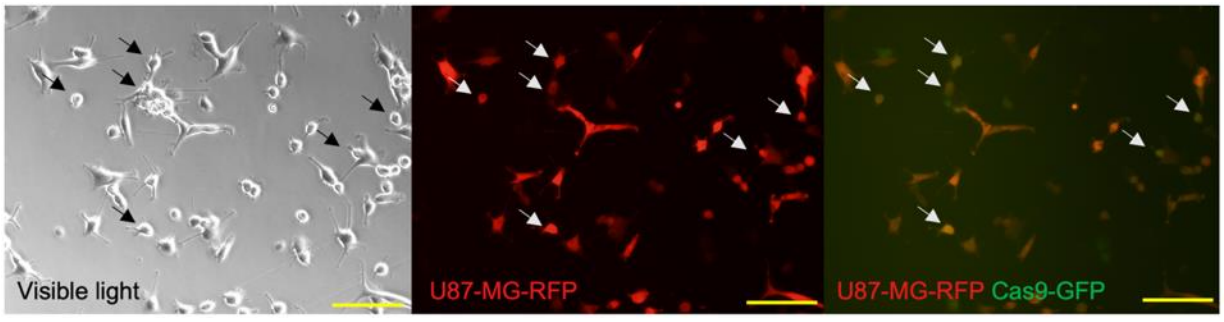

Figure 4.8. Visualization of transfected U87-MG-RFP cells. Representative images of U87-MG-RFP cells 24 h after transfection with the CHI3L1-specific sgRNA and the Cas9-GFP plasmid. Arrows indicate double-positive cells that were successfully transfected. Scale bar represents 50 µm.

U87-MG-RPF cells transfected with the sgCHI3L1 and the Cas9 plasmid were cultured for 24 h and subjected to FACS analysis to sort out transfected cells. Figure 4.9A shows a histogram representing GFP signal from transfected cells. Sorting gates were set to include cells with a high expression of RFP and GFP signal (8.13% of viable cells) (Fig. 4.9B). As a result, 480 cells were sorted into five 96-wells plates to establish single clone cultures.

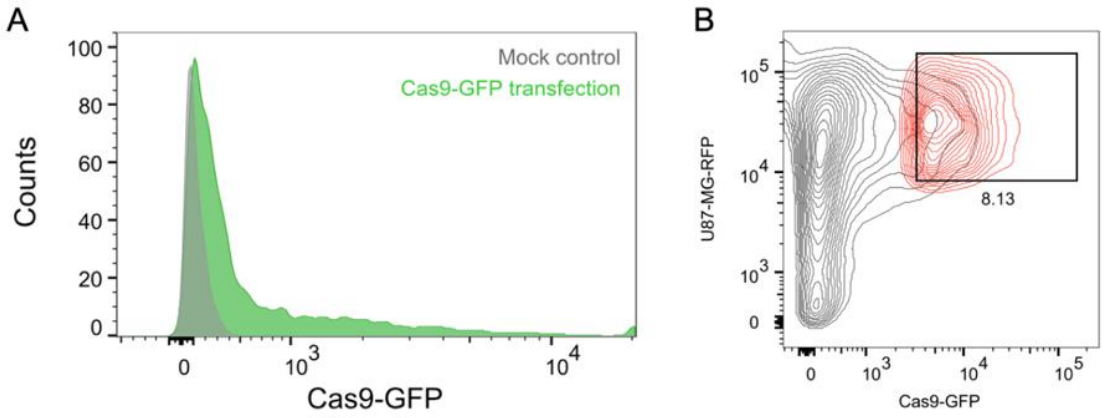

Figure 4.9. Single-cell FACS of U87-MG-RFP sgCHI3L1 transfectants. A. Histogram of U87-MG cells transfected with the pCMV-Cas9-GFP plasmid (green) and mock control (gray). B. Contour plot cytogram of sorted U87-MG-RFP cells transfected with the sgCHI3L1 and the Cas9-GFP plasmid.

4.4.2 The validation of *CHI3L1* knock-out in U87-MG-RFP cells

Upon establishing colonies, proliferating U87-MG-RFP sgCHI3L1 clones were up-scaled and a portion of cells was banked for future use. Levels of *CHI3L1* mRNA and protein were determined in cells using RT-qPCR with two sets of *CHI3L1*-specific primers and CHI3L1-specific ELISA, respectively. Initially, glioma-conditioned medium from 40 clones was subjected to ELISA to select the clones with the lowest concentration of CHI3L1 (Figure 4.10). A threshold of below 15% of wild-type CHI3L1 expression was set to select CHI3L1 KO candidate clones.

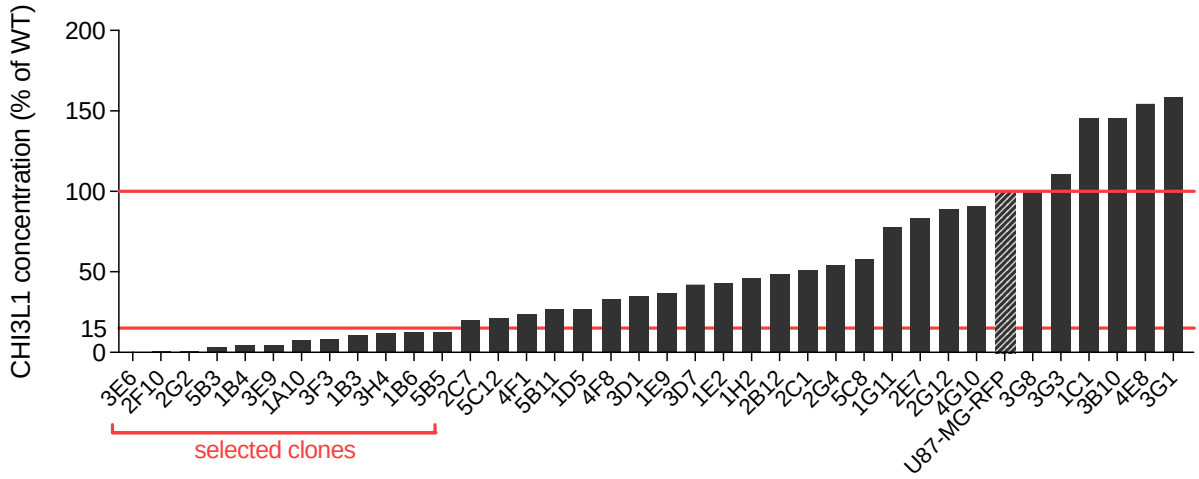

Figure 4.10. CHI3L1 levels in U87-MG-RFP sgCHI3L1 clones. Bar plot showing a ratio pf CHI3L1 concentration in indicated clones compared to WT control (U87-MG-RFP, marked with a striped bar). CHI3L1 was measured in cell culture supernatant. Red line at 100% represents the reference to WT control. Red line at 15% represents the arbitrary threshold to select CHI3L1 KO candidate clones.

The primers for RT-qPCR were designed to target two sites in the *CHI3L1* gene ("887" and "589") to which the two sgRNAs guided the Cas9 nuclease to. The Fig. 4.11A shows a significant decrease in the *CHI3L1* transcript levels in all the selected candidate clones. A second round of ELISA confirmed a significant decrease in the level of secreted CHI3L1 in candidate clones compared to WT (Fig. 4.11B).

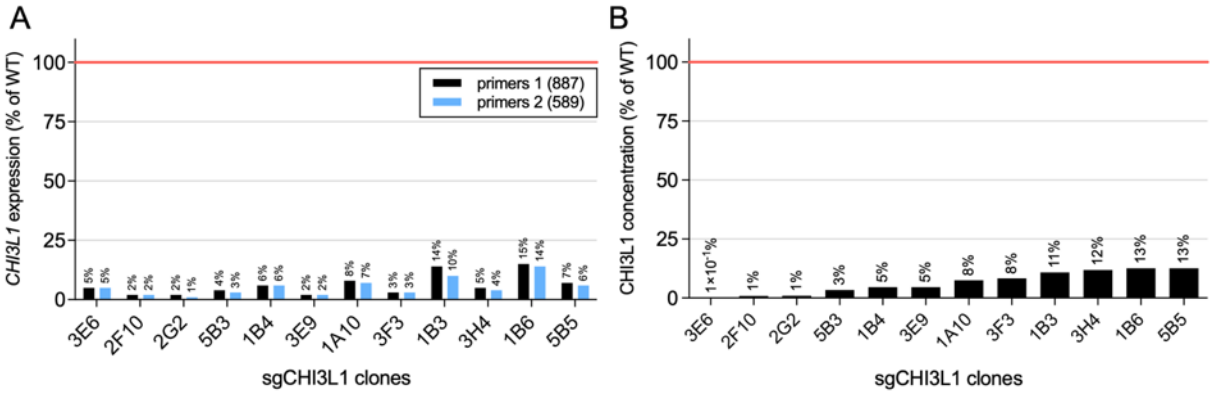

Figure 4.11. Validation of CHI3L1 depletion in selected clones. A. RT-qPCR analysis of *CHI3L1* expression using 2 sets of primers. *CHI3L1* expression given as % of WT control (red line). B. CHI3L1 concentration was determined by ELISA in supernatants of sgCHI3L1 clones and is presented as % of WT control (red line).

Based on the lowest CHI3L1 expression (Fig. 4.11) and cellular morphology resembling the control cells (data not shown), the clone 2G2 (CHI3L1 KO1) was

selected as the best candidate for *in vivo* studies. Clone 5B5 (CHI3L1 KO2) was selected as the second-best candidate with a slightly higher expression of CHI3L1. Both KO1 and KO2 cells were subjected to RT-qPCR and ELISA to confirm a successful decrease of CHI3L1 expression in these cells compared to WT control (Fig. 4.12).

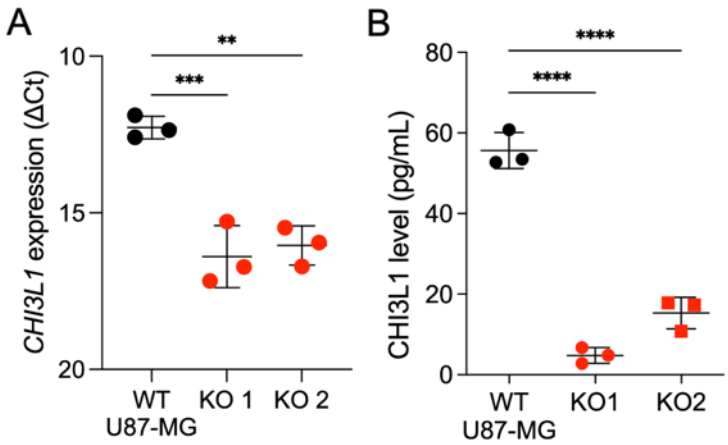

Figure 4.12. Validation of CHI3L1 depletion in selected clones. A. RT-qPCR analysis of *CHI3L1* expression. B. ELISA of cell culture supernatants of KO1 and KO2 clones. Data is presented as mean ± SD; n=3, Unpaired t-test, ** P≤0.01, *** P≤0.001, **** P≤0.0001.

Since the CHI3L1 KO cells and wild type (WT) counterparts were to be used *in vivo* to assess the tumor growth, it was necessary to examine proliferation capacity of these cells as any substantial difference in cell proliferation *in vitro* could diminish the capacity of these cells to establish tumors *in vivo*. Therefore, cell proliferation in CHI3L1 KO1 cells was determined using two assays: dye dilution and BrdU incorporation assays in CHI3L1 KO1 cells. Fig. 4.12 shows that the proliferation of CHI3L1 KO cells was comparable (not significantly different) to that of WT cells (Fig. 4.13A). The results were corroborated by the BrdU assay (Fig. 4.13B). The addition of recombinant human CHI3L1 (rhCHI3L1) at concentrations of 7.5 ng/mL (concentration of CHI3L1 in WT cells conditioned media) or 15 ng/mL (double concentration) did not modulate proliferation of CHI3L1 KO cells (Fig. 4.13C). This shows that extracellular CHI3L1 is not a factor governing glioma cell proliferation *in vitro*.

Notably, CRISPR/Cas9-based gene editing did not change the proliferation of cells. U87-MG-RFP cells were transfected with control non-targeting sgRNA (sgCTR),

then 3 clones were subjected to BrdU incorporation assay. sgCTR cells had comparable proliferation rate as control cells (Fig. 4.12D).

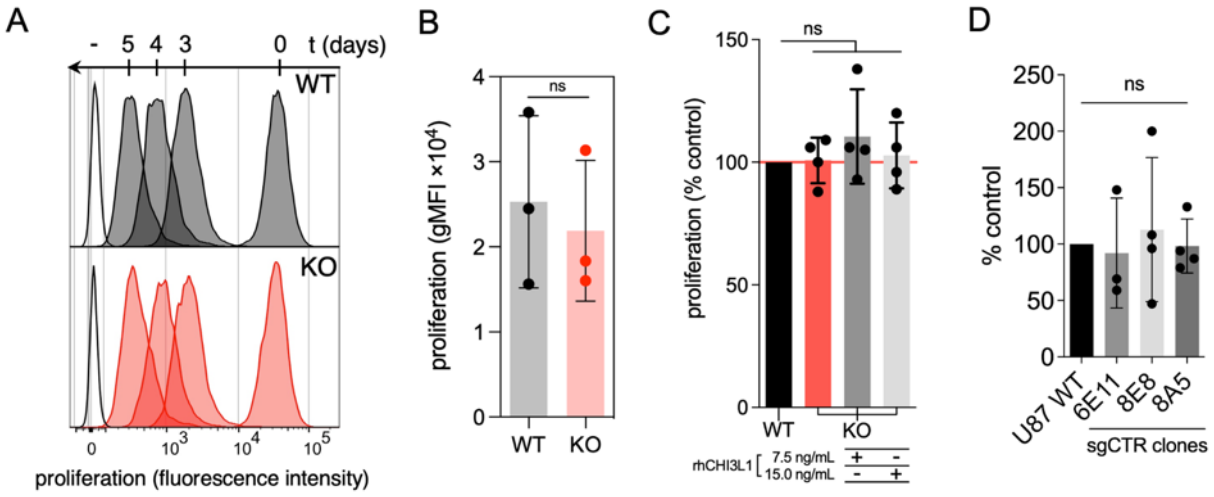

Figure 4.13. CHI3L1 depletion or supplementation do not affect proliferation of glioma cells. A. Cell proliferation dye dilution assay. Histogram of fluorescent dye signal at time points 0, 3, 4 and 5 days of cell culture with the dye. Unstained control is designated "-". B. Quantification of fluorescent dye signal after 72 h of cell culture with the dye; mean ± SD is presented; n=3, parametric unpaired t-test. C. BrdU incorporation assay; mean ± SD is presented; n=4, one-way ANOVA with Dunn's multiple comparison test. Adding recombinant human CHI3L1 to WT and KO cells does not affect cell proliferation. D. BrdU incorporation assay for U87-MG-RFP cells transfected with control non-targeting gRNA. Mean ± SD is presented; n=3, parametric unpaired t-test.

4.5 The determination of transcriptome changes in CHI3L1 KO cells

To study global transcriptomic changes in CHI3L1 deficient cells, total RNA was isolated from CHI3L1 KO cells (clones 1 and 2) and WT U87-MG cells and subjected to RNA sequencing. Differentially expressed genes (DEGs) were identified. A Venn diagram shows the number of commonly up- or down-regulated genes among DEGs in KO1 and KO2 clones compared to WT cells (Fig. 4.14). Around 50% of DEGs were commonly regulated in both KO cell lines.

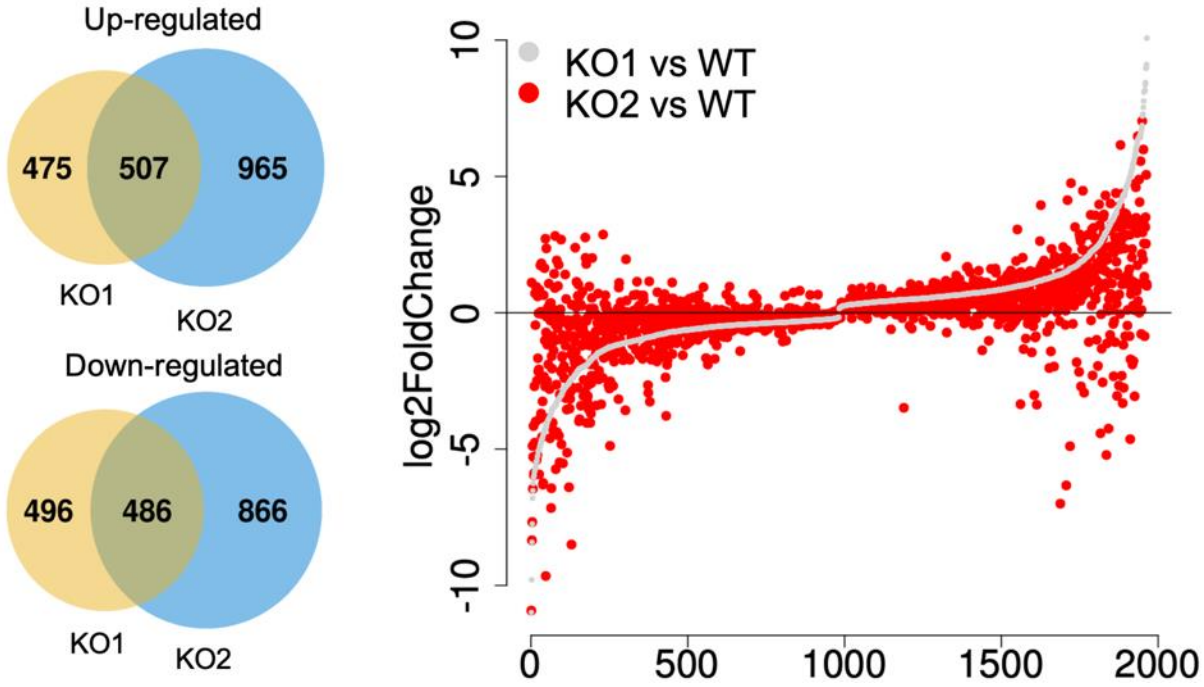

Figure 4.14. Identification of differentially expressed genes CHI3L1 KO1 and KO2 cells. Left.Venn diagrams of differentially expressed genes for up- (top) and down-regulated (bottom) genes between two CHI3L1 KO clones as compared to WT controls. Right. Snakeplot of up- and down-regulated genes in CHI3L1 KO cells vs WT.

A Volcano plot shows genes with significantly altered expression in KO1 cells (Fig. 4.15A). Many of those DEGs are implicated in the regulation of ECM degradation, cell migration, and invasion. Reactome pathway enrichment analysis revealed that many genes down-regulated in CHI3L1 KO clones belong to ECM organization pathway (*MMP2*, *MMP24*, *BMP1*, *PCOLCE*, *PCOLCE2*, *COL5A2*, *COL1A1*, *ADAMTS2*, *ADAMTS9*, *EFEMP1*, *TGFB3*), which suggests that glioma cells depleted of CHI3L1 might exhibit a decreased ability to reorganize the ECM (Fig. 4.15B).

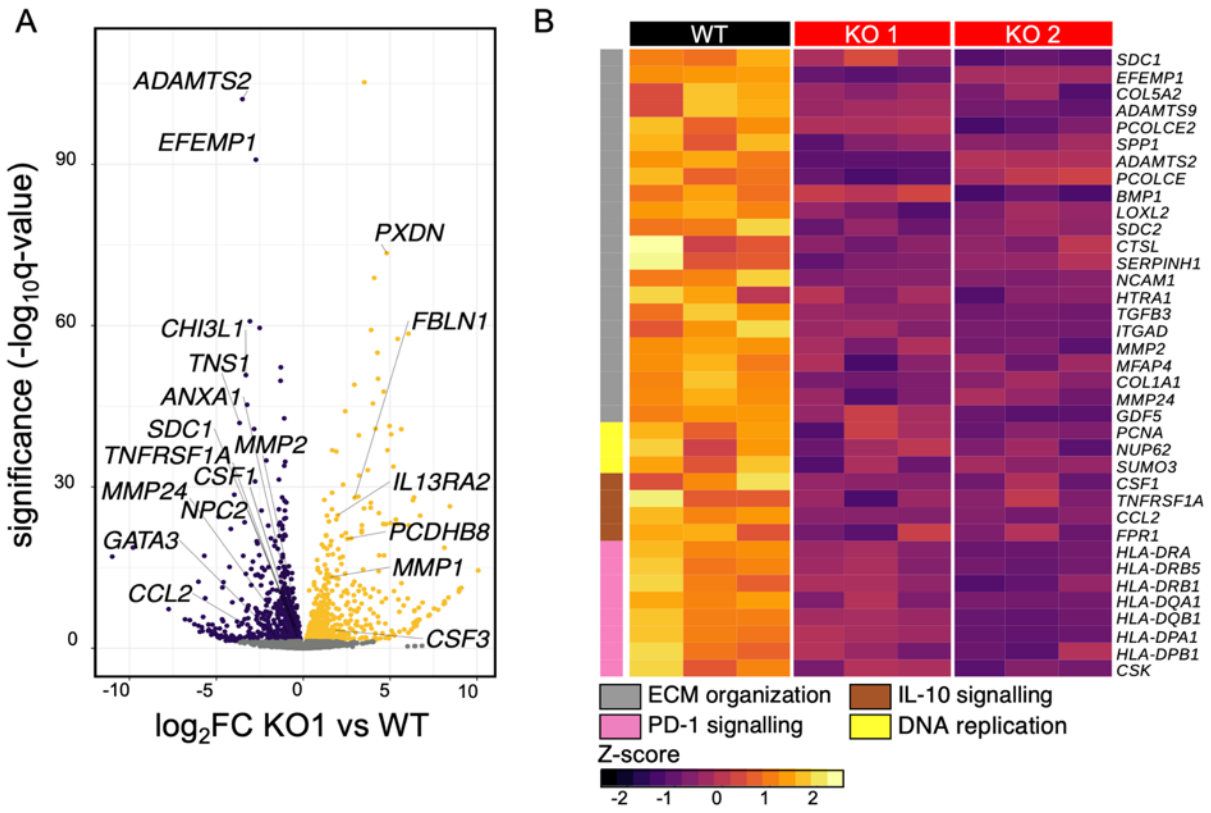

Figure 4.15. Distinct patterns of gene expression in U87 CHI3L1 KO cells. A. Volcano plot of DEGs in the CHI3L1 KO1 cells compared to the WT cells. Common DEGs for KO1 and KO2 are highlighted with a label. B. Z-score heatmap of REACTOME pathway enrichment analysis for CHI3L1 KO1 and KO2.

The heatmap shows similar expression patterns of genes from the selected categories in both KO clones (Fig.14B). GBM is a highly invasive tumor that infiltrates brain parenchyma making complete surgical resection impossible. Glioblastoma cells invade brain parenchyma through production of metalloproteinases, including MMP-2[126], and paving its way through collagen scaffolding. *COL5A2* has been reported as one of the most up-regulated in GBM in comparison to normal brain tissue[71]. *COL1A1* has been implicated in malignant behavior of gliomas[127], thus their reduced expression might decrease tumor invasiveness. *BMP1*, coding for bone morphogenetic protein 1 also known as procollagen C-endopeptidase, was down-regulated in CHI3L1 KO cells. BMP1 has been implicated in gastric cancer progression and was a marker of poor prognosis for gastric cancer patients[128]. The binding of BMP1 to collagen is potentiated by procollagen COOH-terminal proteinase enhancers such as PCOLCE and PCOLCE2[129]. Notably, *PCOLCE* and *PCOLCE2* were down-regulated in CHI3L1 KO

cells. These genes encode glycoproteins which bind and drive the enzymatic cleavage of type I procollagen and heightens C-proteinase activity. Down-regulated genes include *ADAMTS9* and *ADAMTS2,* genes coding for the members of disintegrin-like and metalloprotease with thrombospondin type 1 motif (ADAMTS) family. Members of ADAMTS family are involved in both assembly and disassembly of collagen fibers and play important roles in the proteolytic degradation of the ECM during cancer cell invasion, particularly the degradation of brain ECM component thrombospondin 1 (THBS1)[69,130]. However, the direct role ADAMTS family members in glioblastoma progression has not been yet reported[131]. Of note, *ADAMTS4* and *ADAMTS5* which were detected in surgically resected GBMs[132], were unchanged in CHI3L1 KO cells, which suggests that these members of ADAMTS family might not be dependent on CHI3L1 expression. *EFEMP1* codes for fibulin-3, a member of EGF-containing fibulin ECM proteins. Fibulin-3 has been associated with glioma cell motility and invasiveness contributing to the aggressive nature of glioblastoma[133,134].

Genes highly up-regulated in CHI3L1 KO cells included genes associated with formation and re-organization of ECM and cell-to-cell adhesion (*FBLN1*, *PXDN*, *MMP1*, *PCDHB8*) (Fig. 4.15B). *FBLN1* codes for fibulin 1, an ECM component of blood vessel basement membrane. Fibulin 1 interaction with ADAMTS1 has been shown to exert anti-tumor effect in breast cancer[135]. *PXDN* codes for peroxidasin, an essential enzyme in the cross-linking of collagen IV in endothelial basement membrane[136]. *PCDHB8* codes for protocadherin beta 8, a member of a protocadherin family expressed predominantly in the nervous system during neuronal development[137]. Other protocadherin genes up-regulated in CHI3L1 KO were *PCDHB9*, *PCDHB14* and *PCDHB16*. Protocadherins have been suggested to act as tumor suppressors in multiple malignancies, including astrocytomas[138]. Reactome analysis of RNAseq data revealed two other classes of downregulated genes that have biological significance. Genes involved in PD-1 and IL-10 signaling have been downregulated in CHI3L1 KO cells. Numerous genes coding for HLA-DR, DQ were downregulated. *CSF1* coding for macrophage colony stimulating factor or *TGFB3* encoding transforming growth factor 3 were consistently downregulated in both clones (Fig. 4.15B).

Some of the genes determined as mesenchymal-associated in single-cell database[124]: *ANXA1*, *EFEMP1*, *SPP1*, *NPC2*, *TNFRSF1A*, appeared as most down-

regulated in CHI3L1 KO compared to WT cells (Fig. 4.15B). This suggests that CHI3L1 KO cells lost the mesenchymal transcriptomic prolife.

Altogether, functions of genes differentially expressed in CHI3L1 KO cells suggest reduced ECM reorganization capacity, less immunosuppressive genotype, and loss of the mesenchymal transcription profile of U87-MG glioma cells.

4.6 The impact of CHI3L1 depletion on tumor growth

To assess the impact of glioma-derived CHI3L1 depletion on tumor growth *in vivo*, human WT and CHI3L1 KO U87-MG-RFP glioma cells were implanted intracranially into athymic Foxn1^{nu} mice. Tumor volume was measured by endpoint head magnetic resonance imaging 21 days post implantation. Mice implanted with CHI3L1 KO cells developed significantly smaller tumors compared to WT controls. Depletion of CHI3L1 resulted in over 80% decrease in tumor volume (mean of WT=27.3 mm^3, mean of KO=5.3 mm^3; N=17) (Fig. 4.16A-B). In contrast to WT controls, mice bearing KO tumors have gained weight during the studied period, which is an indicator of a lesser tumor burden and smaller neurological deficits (Fig. 4.16C). Tumor volume and body mass of tumor-bearing animals showed a negative correlation (Fig. 4.16D).

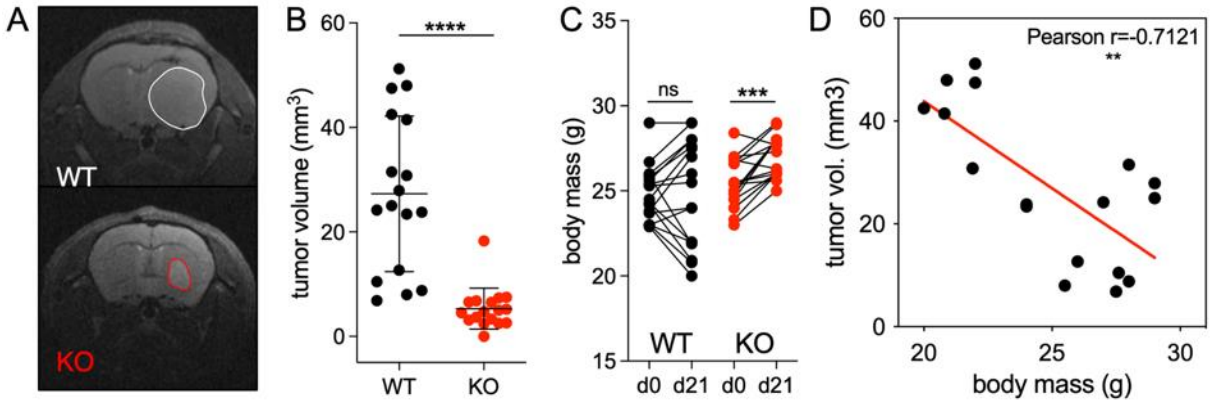

Figure 4.16. Depletion of CHI3L1 in U87-MG human glioblastoma cells reduces tumor growth in recipient mice. A-B. Measurement of tumor growth by magnetic resonance imaging (MRI) 21 days post orthotopic implantation of glioma cells to athymic mice. A. Representative head MRI scans showing tumor size reduction in CHI3L1 KO tumors compared to WT tumors. B. Quantification of tumor volume measurement; mean ± SD, n=17 per group; mean of WT=27.3 mm^3, mean of KO=5.3 mm^3; statistical analysis by parametric, unpaired t-test; **** P≤0.0001. C. Comparison of body mass of recipient mice between day 0 and day 21 post implantation in WT and CHI3L1 KO groups; n=17 per group; parametric,

paired t-test; *** P≤0.001. D. Scatter plot of tumor volume versus corresponding body mass in WT group showing a negative correlation between the two parameters.

4.6.1 CHI3L1 concentration is augmented in blood serum of tumor–bearing mice

The concentration of mouse and human CHI3L1 was measured in the blood serum of WT and CHI3L1 KO tumor-bearing mice. As expected, human CHI3L1 (hCHI3L1) was detected only in the blood of mice bearing WT tumors while the level of hCHI3L1 was very low in mice bearing CHI3L1 KO tumors, and undetectable in the serum of naive mice (Fig. 4.17A, left). A positive correlation (r=0.96) between hCHI3L1 serum level and tumor volume was found in the WT group (Fig. 4.17A, right). On the other hand, mouse CHI3L1 (mCHI3L1) was detectable in the serum of naive mice and increased in mice bearing WT tumors but not CHI3L1 KO tumors (Fig. 4.17B, left). However, no correlation was discovered between stroma-derived CHI3L1 and tumor volume (Fig. 4.17B, right).

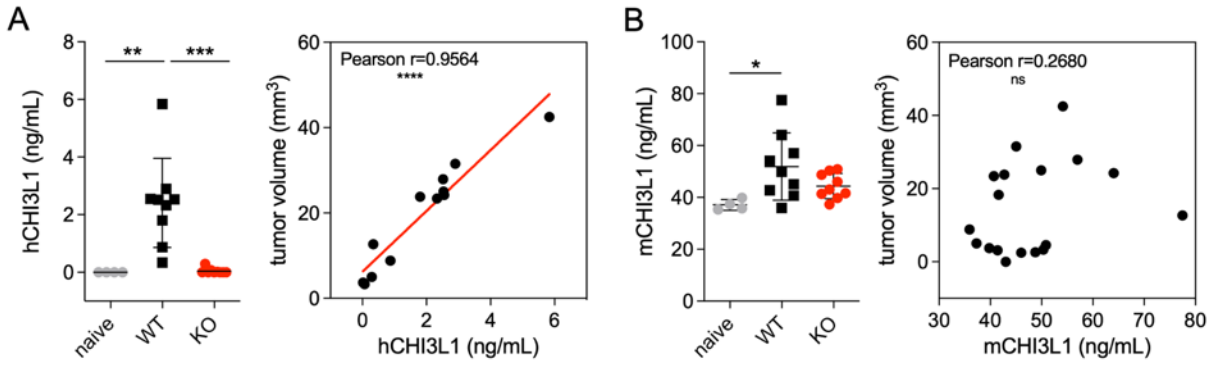

Figure 4.17. Serum concentration of glioma-derived CHI3L1 correlates positively with the tumor volume. A-B. Measurement of concentration of human and mouse CHI3L1 in blood serum of tumor-bearing mice and a correlative analysis with the tumor volume; mean ± SD is presented, n=4 for naïve, n=9 for other groups; parametric, unpaired t-test; * P≤0.05, ** P≤0.01, *** P≤0.001; linear regression line in red.

4.7 The determination of the mechanisms of reduced growth of CHI3L1 KO tumors

Several mechanisms underlying the reduced growth CHI3L1 KO tumors were verified experimentally based on the results of gene expression analysis and well-established features of glioblastoma pathology. Three main aspects were considered:

ECM degradation capacity via metalloproteinases, myeloid cell infiltration and vascular network features.

4.7.1 CHI3L1 KO cells have reduced ECM degradation capacity

The gene expression analysis performed on WT or CHI3L1 depleted U87-MG cells demonstrated a reduced expression of genes coding for metalloproteinases (*MMP2*, *MMP24*), involved in ECM remodeling (Fig. 4.18A). To validate this finding, a gelatin zymography assay that measures the proteolytic gelatinase activity in conditioned media was employed. A significantly lower gelatinolytic activity of MMP-2 was detected in CHI3L1 KO1 glioma cells when compared to wild-type cells. Similar, but non-significant, reduction was noticed in CHI3L1 KO2 cells (Fig. 4.18B).

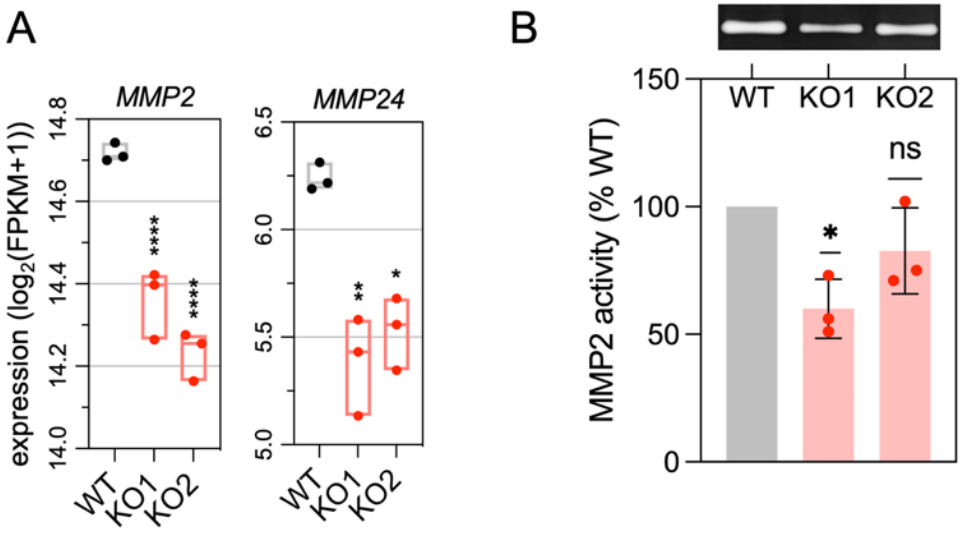

Figure 4.18. Reduced MMP expression and invasiveness of CHI3L1 KO glioma cells. A. Boxplots of *MMP2* and *MMP24* expression in CHI3L1 KO clones compared to WT control in the RNA-seq analysis; * Padj≤0.05, ** Padj≤0.01, **** Padj≤0.0001. B. The gelatinolytic activity in the U87-conditioned medium measured using gelatin zymography. Upper panel shows representative bands on the electrophoretic gel corresponding to the gelatinase activity. Lower panel shows the quantification of three biological repeats; data are shown as mean ± SD; statistical analysis with one-sample t-test with a hypothetical value of 100%; * P≤0.05.

It has been demonstrated that glioma invasion is strongly enhanced by microglial cells as those cells produce membrane type 1 metalloproteinase (MT1-MMP), an enzyme activating MMP-2[77,139,140]. Therefore, the invasiveness of WT and CHI3L1 KO1 glioma cells in the presence or absence of human microglial HM-SV40 cells (SV40 immortalized microglial cells) was determined using a matrigel assay. The

presence of HM-SV40 microglial cells strongly enhanced the tumor cell invasion in WT cells. A significant decrease in the invasion of CHI3L1 KO cells was found (Fig. 4.19).

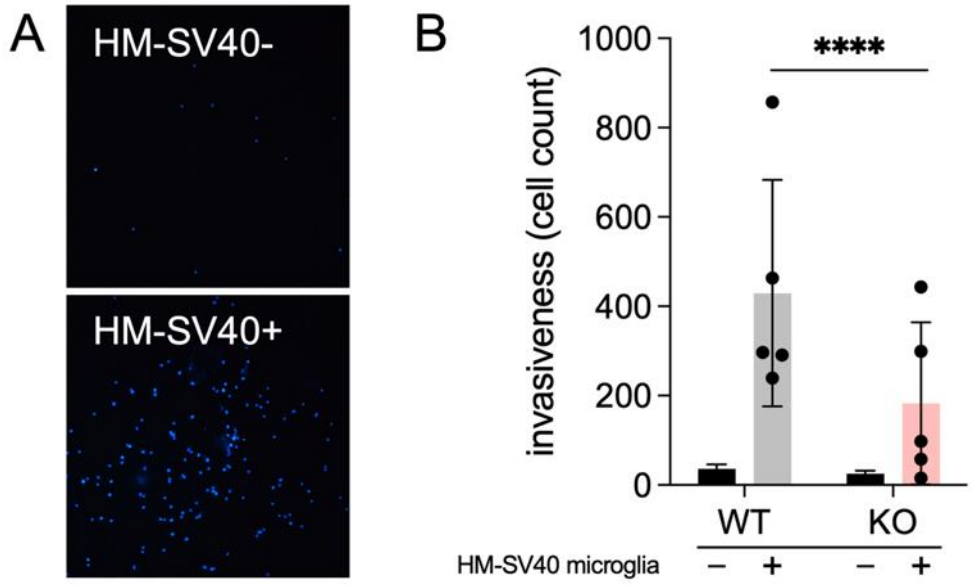

Figure 4.19. Reduced microglia-dependent invasion of CHI3L1 KO cells. A. Representative microscopy images of porous membranes with U87-MG cell nuclei stained with DAPI after 18 h incubation without (upper image) or with HM-SV40 microglia cells (lower image). **B.** Quantification of Matrigel invasion assay. Black bars represent the baseline invasiveness of glioma cells; grey and red dots/bars represent the invasiveness of WT and CHI3L1 KO cells when co-cultured with HM-SV40 human microglial cells; mean ± SD is presented; chi-squared test; odds ratio=2.37; **** P≤0.0001.

Altogether, the presented data demonstrate the crucial role of CHI3L1 in the enhanced remodeling of local ECM via regulation of MMP-2 activity.

4.7.2 Myeloid cells infiltration is reduced in CHI3L1 KO tumors

The immune cell landscape in malignant gliomas is dominated by myeloid cells, mostly monocytes, monocyte-derived macrophages, dendritic cells, and brain resident microglia[81,141]. These cells have been shown to drive GBM immunosuppression and resistance to therapy[142]. The important role of tumor-derived SPP1 (secreted phosphoprotein 1/osteopontin) as one of the main attractants of myeloid cells in GBM was previously reported[139]. The expression of *SPP1,* which was high in U87-MG glioma cells, was significantly down-regulated in CHI3L1 KO cells (Fig. 4.20A). The results were corroborated by the SPP1-specific ELISA showing a significant decrease of SPP1 concentration in conditioned media collected from both CHI3L1 KO cell

cultures compared to WT cells (Fig. 4.20B). Subsequently, the infiltration of myeloid cells in intracranial gliomas was determined by detecting IBA1 positive (IBA1+) cells in sections from tumor-bearing brains. A significant decrease in the density of IBA1+ cells was detected in CHI3L1 KO tumors compared to WT gliomas (Fig. 4.20C-D).

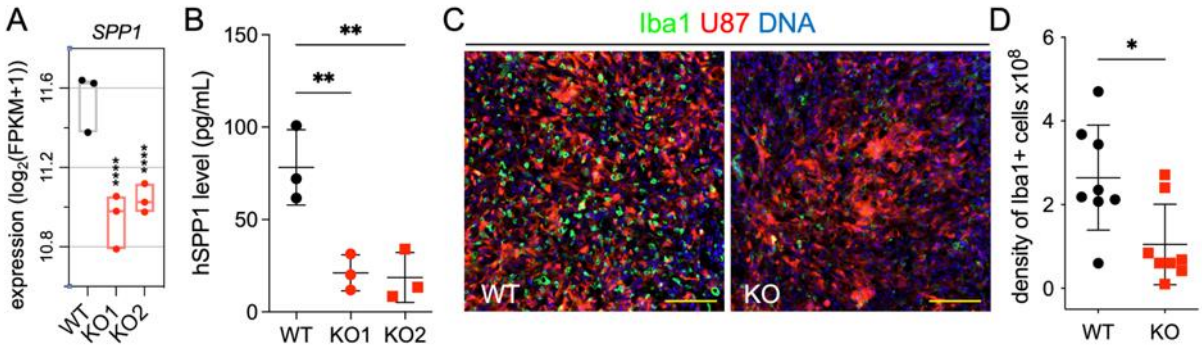

Figure 4.20. Reduced SPP1 levels are associated with lessened myeloid cell infiltration into CHI3L1 KO tumors. A. A boxplot of *SPP1* expression in CHI3L1 KO cells compared to WT controls in the RNA-seq data; **** Padj≤0.0001. **B.** A measurement of SPP1 levels in U87-conditioned media from CHI3L1 KO cells compared to WT control cells. Cytokine concentration was normalized to the cell lysate proteins; unpaired, parametric t-test; ** P≤0.01, n=3. **C.** An immunofluorescent staining of a pan-myeloid cell marker Iba1 (green) in the U87-MG gliomas in athymic mice. Scale bar represents 150 µm. **D.** The quantification of IBA1 immunostaining in tumor-bearing brain sections; unpaired, parametric t-test; ** P≤0.01, n=8.

Overall, these results demonstrate two mechanisms through which CHI3L1 depletion may result in the reduced glioma growth: one involving reduced MMP-2 expression/activity leading to diminished ECM degradation and reduced glioma cell invasion and the second one involving a decrease in the tumor-derived SPP1 production which results in reduced myeloid cell infiltration.

4.7.3 The impact of CHI3L1 depletion on the glioma vasculature

GBM is one of the most highly vascularized solid tumors. The tumor uses an extensive network of aberrant blood vessels to support heightened demands for nutrients and oxygen. One of the characteristics of the GBM vessel network is the extensive proliferation of microvessels[143], which leads to a high microvessel density (MVD). While the potential role of CHI3L1 in promoting glioblastoma neoangiogenesis has been proposed, direct evidence on the mechanisms underpinning the CHI3L1-dependent organization of the glioma vascular network is lacking.

The vasculature of WT and CHI3L1 KO U87-MG tumors was compared using immunofluorescent staining for von Willebrand Factor (vWF), a marker of activated endothelium (Fig. 4.21A). The gross vasculature differed considerably in WT and CHI3L1 KO tumors. The quantification of vessels number and microvessel density shows an increased number of larger vessels in CHI3L1 KO tumors and reduced microvessel density (Fig. 4.21B-C).

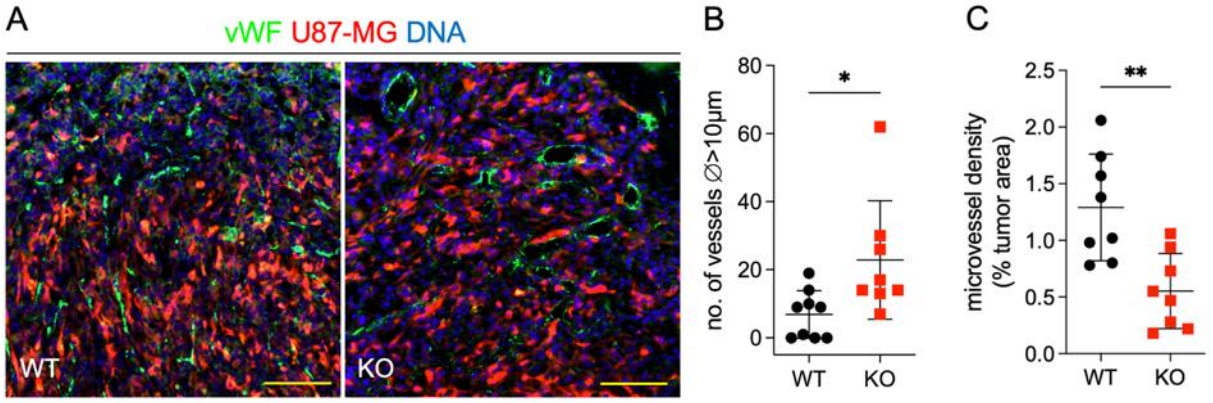

Figure 4.21. Changes in vessel number and microvessel density in CHI3L1 KO tumors. An immunofluorescence staining for the von Willebrand Factor (vWF) in WT and CHI3L1 KO tumors. A. Representative images for WT and CHI3L1 KO tumors. Color code indicated above the images. Scale bar represents 150 µm. B-C. The quantification of non-capillary vessels (⌀ >10 µm) (B) and microvessel density (C) based on the vWF staining. Mean ± SD is shown; data were analyzed with the unpaired, parametric t-test; * P≤0.05, ** P ≤0.01.

The number of vessels and microvessel density did not correlate with the tumor volume in either group (Fig. 4.22), suggesting that the increase in non-capillary vessels in CHI3L1 KO tumors was not due to their smaller volume but a result of CHI3L1 depletion. This is also depicted in representative scale-matched whole-tumor images in Fig. 4.23.

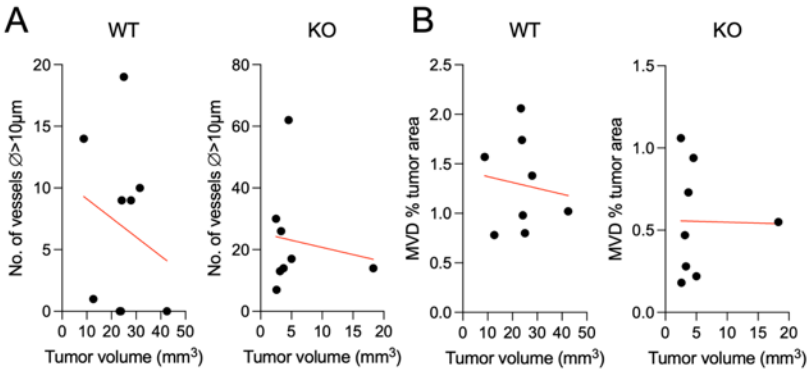

Figure 4.22. A linear regression analysis for number of non-capillary vessels (A) and microvessel density (B) and tumor volume. No correlations were found.

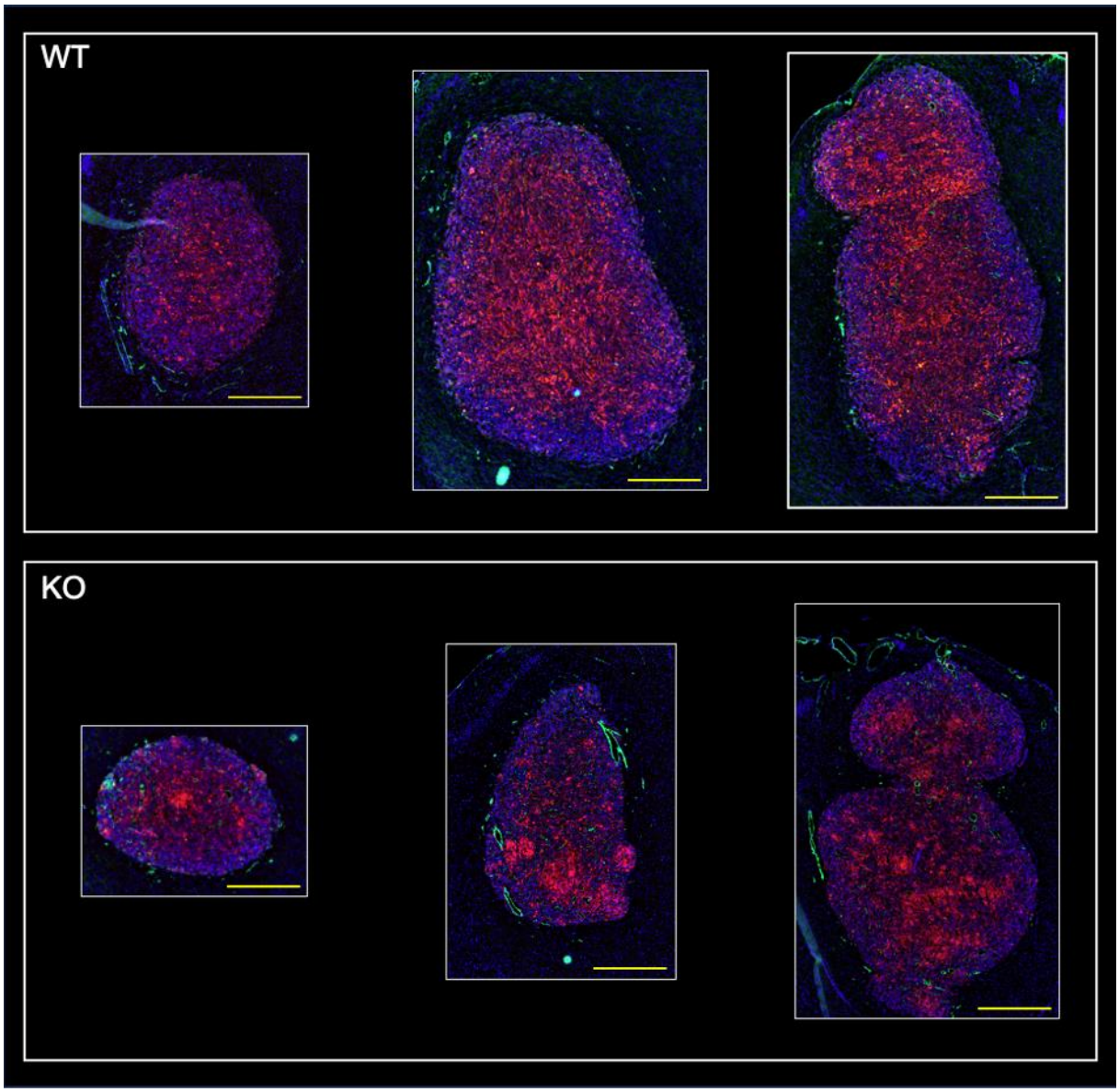

Figure 4.23. Representative immunofluorescence microscopy images for the von Willebrand factor staining. Upper and lower panels depict WT and CHI3L1 KO tumors, respectively. Specimen were chosen to show three different tumor section areas. Red: U87-MG-RFP, blue: DAPI (DNA), green: von Willebrand factor. Scale bars represent 500 µm. Size ratios between specimen are matching.

To determine if CHI3L1 contributes to the aberrant network of capillary vessels in glioblastoma, the structure of the blood vessel walls was examined. It was hypothesized that the depletion of CHI3L1 should result in a normalization of the vessel structure. Tumor sections were stained for laminin, an endothelium basement

membrane marker (Fig. 4.24A). In CHI3L1 KO gliomas both capillary and non-capillary blood vessels were continuously lined with laminin in contrast to WT tumors and there was a significant increase in laminin signal in CHI3L1 KO gliomas compared to WT (Fig. 4.24B).

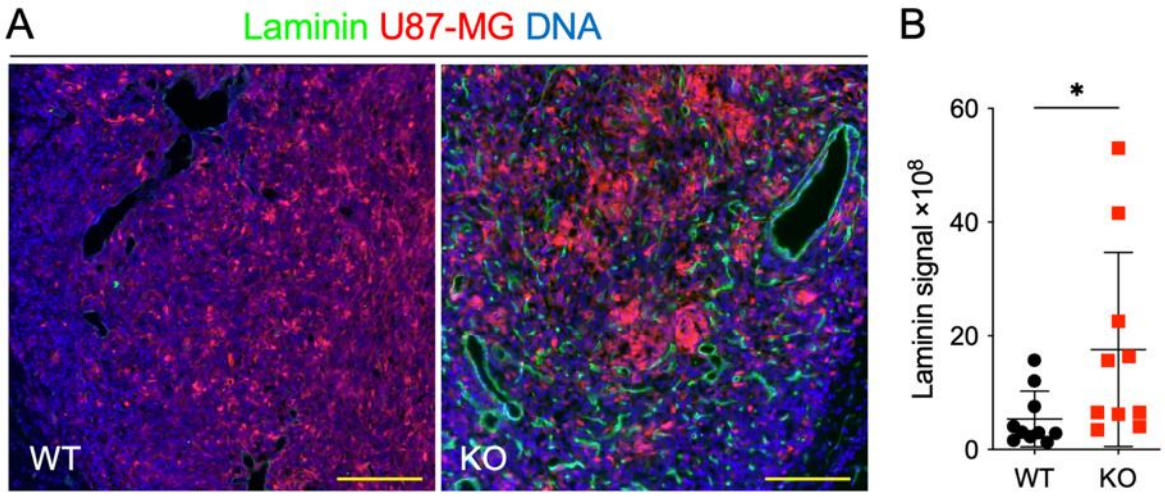

Figure 4.24. The detection of laminin at the endothelial basement membrane. A. Representative immunofluorescence images for WT and CHI3L1 KO tumors. Color code indicated above the images. Scale bar represents 300 μm. B. The quantification of laminin signal; mean ± SD is shown; unpaired, parametric t-test; * P≤0.05.

The integrity of morphologically abnormal vessels was also assessed using CD31 staining and 3D rendering. The CD31+ vessels formed continuous tubes in CHI3L1 KO tumors compared to those in WT (Fig. 4.25). These findings show that in the absence of tumor-derived CHI3L1, blood vessels are better structured and probably more functional.

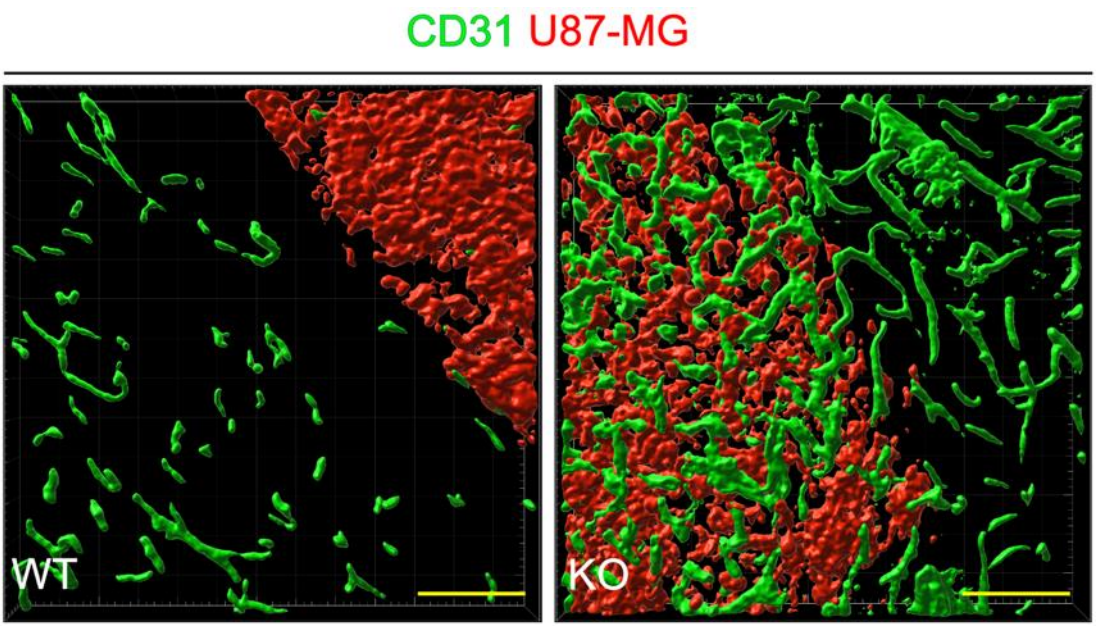

Figure 4.25. An analysis of vessel integrity. The 3D rendering of CD31 immunofluorescence staining images in Imaris software has been applied. Color code indicated above the images. Scale bar represents 150 µm.

An important property of cerebral blood vessels is their coverage by astrocytic endfeet. Astrocytes contribute to the blood-brain barrier by releasing factors that seal endothelial cell junctions and controlling the intake of nutrients from circulation[144]. Astrocytes are responsible for clearing waste and excess of extracellular fluid *via* perivascular space[145]. One of the crucial molecules involved in the latter function is an astrocytic water channel aquaporin 4 (AQP4), localized at the astrocytic endfeet that covers cerebral blood vessels and controls the volume of interstitial fluid.

The expression of AQP4 was found to be very low in U87-MG gliomas but strongly increased in the absence of CHI3L1 (Fig. 4.26A-B). A linear regression analysis for the expression of CHI3L1 and AQP4 at a protein level on data from BPA database was performed. A statistically significant negative correlation between the two proteins was found (Fig. 4.26C). Reduced staining for astrocytic marker glial fibrillary acidic protein (GFAP) demonstrates that astrocytes were less activated in CHI3L1 KO tumors in comparison to WT controls (Fig. 4.26D-E). The association of AQP4 with the astrocytic endfeet was confirmed by double staining for AQP4 and GFAP. Aquaporin 4 was localized at the GFAP+ cell protrusions covering blood vessels (Fig. 4.26F).

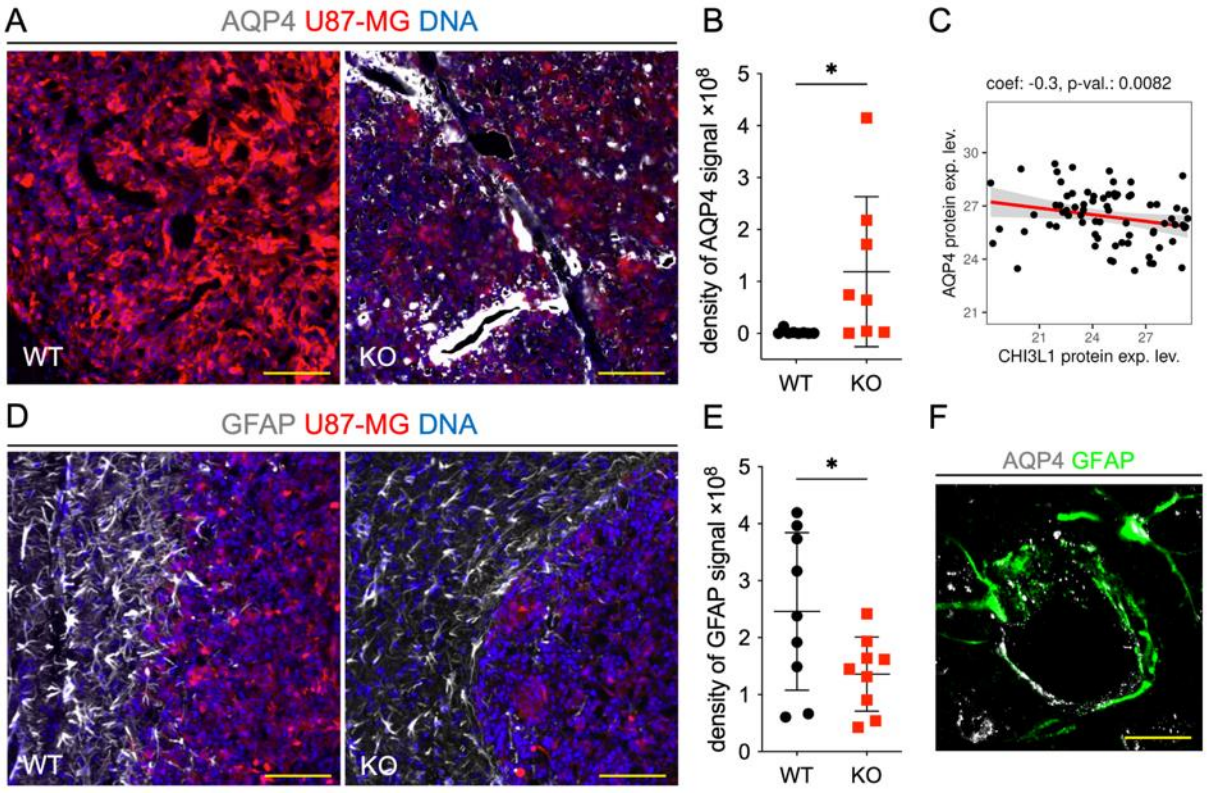

Figure 4.26. Immunofluorescence microscopy images show the localization of AQP4 and GFAP. A, D. The representative images of AQP4 (A) and GFAP (D) staining for WT and CHI3L1 KO tumors. Color code indicated above the images. Scale bar represents 150 µm. **B, E.** The quantification of AQP4 (B) and GFAP (E) signal based on respective staining shown in A and D. Mean ± SD is shown; unpaired, parametric t-test; * P≤0.05. **C.** A linear regression analysis of CHI3L1 and AQP4 protein expression in the Brain Protein Atlas: proteomic data from patient GBM samples. **F.** A co-staining of AQP4 (in light gray) and GFAP (in green) immunofluorescent staining at confocal resolution. Astrocytic endfeet around a blood vessel are captured. Scale bar represents 50 µm.

The impact of CHI3L1 on neoangiogenesis was associated with VEGF signaling[1,15,94]. Therefore, available databases and experimental resources were explored for the association between VEGF and CHI3L1. A positive correlation for VEGFA and CHI3L1 was found in the Ivy GAP database[121] (Fig. 4.27A). Moreover, the concentrations of mVEGF and mCHI3L1 in the blood of the tumor-bearing mice showed a positive correlation in CHI3L1 KO group (Fig. 4.27B).

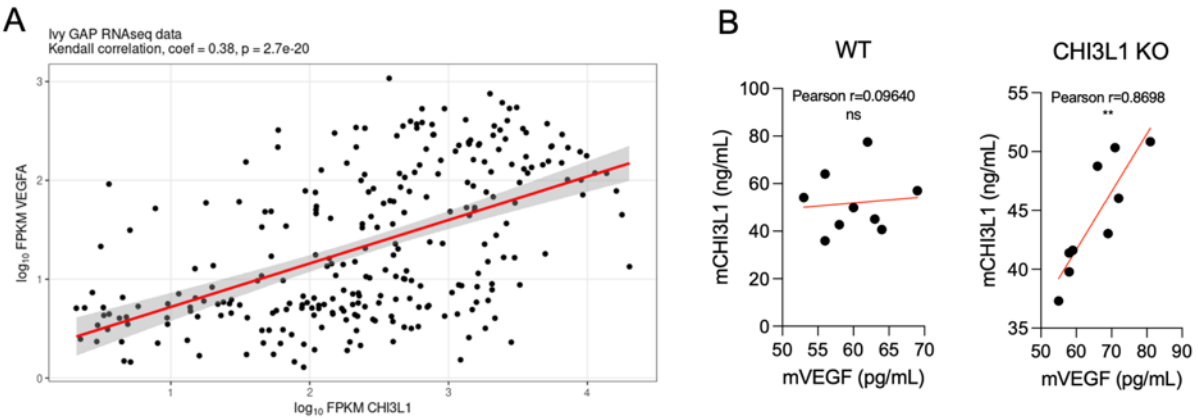

Figure 4.27. Correlation analysis for VEGFA and CHI3L1. A. A linear regression analysis of *VEGFA* and *CHI3L1* expression in Ivy GAP RNAseq database. B. A linear regression analysis of mVEGF and mCHI3L1 concentrations in the sera of tumor-bearing mice determined by ELISA.

The presented results show that CHI3L1 promotes the deregulation of the vascular network in glioma by increasing the number of endothelial sprouts, altering the structure of vascular walls, decreasing the coverage of blood vessels by astrocytes, and thus disrupting the perivascular space.

5. Discussion

In the presented thesis, the expression, and roles of CHI3L1 in gliomas have been addressed based on the exploration of new single-cell databases, two Polish glioma patient cohorts and multiple cell lines. Using genetically engineered human glioma cells and an orthotopic mouse model, it has been shown that CHI3L1-deficient gliomas establish considerably smaller tumors compared to wild-type controls. Several mechanisms through which CHI3L1 influences tumor growth have been highlighted: the rearrangement of ECM, the induction of glioma invasiveness, the stimulation of myeloid cells infiltration and the enhanced neoangiogenesis. It has been shown that blood vessels in tumors established with CHI3L1-deficient cells have larger diameter, thicker walls lined with laminin and normalized perivascular space with the high expression of AQP4 in astrocytic endfeet when compared to wild-type controls.

5.1 The overexpression of *CHI3L1* in high- and low-grade gliomas

Several reports based on gene microarrays[105] and bulk RNA sequencing[107] demonstrated the overexpression of *CHI3L1* in many human malignancies, including high grade gliomas[1]. Recently, many new databases have been published and made accessible, including ones integrating multiple previously published datasets or single-cell databases. These newly published databases have been explored to investigate CHI3L1 expression in a broader context and greater detail. The exploration of publicly available single-cell data shows that malignant cells are the predominant source of *CHI3L1* expression in GBMs. The expression of *CHI3L1* correlates positively with the MESlike1 signature which represents the mesenchymal gene expression profile of GBM, which is in line with previous findings[107]. Moreover, a positive correlation was found between genes listed in the MESlike1 signature and the CHI3L1 protein in the Brain Protein Atlas, which further strengthens the link between CHI3L1 and the mesenchymal phenotype of GBM which is the most aggressive, invasive, and immunosuppressive primary brain tumor in adults.

In a recently published study, Guetta-Terrier and colleagues[146] report that CHI3L1 is not only associated with the mesenchymal signature but is a driver of the mesenchymal phenotype of glioma stem cells (GCS). This is also in line with the

obtained RNAseq results where genes associated with the mesenchymal subtype are among the most down-regulated DEGs along with *CHI3L1* in CHI3L1 KO glioma cells (Fig. 4.15). U87-MG glioma cells used in this study have been shown as being a rich source of GSCs[147].

In the studied glioma cohorts, an increased expression of *CHI3L1* was found in both GBM and, unexpectedly, in pilocytic astrocytomas (PAs) which are benign, non-invasive brain tumors[148]. The high level of *CHI3L1* mRNA in PA might not, however, be reflected at the protein level as low levels of CHI3L1 have been reported in PAs using protein detection assays[108]. CHI3L1 content was determined at mRNA and protein level in several glioma cell lines and human astrocytes. Interestingly, human astrocytes showed a level of *CHI3L1* mRNA comparable to U87-MG cells (Fig. 4.5A), but at the protein level they had much less CHI3L1 protein than U87-MG (Fig. 4.5B). These results, together with the results of *CHI3L1* overexpression in PAs, suggest that in high-grade gliomas *CHI3L1* mRNA is either more stable or more readily translated into protein. This might be due to the presence of mRNA-stabilizing protein HuR that is known to be up-regulated in cancer, including high-grade gliomas[149], and drives excessive protein synthesis.

5.2 The characteristics of glioma cells depleted of CHI3L1

CRISPR Cas9 mediated gene editing is currently the most effective, efficient, and accurate method of genome editing. It employs guide RNA (gRNA) that recognizes the target sequence in the gene of interest through a complementary base pair and CRISPR-associated (Cas-9) proteins that perform three steps: recognition, cleavage, and repair. The Cas-9 nuclease makes double-stranded breaks at a site 3 base pair upstream to protospacer adjacent motif, then the double-stranded break is repaired by either non-homologous end joining or homology-directed repair cellular mechanisms.

A validated set of two gRNAs and a Cas9 carrying vector were used in this study. The generated cell lines were grown and clones with the lowest CHI3L1 were selected through several rounds of protein testing by ELISA and qPCR. The cells transfected with specific and control gRNAs had similar basic properties when compared with parental cells. Cell morphology, MTT metabolism and proliferation were not

significantly affected by CRISPR Cas9 editing. The exogenous CHI3L1 did not change the proliferation rate of obtained cells suggesting that CHI3L1 does not regulate cell proliferation as an exogenous/extracellular factor.

5.3 The transcriptional changes in glioma cells depleted of CHI3L1

Transcriptomic analysis allows for the determination of global changes ongoing in cells devoid of a specific gene. It helps to identify the important pathways affected and provide signaling hubs for further validation. Performing transcriptomic analysis of parental and CHI3L1 KO followed by the comparative analysis allowed identification of the genes affected by CHI3L1 depletion. The genes affected in the similar manner in both KO cell lines were focused on. Differential gene expression analysis of the WT and CHI3L1 KO cells showed that genes up-regulated in CHI3L1 KO cells were associated with formation of ECM, and cell-to-cell adhesion. A substantial number of genes down-regulated in CHI3L1 KO cells belongs to the ECM organization category, which suggests that glioma cells depleted of CHI3L1 might exhibit a decreased ability to reorganize the ECM and become less invasive. Two other classes of reported DEGs were considered biologically important. Genes associated with PD-1 and IL-10 signaling were down-regulated in CHI3L1 KO cells, including genes coding for HLA-DR, DQ proteins and immunomodulating cytokines such as CSF1, CCL2 and TGFB3. CSF1 and CCL2 are crucial cytokines driving the accumulation of myeloid cells in glioblastoma[150] and TGFβ is a cytokine implicated in glioma invasion and immunosuppression[151,152]. The genes associated with the mesenchymal signature (*ANXA1*, *EFEMP1*, *SPP1*, *NPC2*, *TNFRSF1A*) from the single-cell human glioblastoma database[124] were strongly down-regulated in CHI3L1 KO cells.

Genes associated with “DNA replication” (*PCNA*, *NUP62* and *SUMO3)* were down-regulated in CHI3L1 KO cells but the proliferation rate of CHI3L1 KO cells was comparable with WT cells, thus the observed reduction of tumor growth was not a result of decreased cell proliferation of the CHI3L1 KO cells. To make sure CRISPR/Cas9 gene editing did not impact cell proliferation, three clones of U87-MG transfected with non-targeting control gRNA were tested in a proliferation assay and found to proliferate comparably as WT controls (Fig. 4.13D).

In the light of those results, it was concluded that CHI3L1, apart from being a member of mesenchymal signature, might be a potential positive regulator of some of the mesenchymal signature genes. The results also suggest that CHI3L1 KO cells become less invasive and immunosuppressive.

5.4 The mechanisms of the reduction of tumor volume in CHI3L1 depletion

The results obtained using magnetic resonance imaging demonstrated that the CHI3L1 KO cells formed significantly smaller tumors compared to WT cells, which indicates that CHI3L1 plays a role in tumor progression. The mice bearing CHI3L1 KO tumors gained body mass during the tumor growth period corroborating the observation that tumor progression was halted. This conclusion is in line with the results obtained by Chen *et al*.[153] showing the overexpression of CHI3L1 yielded larger tumors in recipient mice. Several potential mechanisms that could be responsible for the impaired growth were verified, guided by the results of transcriptomic analyses.

MMP-2 is a crucial ECM degrading enzyme that is produced by glioma cells and activated through interactions with MMP-14 (also known as MT1-MMP) expressed on activated microglia[77]. The reduced *MMP2* expression in CHI3L1 KO cells resulting in reduced invasiveness was corroborated by functional assays: gelatin zymography and matrigel invasion assays. CHI3L1 KO1 cells exhibited a reduced proteolytic and invasive activity compared to WT cells. The CHI3L1 KO2 cells showed a weaker, but statistically insignificant, reduction of the gelatinolytic activity than WT cells, likely due to the remaining production of CHI3L1 in those cells (Fig. 4.12B) or differences in DEGs between CHI3L1 KO1 and KO2 (Fig. 4.14A). These results demonstrate that CHI3L1 has a profound impact on the neoplastic outgrowth. The results are in line with the report of Ku *et al*.[110] who showed that a transient silencing of CHI3L1 in U87-MG cells results in a decreased MMP-2 production and lowered gelatinolytic activity of these cells *in vitro*. The integrity of these results is an important validation of a successful knock-out of *CHI3L1* with CRISPR/Cas9 technology in the cells used for the presented study. Lee and colleagues[60] showed that a pharmacological blockade of CHI3L1 reduces the number and size of lung metastases of melanoma and lung cancer, and diminishes the level of several proteins in those metastases including

MMP-2 and MMP-9. Scully and colleagues[58] showed that CHI3L1 induces MMP-9 levels in mammary epithelium *in vitro*, which was impeded by the addition of CHI3L1-neutralizing antibody. These reports show that CHI3L1-MMP link is not glioma-specific but is a biological phenomenon applicable to other malignancies. It is also a proof that CHI3L1 can be pharmacologically blocked *in vivo*, resulting in changes congruent with *in vitro* data. This shows that MMP expression might be dependent on CHI3L1 signaling, however, more mechanistic research needs to be done to pinpoint underlaying regulatory pathways.

Certain matrix metalloproteinases play a key role in the mechanisms of glioblastoma invasion[154,155]. These enzymes are involved in the degradation and remodeling of ECM but also contribute to the overall pathology by cleaving and activating/deactivating cytokines, chemokines, and growth factors[156]. Accumulated evidence shows that lowering MMP activity in glioblastoma TME would be a desirable outcome in the GBM therapy, however, clinical trials with the MMP inhibitor marimastat in the 2000s failed to yield any survival benefits for GBM patients[157]. Recently, new insights into the MMP role in health and disease have been highlighted: the non-enzymatic signaling function that these proteins exert in the cytoplasm and cell nucleus[158,159]. It is possible that previous attempts of interfering with MMPs activity in GBM did not consider the intracellular functions of MMPs, and that perhaps, the topic of targeting MMPs in GBM is not exhausted. Assuming that CHI3L1 is regulating the expression of certain MMPs, the blockade of CHI3L1 in TME might improve the outcomes of anti-GBM therapy.

CHI3L1 KO cells exhibited a diminished expression/production of SPP1 (osteopontin), a well-established multifunctional protein associated with the regulation of tumor invasion and immunosuppression in GBM[139,147]. The accumulation of myeloid cells in CHI3L1 KO tumors was diminished compared to tumors in the WT group (Fig. 4.20), which was attributed to the lower concentration of tumor-derived SPP1 in TME. There are a few reports exploring the CHI3L1-SPP1 link in GBM or other pathologies. These proteins are often reported together as reliable prognostic/diagnostic biomarkers (or combined biomarker scores) in astrocytomas[160], cancer[161], neurodegenerative diseases[22–24], neuroinflammation[26–29] or other inflammatory diseases[162], but the mechanical basis of this association is unknown. Urakami and

colleagues[163] reported that CHI3L1 and SPP1 are signaling through a mutual integrin β4-p70S6K axis in macrophages in esophageal squamous cell carcinoma, but the common regulation mechanisms of these two proteins remain unspecified. Given the reported role of CHI3L1 as a driver of GSC stemness[146], it is likely that the expression of other genes known to be involved in this process such as *SPP1* is down-regulated when *CHI3L1* is silenced. This conclusion is also in line with the fact that SPP1 is associated with the mesenchymal signature in large scale gene expression studies[124] along with CHI3L1. Moreover, Kijewska and colleagues[147] reported an important role of tumor derived SPP1 in the maintenance and self-renewal of human and rat GSCs.

A substantial increase of the serum mCHI3L1 levels was detected in mice bearing WT tumors (Fig. 4.17B, left) – an increase that can be associated with the response of the tumor microenvironment i.e., astrocytes, pericytes, endothelium, accumulated macrophages. Interestingly, the level of mCHI3L1 decreased in mice bearing CHI3L1 KO tumors but the difference was not significant in comparison to neither naïve nor the WT group (Fig. 4.17B, left). This suggests that growing tumors stimulate the TME to release CHI3L1 in the presence of glioma-derived CHI3L1 but when the glioma-derived CHI3L1 is absent, the TME ceases to respond this way. No correlation between TME-derived CHI3L1 and tumor volume was detected (Fig. 4.17B, right), which implies that the microenvironment response to a growing tumor is not linear in terms of CHI3L1 release and may be dependent on other, unidentified factors. These results suggest that either tumor growth is dependent predominantly on the glioma-derived CHI3L1, which suggests autocrine signaling of CHI3L1 in glioma cells, or that human glioma cells do not respond to mouse CHI3L1 as they respond to a human counterpart. However, the addition of exogenous CHI3L1 did not modulate WT and CHI3L1 KO cell proliferation, so there is no evidence of autocrine signaling via CHI3L1 in glioma cells.

Serum levels of hCHI3L1 were substantially heightened in mice bearing WT tumors and reduced to the level of naïve mice in mice bearing CHI3L1 KO tumors (Fig. 4.17A, left). Serum hCHI3L1 correlated positively with the tumor volume in the WT group (Fig. 4.17A, right) indicating the supportive role of the tumor derived protein in glioma growth. This result shows also that CHI3L1 readily enters circulation and can be used to assess the tumor burden in mice.

5.5 The normalization of blood vessel network in tumors depleted of CHI3L1

The presence of aberrant vasculature is a fundamental hallmark of GBM pathology. Abnormal blood vessels in GBM impede delivery of nutrients, oxygen, drugs, and effector immune cells. The organization of blood vessels is disrupted, which leads to the formation of abnormal vessels that are leaky, collapsed, and disorganized. This contributes to hypoxia and immune suppression, alters tumor metabolism and creates a specific TME[94–96]. The perivascular space is also disrupted by the displacement of astrocytes by glioblastoma cells and accumulation of macromolecules and an excessive extravascular fluid, which leads to an enhanced permeability and retention (EPR) effect[100]. The increased permeability of blood-tumor barrier (BTB) does not however facilitate the delivery of therapeutics to a GBM tumor. On the contrary, the delivery of drugs to tumors remains a key challenge in the treatment of GBM[101]. Therefore, normalization of GBM vasculature is highly desirable for effective anti-tumor activity.

Several previous studies reported on the impact of CHI3L1 on vasculature in GBMs based on *in vitro* studies of tube formation assays with human umbilical vein cord (HUVEC) or extracranial mouse models[15,111,164]. In the intracranial orthotopic model presented here, tumors depleted of glioma-derived CHI3L1 exhibited features of normalized vasculature and vessel lining, along with AQP4 localized to the astrocytic endfeet surrounding the vessels. The role of AQP4 and glymphatic system in the pathology of gliomas is double-edged. On the one hand, the disruption of the glymphatic system and the loss of polarization of AQP4 at the astrocytic endfeet around blood vessels contributes to the retention of glioma-derived metabolites and signaling molecules in the TME[165], which contributes to the pathology. On the other hand, however, the excess of perivascular AQP4 has been considered a causative of CNS edema in various neuropathologies and the peritumoral brain edema in gliomas[165–167]. The overall contribution of AQP4 to the glioma TME depends probably on the structure and function the vascular network: the degree of leakiness of the vessels, the degree of disruption of the vascular blood flow and/or the level of microvascular density. If these parameters are heightened, the drainage of the excess of peritumoral fluids is perhaps necessary. However, when there is an excess of AQP4,

especially if it is localized to glioma cells (and not astrocytes), it might contribute to aberrant water flow in the brain and result in peritumoral edema.

In the Figure 4.28 a proposed model of the brain vasculature and perivascular space in CHI3L1 depleted gliomas is presented.

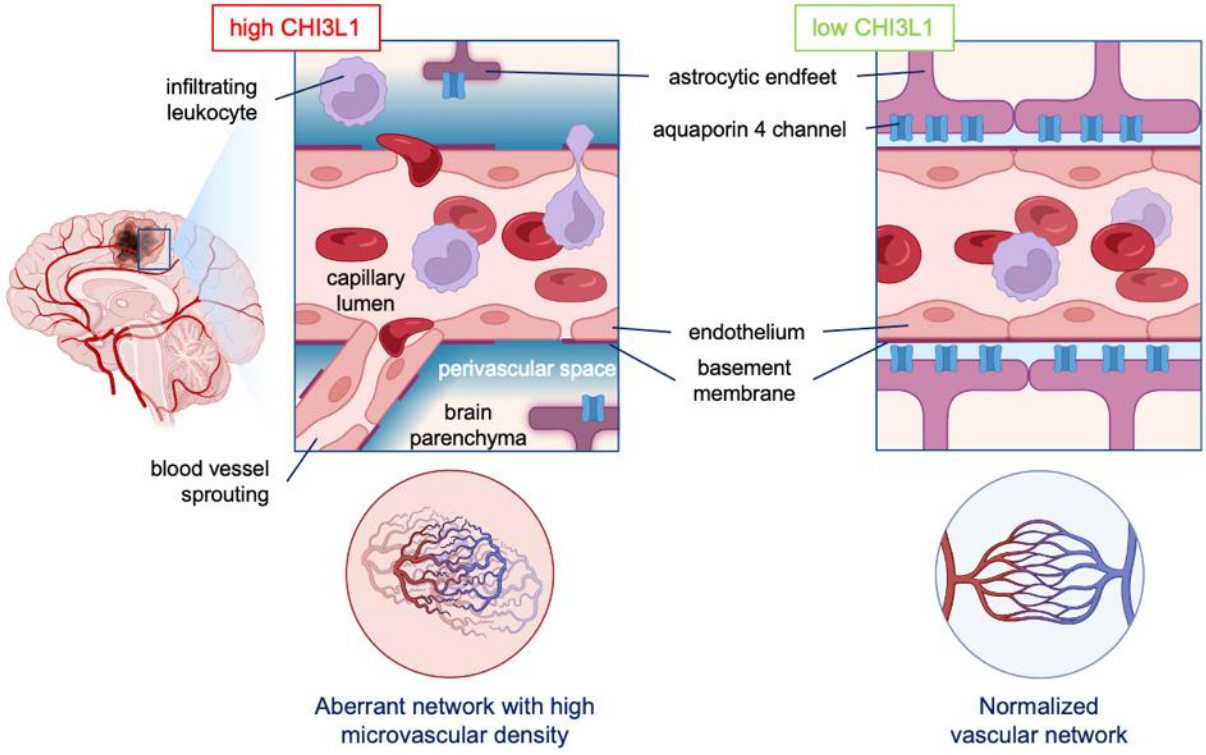

Figure 4.28. A proposed model of the brain vasculature and perivascular space in CHI3L1 depleted gliomas.

In tumors with high CHI3L1 production the number of large vessels decreases and the expanse of microvessels forming disorganized vascular network increases. The vascular laminar basement membrane is fenestrated and thin. The aberrant vessels may facilitate the penetration of myeloid cells from the periphery. The blood-brain barrier is disrupted: astrocytes retract from vessels and the perivascular space is not sealed by astrocytic endfeet with a crucial water channel AQP4. In CHI3L1 KO gliomas, the vascular network is normalized, less leaky and more efficient in carrying blood flow. Endothelial basement membrane is well structured and thick. The number of activated astrocytes is reduced, an astrocytic endfeet covers the blood vessels and seals the perivascular space. AQP4 in the astrocytic endfeet facilitates clearance of harmful substances and water excess from the perivascular space.

In previous studies, CHI3L1 impact on neoangiogenesis was associated with VEGF signaling[1,94,164]. A positive correlation for VEGFA and CHI3L1 was found in the Ivy GAP RNAseq database[121] (Fig. 4.27A). Moreover, a positive correlation for mVEGF and mCHI3L1 concentration was detected in blood sera of tumor-bearing mice, but only in the CHI3L1 KO group (Fig. 4.27B). Neoangiogenesis is controlled by a balance of pro- and anti-angiogenic factors. It is likely that CHI3L1 and VEGF impact neoangiogenesis as pro-angiogenic factors synergistically, however, the exact interplay between CHI3L1 and VEGF is more complex and remains elusive.

6. Conclusions

In this PhD thesis I presented a set of experiments exploring expression patterns of CHI3L1 in human gliomas and its role in driving progression of malignant gliomas.

The specific aims of this study were achieved, and the following conclusions have been reached:

1. While *CHI3L1* mRNA levels were high in benign and malignant human gliomas, the CHI3L1 protein levels were upregulated only in malignant tumors and high-grade glioma-derived cell lines.
2. CRISPR-Cas9 mediated CHI3L1 depletion does not change basal cellular behavior of cells but strongly modifies global gene transcription.
3. CHI3L1 depletion downregulates genes involved in ECM rearrangement, myeloid cell infiltration and immunosuppression.
4. CHI3L1 depletion in human glioma cells decreases tumor growth *in vivo*.

Inhibition of tumor growth in CHI3L1 KO tumors could result from reduced MMP-2 dependent invasion, diminished Spp1-driven myeloid cells infiltration/activation and a restoration of effective angiogenesis. Altogether, the results presented in this study indicate that CHI3L1 is an important therapeutic target in GBM, and the presented findings document speculated roles of CHI3L1 in driving or maintaining GBM progression. If CHI3L1 regulates many pathogenic proteins in GBM, such as MMP-2, SPP1 or AQP4, pharmacological blocking of CHI3L1 might yield multiple benefits in the anti-GBM therapy. However, more research must be conducted to test that hypothesis. Given the notorious resistance of GBM to therapies, it might be beneficial to combine anti-CHI3L1 drugs with other therapeutic approaches, such as immunotherapy, to maximize the outcomes.

7. References

1. Zhao, T., Su, Z., Li, Y., Zhang, X. & You, Q. Chitinase-3 like-protein-1 function and its role in diseases. *Signal Transduct. Target. Ther.* **5**, 201 (2020).

2. Ober, C. & Chupp, G. L. The chitinase and chitinase-like proteins: a review of genetic and functional studies in asthma and immune-mediated diseases. *Curr. Opin. Allergy Clin. Immunol.* **9**, 401–408 (2009).

3. Bussink, A. P., Speijer, D., Aerts, J. M. F. G. & Boot, R. G. Evolution of Mammalian Chitinase(-Like) Members of Family 18 Glycosyl Hydrolases. *Genetics* **177**, 959–970 (2007).

4. Lee, C.-M. *et al.* IL-13Rα2 uses TMEM219 in chitinase 3-like-1-induced signalling and effector responses. *Nat. Commun.* **7**, 12752 (2016).

5. Pinteac, R., Montalban, X. & Comabella, M. Chitinases and chitinase-like proteins as biomarkers in neurologic disorders. *Neurol. - Neuroimmunol. Neuroinflammation* **8**, e921 (2021).

6. Zhou, Y. *et al.* Galectin-3 Interacts with the CHI3L1 Axis and Contributes to Hermansky–Pudlak Syndrome Lung Disease. *J. Immunol.* **200**, 2140–2153 (2018).

7. Geng, B. *et al.* Chitinase 3-like 1-CD44 interaction promotes metastasis and epithelial-to-mesenchymal transition through β-catenin/Erk/Akt signaling in gastric cancer. *J. Exp. Clin. Cancer Res.* **37**, 208 (2018).

8. Kioi, M. *et al.* N-linked glycosylation of IL-13R0'2 is essential for optimal IL-13 inhibitory activity. *FASEB J.* **20**, 2378–2380 (2006).

9. He, C. H. *et al.* Chitinase 3-like 1 Regulates Cellular and Tissue Responses via IL-13 Receptor α2. *Cell Rep.* **4**, 830–841 (2013).

10. Coffman, F. D. Chitinase 3-Like-1 (CHI3L1): A Putative Disease Marker at the Interface of Proteomics and Glycomics. *Crit. Rev. Clin. Lab. Sci.* **45**, 531–562 (2008).

11. Kognole, A. A. & Payne, C. M. Inhibition of Mammalian Glycoprotein YKL-40. *J. Biol. Chem.* **292**, 2624–2636 (2017).

12. Iwata, T. *et al.* YKL-40 secreted from adipose tissue inhibits degradation of type I collagen. *Biochem. Biophys. Res. Commun.* **388**, 511–516 (2009).

13. Bigg, H. F., Wait, R., Rowan, A. D. & Cawston, T. E. The Mammalian Chitinase-like Lectin, YKL-40, Binds Specifically to Type I Collagen and Modulates the Rate of Type I Collagen Fibril Formation. *J. Biol. Chem.* **281**, 21082–21095 (2006).

14. Pouyafar, A., Heydarabad, M. Z., Mahboob, S., Mokhtarzadeh, A. & Rahbarghazi, R. Angiogenic potential of YKL-40 in the dynamics of tumor niche. *Biomed. Pharmacother.* **100**, 478–485 (2018).

15. Francescone, R. A. *et al.* Role of YKL-40 in the Angiogenesis, Radioresistance, and Progression of Glioblastoma. *J. Biol. Chem.* **286**, 15332–15343 (2011).

16. Libreros, S., Garcia-Areas, R. & Iragavarapu-Charyulu, V. CHI3L1 plays a role in cancer through enhanced production of pro-inflammatory/pro-tumorigenic and angiogenic factors. *Immunol. Res.* **57**, 99–105 (2013).

17. Rehli, M., Krause, S. W. & Andreesen, R. Molecular Characterization of the Gene for Human Cartilage gp-39 (CHI3L1), a Member of the Chitinase Protein Family and Marker for Late Stages of Macrophage Differentiation. *Genomics* **43**, 221–225 (1997).

18. Rehli, M. *et al.* Transcriptional Regulation of CHI3L1, a Marker Gene for Late Stages of Macrophage Differentiation. *J. Biol. Chem.* **278**, 44058–44067 (2003).

19. Craig-Schapiro, R. *et al.* YKL-40: A Novel Prognostic Fluid Biomarker for Preclinical Alzheimer's Disease. *Biol. Psychiatry* **68**, 903–912 (2010).

20. Malmeström, C. *et al.* CSF levels of YKL-40 are increased in MS and decrease with immunosuppressive treatment. *J. Neuroimmunol.* **269**, 87–89 (2014).

21. Llorens, F. *et al.* YKL-40 in the brain and cerebrospinal fluid of neurodegenerative dementias. *Mol. Neurodegener.* **12**, 83 (2017).

22. Paterson, R. W. *et al.* A targeted proteomic multiplex CSF assay identifies increased malate dehydrogenase and other neurodegenerative biomarkers in individuals with Alzheimer's disease pathology. *Transl. Psychiatry* **6**, e952–e952 (2016).

23. Zhou, M. *et al.* Targeted mass spectrometry to quantify brain-derived cerebrospinal fluid biomarkers in Alzheimer's disease. *Clin. Proteomics* **17**, 19 (2020).

24. Li, Y. *et al.* Identification of hub proteins in cerebrospinal fluid as potential biomarkers of Alzheimer's disease by integrated bioinformatics. *J. Neurol.* **270**, 1487–1500 (2023).

25. Lucchini, M. *et al.* CSF CXCL13 and Chitinase 3-like-1 Levels Predict Disease Course in Relapsing Multiple Sclerosis. *Mol. Neurobiol.* **60**, 36–50 (2023).

26. De Fino, C. *et al.* The predictive value of CSF multiple assay in multiple sclerosis: A single center experience. *Mult. Scler. Relat. Disord.* **35**, 176–181 (2019).

27. Oset, M. *et al.* Predictive value of brain atrophy, serum biomarkers and information processing speed for early disease progression in multiple sclerosis. *Front. Neurol.* **14**, 1223220 (2023).

28. Kim, J.-S. Protein biomarkers in multiple sclerosis. *encephalitis* **3**, 54–63 (2023).

29. Zhao, J. *et al.* Elevated CHI3L1 and OPN levels in patients with anti-N-methyl-d-aspartate receptor encephalitis. *J. Neuroimmunol.* **334**, 577005 (2019).

30. Yilmazer-Hanke, D. *et al.* Differential Glial Chitotriosidase 1 and Chitinase 3-like Protein 1 Expression in the Human Primary Visual Cortex and Cerebellum after Global Hypoxia-Ischemia. *Neuroscience* **506**, 91–113 (2022).

31. Lananna, B. V. *et al. Chi3l1* /YKL-40 is controlled by the astrocyte circadian clock and regulates neuroinflammation and Alzheimer's disease pathogenesis. *Sci. Transl. Med.* **12**, eaax3519 (2020).

32. Matute-Blanch, C. *et al.* Chitinase 3-like 1 is neurotoxic in primary cultured neurons. *Sci. Rep.* **10**, 7118 (2020).

33. Im, J. H. *et al.* Deletion of Chitinase-3-like 1 accelerates stroke development through enhancement of Neuroinflammation by STAT6-dependent M2 microglial inactivation in Chitinase-3-like 1 knockout mice. *Exp. Neurol.* **323**, 113082 (2020).

34. Verheijden, G. F. M. *et al.* Human cartilage glycoprotein-39 as a candidate autoantigen in rheumatoid arthritis. *Arthritis Rheum.* **40**, 1115–1125 (1997).

35. Morgante, M., Di Munno, O. & Morgante, D. [YKL 40: marker of disease activity in rheumatoid arthritis?]. *Minerva Med.* **90**, 437–441 (1999).

36. Johansen, J. S., Jensen, H. S. & Price, P. A. A NEW BIOCHEMICAL MARKER FOR JOINT INJURY. ANALYSIS OF YKL-40 IN SERUM AND SYNOVIAL FLUID. *Rheumatology* **32**, 949–955 (1993).

37. Moffatt, M. F. Genes in asthma: new genes and new ways. *Curr. Opin. Allergy Clin. Immunol.* **8**, 411–417 (2008).

38. Mizoguchi, E. & Mizoguchi, A. Is the sugar always sweet in intestinal inflammation? *Immunol. Res.* **37**, 47–60 (2007).

39. Vignon, É. Is glycoprotein YKL40 a new marker for joint disorders? *Joint Bone Spine* **68**, 454–456 (2001).

40. Mikuls, T. & Moreland, L. Predicting outcomes in early rheumatoid arthritis. *Curr. Rheumatol. Rep.* **4**, 193–194 (2002).

41. Rathcke, C. N. & Vestergaard, H. YKL-40, a new inflammatory marker with relation to insulin resistance and with a role in endothelial dysfunction and atherosclerosis. *Inflamm. Res.* **55**, 221–227 (2006).

42. Cintin, C. *et al.* Serum YKL-40 and colorectal cancer. *Br. J. Cancer* **79**, 1494–1499 (1999).

43. Eurich, K., Segawa, M., Toei-Shimizu, S. & Mizoguchi, E. Potential role of chitinase 3-like-1 in inflammationassociated carcinogenic changes of epithelial cells. *World J. Gastroenterol.* **15**, 5249 (2009).

44. Johansen, J. S., Jensen, B. V., Roslind, A., Nielsen, D. & Price, P. A. Serum YKL-40, A New Prognostic Biomarker in Cancer Patients? *Cancer Epidemiol. Biomarkers Prev.* **15**, 194–202 (2006).

45. Johansen, J. S. Studies on serum YKL-40 as a biomarker in diseases with inflammation, tissue remodelling, fibroses and cancer. *Dan. Med. Bull.* **53**, 172–209 (2006).

46. Johansen, J. S., Cintin, C., Jørgensen, M., Kamby, C. & Price, P. A. Serum YKL-40: A new potential marker of prognosis and location of métastases of patients with recurrent breast cancer. *Eur. J. Cancer* **31**, 1437–1442 (1995).

47. Tang, Z. *et al.* GEPIA: a web server for cancer and normal gene expression profiling and interactive analyses. *Nucleic Acids Res.* **45**, W98–W102 (2017).

48. Hakala, B. E., White, C. & Recklies, A. D. Human cartilage gp-39, a major secretory product of articular chondrocytes and synovial cells, is a mammalian member of a chitinase protein family. *J. Biol. Chem.* **268**, 25803–25810 (1993).

49. Volck, B. *et al.* YKL-40, a mammalian member of the chitinase family, is a matrix protein of specific granules in human neutrophils. *Proc. Assoc. Am. Physicians* **110**, 351–360 (1998).

50. Johansen, J. S. *et al.* YKL-40 in giant cells and macrophages from patients with giant cell arteritis. *Arthritis Rheum.* **42**, 2624–2630 (1999).

51. Park, K.-R. *et al.* Chitinase 3 like 1 suppresses the stability and activity of p53 to promote lung tumorigenesis. *Cell Commun. Signal.* **18**, 5 (2020).

52. Liu, K., Jin, M., Ye, S. & Yan, S. CHI3L1 promotes proliferation and improves sensitivity to cetuximab in colon cancer cells by down-regulating p53. *J. Clin. Lab. Anal.* **34**, (2020).

53. Qiu, Q.-C. *et al.* CHI3L1 promotes tumor progression by activating TGF-β signaling pathway in hepatocellular carcinoma. *Sci. Rep.* **8**, 15029 (2018).

54. Low, D. *et al.* High Endogenous Expression of Chitinase 3-Like 1 and Excessive Epithelial Proliferation with Colonic Tumor Formation in MOLF/EiJ Mice. *PLOS ONE* **10**, e0139149 (2015).

55. Kawada, M. *et al.* Chitinase 3-like 1 promotes macrophage recruitment and angiogenesis in colorectal cancer. *Oncogene* **31**, 3111–3123 (2012).

56. Chen, A. *et al.* Chitinase-3-like 1 protein complexes modulate macrophage-mediated immune suppression in glioblastoma. *J. Clin. Invest.* **131**, e147552 (2021).

57. Morera, E. *et al.* YKL-40/CHI3L1 facilitates migration and invasion in HER2 overexpressing breast epithelial progenitor cells and generates a niche for capillary-like network formation. *Vitro Cell. Dev. Biol. - Anim.* **55**, 838–853 (2019).

58. Scully, S., Yan, W., Bentley, B., Cao, Q. J. & Shao, R. Inhibitory Activity of YKL-40 in Mammary Epithelial Cell Differentiation and Polarization Induced by Lactogenic Hormones: A Role in Mammary Tissue Involution. *PLoS ONE* **6**, e25819 (2011).

59. Chen, Y., Zhang, S., Wang, Q. & Zhang, X. Tumor-recruited M2 macrophages promote gastric and breast cancer metastasis via M2 macrophage-secreted CHI3L1 protein. *J. Hematol. Oncol.J Hematol Oncol* **10**, 36 (2017).

60. Lee, Y. S. *et al.* A small molecule targeting CHI3L1 inhibits lung metastasis by blocking IL-13Rα2-mediated JNK-AP-1 signals. *Mol. Oncol.* **16**, 508–526 (2022).

61. Ma, B. *et al.* CHI3L1 regulates PD-L1 and anti–CHI3L1–PD-1 antibody elicits synergistic antitumor responses. *J. Clin. Invest.* **131**, e137750 (2021).

62. Ostrom, Q. T. *et al.* CBTRUS Statistical Report: Primary Brain and Other Central Nervous System Tumors Diagnosed in the United States in 2013–2017. *Neuro-Oncol.* **22**, iv1–iv96 (2020).

63. Louis, D. N. *et al.* The 2007 WHO Classification of Tumours of the Central Nervous System. *Acta Neuropathol. (Berl.)* **114**, 97–109 (2007).

64. Louis, D. N. *et al.* The 2016 World Health Organization Classification of Tumors of the Central Nervous System: a summary. *Acta Neuropathol. (Berl.)* **131**, 803–820 (2016).

65. Louis, D. N. *et al.* The 2021 WHO Classification of Tumors of the Central Nervous System: a summary. *Neuro-Oncol.* **23**, 1231–1251 (2021).

66. Koshy, M. *et al.* Improved survival time trends for glioblastoma using the SEER 17 population-based registries. *J. Neurooncol.* **107**, 207–212 (2012).

67. Lin, Z. *et al.* Establishment of age group classification for risk stratification in glioma patients. *BMC Neurol.* **20**, 310 (2020).

68. Bruno, F., Pellerino, A., Pronello, E. & Rudà, R. Newly diagnosed glioblastoma: A review on clinical management. in *New Insights Into Glioblastoma* 101–123 (Elsevier, 2023). doi:10.1016/B978-0-323-99873-4.00026-8.

69. Fabian, C., Han, M., Bjerkvig, R. & Niclou, S. P. Novel facets of glioma invasion. in *International Review of Cell and Molecular Biology* vol. 360 33–64 (Elsevier, 2021).

70. Hadjipanayis, C. G., Widhalm, G. & Stummer, W. What is the Surgical Benefit of Utilizing 5-Aminolevulinic Acid for Fluorescence-Guided Surgery of Malignant Gliomas? *Neurosurgery* **77**, 663–673 (2015).

71. Payne, L. S. & Huang, P. H. The Pathobiology of Collagens in Glioma. *Mol. Cancer Res.* **11**, 1129–1140 (2013).

72. De Gooijer, M. C., Guillén Navarro, M., Bernards, R., Wurdinger, T. & Van Tellingen, O. An Experimenter's Guide to Glioblastoma Invasion Pathways. *Trends Mol. Med.* **24**, 763–780 (2018).

73. Ellert-Miklaszewska, A., Poleszak, K., Pasierbinska, M. & Kaminska, B. Integrin Signaling in Glioma Pathogenesis: From Biology to Therapy. *Int. J. Mol. Sci.* **21**, 888 (2020).

74. Hagemann, C. A complete compilation of matrix metalloproteinase expression in human malignant gliomas. *World J. Clin. Oncol.* **3**, 67 (2012).

75. Hatoum, A., Mohammed, R. & Zakieh, O. The unique invasiveness of glioblastoma and possible drug targets on extracellular matrix. *Cancer Manag. Res.* **Volume 11**, 1843–1855 (2019).

76. Bowman, R. L., Wang, Q., Carro, A., Verhaak, R. G. W. & Squatrito, M. GlioVis data portal for visualization and analysis of brain tumor expression datasets. *Neuro-Oncol.* **19**, 139–141 (2017).

77. Markovic, D. S. *et al.* Gliomas induce and exploit microglial MT1-MMP expression for tumor expansion. *Proc. Natl. Acad. Sci.* **106**, 12530–12535 (2009).

78. Mentlein, R., Hattermann, K. & Held-Feindt, J. Lost in disruption: Role of proteases in glioma invasion and progression. *Biochim. Biophys. Acta BBA - Rev. Cancer* **1825**, 178–185 (2012).

79. Chen, S. & Parney, I. F. Immune Response: Glioma-Associated Immunosuppression. in *Glioma Cell Biology* (eds. Sedo, A. & Mentlein, R.) 221–239 (Springer Vienna, 2014). doi:10.1007/978-3-7091-1431-5_8.

80. Nduom, E. K., Weller, M. & Heimberger, A. B. Immunosuppressive mechanisms in glioblastoma: Fig. 1. *Neuro-Oncol.* **17**, vii9–vii14 (2015).

81. Ochocka, N. *et al.* Single-cell RNA sequencing reveals functional heterogeneity of glioma-associated brain macrophages. *Nat. Commun.* **12**, 1151 (2021).

82. Nakano, Y., Kuroda, E., Kito, T., Yokota, A. & Yamashita, U. Induction of macrophagic prostaglandin E2 synthesis by glioma cells. *J. Neurosurg.* **104**, 574–582 (2006).

83. Golán, I., Rodríguez De La Fuente, L. & Costoya, J. NK Cell-Based Glioblastoma Immunotherapy. *Cancers* **10**, 522 (2018).

84. Wang, H. *et al.* Different T-cell subsets in glioblastoma multiforme and targeted immunotherapy. *Cancer Lett.* **496**, 134–143 (2021).

85. Chongsathidkiet, P. *et al.* Sequestration of T cells in bone marrow in the setting of glioblastoma and other intracranial tumors. *Nat. Med.* **24**, 1459–1468 (2018).

86. Curry, W. T. & Lim, M. Immunomodulation: checkpoint blockade etc.: Fig. 1. *Neuro-Oncol.* **17**, vii26–vii31 (2015).

87. Simmons, G. W. *et al.* Neurofibromatosis-1 Heterozygosity Increases Microglia in a Spatially and Temporally Restricted Pattern Relevant to Mouse Optic Glioma Formation and Growth. *J. Neuropathol. Exp. Neurol.* **70**, 51–62 (2011).

88. Tirosh, I. *et al.* Single-cell RNA-seq supports a developmental hierarchy in human oligodendroglioma. *Nature* **539**, 309–313 (2016).

89. Gieryng, A., Pszczolkowska, D., Walentynowicz, K. A., Rajan, W. D. & Kaminska, B. Immune microenvironment of gliomas. *Lab. Invest.* **97**, 498–518 (2017).

90. Chung, A. S., Lee, J. & Ferrara, N. Targeting the tumour vasculature: insights from physiological angiogenesis. *Nat. Rev. Cancer* **10**, 505–514 (2010).

91. Ahir, B. K., Engelhard, H. H. & Lakka, S. S. Tumor Development and Angiogenesis in Adult Brain Tumor: Glioblastoma. *Mol. Neurobiol.* **57**, 2461–2478 (2020).

92. Kuczynski, E. A., Vermeulen, P. B., Pezzella, F., Kerbel, R. S. & Reynolds, A. R. Vessel co-option in cancer. *Nat. Rev. Clin. Oncol.* **16**, 469–493 (2019).

93. El Hallani, S. *et al.* A new alternative mechanism in glioblastoma vascularization: tubular vasculogenic mimicry. *Brain* **133**, 973–982 (2010).

94. Holst, C. B. *et al.* Perspective: targeting VEGF-A and YKL-40 in glioblastoma – matter matters. *Cell Cycle* **20**, 702–715 (2021).

95. Ghosh, M., Lenkiewicz, A. M. & Kaminska, B. The Interplay of Tumor Vessels and Immune Cells Affects Immunotherapy of Glioblastoma. *Biomedicines* **10**, 2292 (2022).

96. Maddison, K., Bowden, N. A., Graves, M. C. & Tooney, P. A. Characteristics of vasculogenic mimicry and tumour to endothelial transdifferentiation in human glioblastoma: a systematic review. *BMC Cancer* **23**, 185 (2023).

97. Kane, J. R. The Role of Brain Vasculature in Glioblastoma. *Mol. Neurobiol.* **56**, 6645–6653 (2019).

98. Sukriti, S., Tauseef, M., Yazbeck, P. & Mehta, D. Mechanisms Regulating Endothelial Permeability. *Pulm. Circ.* **4**, 535–551 (2014).

99. Iliff, J. J. *et al.* Brain-wide pathway for waste clearance captured by contrast-enhanced MRI. *J. Clin. Invest.* **123**, 1299–1309 (2013).

100. Hempel, C., Johnsen, K. B., Kostrikov, S., Hamerlik, P. & Andresen, T. L. Brain tumor vessels—a barrier for drug delivery. *Cancer Metastasis Rev.* **39**, 959–968 (2020).

101. Mitusova, K. *et al.* Overcoming the blood–brain barrier for the therapy of malignant brain tumor: current status and prospects of drug delivery approaches. *J. Nanobiotechnology* **20**, 412 (2022).

102. Magnussen, A. L. & Mills, I. G. Vascular normalisation as the stepping stone into tumour microenvironment transformation. *Br. J. Cancer* **125**, 324–336 (2021).

103. Bonneh-Barkay, D. *et al.* Astrocyte and Macrophage Regulation of YKL-40 Expression and Cellular Response in Neuroinflammation: YKL-40 Expression in Macrophages and Astrocytes. *Brain Pathol.* **22**, 530–546 (2012).

104. Bonneh-Barkay, D., Wang, G., Starkey, A., Hamilton, R. L. & Wiley, C. A. In vivo CHI3L1 (YKL-40) expression in astrocytes in acute and chronic neurological diseases. *J. Neuroinflammation* **7**, 34 (2010).

105. Tanwar, M. K., Gilbert, M. R. & Holland, E. C. Gene expression microarray analysis reveals YKL-40 to be a potential serum marker for malignant character in human glioma. *Cancer Res.* **62**, 4364–4368 (2002).

106. Steponaitis, G. *et al.* High CHI3L1 expression is associated with glioma patient survival. *Diagn. Pathol.* **11**, 42 (2016).

107. Verhaak, R. G. W. *et al.* Integrated Genomic Analysis Identifies Clinically Relevant Subtypes of Glioblastoma Characterized by Abnormalities in PDGFRA, IDH1, EGFR, and NF1. *Cancer Cell* **17**, 98–110 (2010).

108. Zhang, W. *et al.* Association between YKL-40 and adult primary astrocytoma. *Cancer* NA-NA (2010) doi:10.1002/cncr.25084.

109. Pelloski, C. E. *et al.* YKL-40 Expression is Associated with Poorer Response to Radiation and Shorter Overall Survival in Glioblastoma. *Clin. Cancer Res.* **11**, 3326–3334 (2005).

110. Ku, B. M. *et al.* CHI3L1 (YKL-40) is expressed in human gliomas and regulates the invasion, growth and survival of glioma cells. *Int. J. Cancer* **128**, 1316–1326 (2011).

111. Shao, R. *et al.* YKL-40, a secreted glycoprotein, promotes tumor angiogenesis. *Oncogene* **28**, 4456–4468 (2009).

112. Król, S. K. *et al.* Aberrantly Expressed RECQL4 Helicase Supports Proliferation and Drug Resistance of Human Glioma Cells and Glioma Stem Cells. *Cancers* **12**, 2919 (2020).

113. Stępniak, K. *et al.* Mapping chromatin accessibility and active regulatory elements reveals pathological mechanisms in human gliomas. *Nat. Commun.* **12**, 3621 (2021).

114. Ciechomska, I. A. *et al.* Exploring Novel Therapeutic Opportunities for Glioblastoma Using Patient-Derived Cell Cultures. *Cancers* **15**, 1562 (2023).

115. Dobin, A. *et al.* STAR: ultrafast universal RNA-seq aligner. *Bioinformatics* **29**, 15–21 (2013).

116. Liao, Y., Smyth, G. K. & Shi, W. The R package Rsubread is easier, faster, cheaper and better for alignment and quantification of RNA sequencing reads. *Nucleic Acids Res.* **47**, e47–e47 (2019).

117. Love, M. I., Huber, W. & Anders, S. Moderated estimation of fold change and dispersion for RNA-seq data with DESeq2. *Genome Biol.* **15**, 550 (2014).

118. Jassal, B. *et al.* The reactome pathway knowledgebase. *Nucleic Acids Res.* gkz1031 (2019) doi:10.1093/nar/gkz1031.

119. Yu, G., Wang, L.-G., Han, Y. & He, Q.-Y. clusterProfiler: an R Package for Comparing Biological Themes Among Gene Clusters. *OMICS J. Integr. Biol.* **16**, 284–287 (2012).

120. Müller, B. *et al.* High-resolution tomographic imaging of microvessels. in (ed. Stock, S. R.) 70780B (2008). doi:10.1117/12.794157.

121. Puchalski, R. B. *et al.* An anatomic transcriptional atlas of human glioblastoma. *Science* **360**, 660–663 (2018).

122. Lam, K. H. B. *et al.* Topographic mapping of the glioblastoma proteome reveals a triple-axis model of intra-tumoral heterogeneity. *Nat. Commun.* **13**, 116 (2022).

123. Lam, K. H. B., Faust, K., Yin, R., Fiala, C. & Diamandis, P. The Brain Protein Atlas: A conglomerate of proteomics datasets of human neural tissue. *PROTEOMICS* **22**, 2200127 (2022).

124. Neftel, C. *et al.* An Integrative Model of Cellular States, Plasticity, and Genetics for Glioblastoma. *Cell* **178**, 835-849.e21 (2019).

125. Tsherniak, A. *et al.* Defining a Cancer Dependency Map. *Cell* **170**, 564-576.e16 (2017).

126. Forsyth, P. A. *et al.* Gelatinase-A (MMP-2), gelatinase-B (MMP-9) and membrane type matrix metalloproteinase-1 (MT1-MMP) are involved in different aspects of the pathophysiology of malignant gliomas. *Br. J. Cancer* **79**, 1828–1835 (1999).

127. Comba, A. *et al.* Spatiotemporal analysis of glioma heterogeneity reveals COL1A1 as an actionable target to disrupt tumor progression. *Nat. Commun.* **13**, 3606 (2022).

128. Rafi, J. H. *et al.* High expression of bone morphogenetic protein 1 (BMP1) is associated with a poor survival rate in human gastric cancer, a dataset approaches. *Genomics* **113**, 1141–1154 (2021).

129. Steiglitz, B. M., Keene, D. R. & Greenspan, D. S. PCOLCE2 Encodes a Functional Procollagen C-Proteinase Enhancer (PCPE2) That Is a Collagen-binding Protein Differing in Distribution of Expression and Post-translational Modification from the Previously Described PCPE1. *J. Biol. Chem.* **277**, 49820–49830 (2002).

130. Takahashi, H. *et al.* Differential Expression of ADAM (a Disintegrin and Metalloproteinase) Genes between Human First Trimester Villous and Extravillous Trophoblast Cells. *J. Nippon Med. Sch.* **81**, 122–129 (2014).

131. Wang, S. *et al.* Novel Brain-Stiffness-Mimicking Matrix Gel Enables Comprehensive Invasion Analysis of 3D Cultured GBM Cells. *Front. Mol. Biosci.* **9**, 885806 (2022).

132. Held-Feindt, J. *et al.* Matrix-degrading proteases ADAMTS4 and ADAMTS5 (disintegrins and metalloproteinases with thrombospondin motifs 4 and 5) are expressed in human glioblastomas. *Int. J. Cancer* **118**, 55–61 (2006).

133. Fontanil, T., Mohamedi, Y., Cobo, T., Cal, S. & Obaya, Á. J. Novel Associations Within the Tumor Microenvironment: Fibulins Meet ADAMTSs. *Front. Oncol.* **9**, 796 (2019).

134. Hu, B., Thirtamara-Rajamani, K. K., Sim, H. & Viapiano, M. S. Fibulin-3 Is Uniquely Upregulated in Malignant Gliomas and Promotes Tumor Cell Motility and Invasion. *Mol. Cancer Res.* **7**, 1756–1770 (2009).

135. Mohamedi, Y. *et al.* The molecular interaction of ADAMTS-1 and fibulin-1 and its potential contribution to breast cancer biology. *J. Cancer Metastasis Treat.* **2019**, (2019).

136. He, C. *et al.* Peroxidasin-mediated bromine enrichment of basement membranes. *Proc. Natl. Acad. Sci.* **117**, 15827–15836 (2020).

137. Morishita, H. & Yagi, T. Protocadherin family: diversity, structure, and function. *Curr. Opin. Cell Biol.* **19**, 584–592 (2007).

138. Waha, A. *et al.* Epigenetic Silencing of the Protocadherin Family Member PCDH-γ-All in Astrocytomas. *Neoplasia* **7**, 193–199 (2005).

139. Ellert-Miklaszewska, A. *et al.* Tumour-processed osteopontin and lactadherin drive the protumorigenic reprogramming of microglia and glioma progression. *Oncogene* **35**, 6366–6377 (2016).

140. Sliwa, M. *et al.* The invasion promoting effect of microglia on glioblastoma cells is inhibited by cyclosporin A. *Brain* **130**, 476–489 (2007).

141. Kaminska, B., Ochocka, N. & Segit, P. Single-Cell Omics in Dissecting Immune Microenvironment of Malignant Gliomas—Challenges and Perspectives. *Cells* **10**, 2264 (2021).

142. Quail, D. F. & Joyce, J. A. The Microenvironmental Landscape of Brain Tumors. *Cancer Cell* **31**, 326–341 (2017).

143. Ghochani, Y. *et al.* A molecular interactome of the glioblastoma perivascular niche reveals integrin binding sialoprotein as a mediator of tumor cell migration. *Cell Rep.* **41**, 111511 (2022).

144. Cabezas, R. *et al.* Astrocytic modulation of blood brain barrier: perspectives on Parkinsonâ€™s disease. *Front. Cell. Neurosci.* **8**, (2014).

145. Troili, F. *et al.* Perivascular Unit: This Must Be the Place. The Anatomical Crossroad Between the Immune, Vascular and Nervous System. *Front. Neuroanat.* **14**, 17 (2020).

146. Guetta-Terrier, C. *et al.* Chi3l1 Is a Modulator of Glioma Stem Cell States and a Therapeutic Target in Glioblastoma. *Cancer Res.* **83**, 1984–1999 (2023).

147. Kijewska, M. *et al.* The embryonic type of *SPP1* transcriptional regulation is re-activated in glioblastoma. *Oncotarget* **8**, 16340–16355 (2017).

148. Collins, V. P., Jones, D. T. W. & Giannini, C. Pilocytic astrocytoma: pathology, molecular mechanisms and markers. *Acta Neuropathol. (Berl.)* **129**, 775–788 (2015).

149. Filippova, N. *et al.* Hu antigen R (HuR) multimerization contributes to glioma disease progression. *J. Biol. Chem.* **292**, 16999–17010 (2017).

150. Pyonteck, S. M. *et al.* CSF-1R inhibition alters macrophage polarization and blocks glioma progression. *Nat. Med.* **19**, 1264–1272 (2013).

151. Kaminska, B. & Cyranowski, S. Recent Advances in Understanding Mechanisms of TGF Beta Signaling and Its Role in Glioma Pathogenesis. in *Glioma Signaling* (ed. Barańska, J.) vol. 1202 179–201 (Springer International Publishing, 2020).

152. Chang, A. L. *et al.* CCL2 Produced by the Glioma Microenvironment Is Essential for the Recruitment of Regulatory T Cells and Myeloid-Derived Suppressor Cells. *Cancer Res.* **76**, 5671–5682 (2016).

153. Chen, C.-C., Llado, V., Eurich, K., Tran, H. T. & Mizoguchi, E. Carbohydrate-binding motif in chitinase 3-like 1 (CHI3L1/YKL-40) specifically activates Akt signaling pathway in colonic epithelial cells. *Clin. Immunol.* **140**, 268–275 (2011).

154. Zhang, J.-F. *et al.* IL-33 enhances glioma cell migration and invasion by upregulation of MMP2 and MMP9 via the ST2-NF-κB pathway. *Oncol. Rep.* **38**, 2033–2042 (2017).

155. Coniglio, S. J. & Segall, J. E. Review: Molecular mechanism of microglia stimulated glioblastoma invasion. *Matrix Biol.* **32**, 372–380 (2013).

156. Chopra, S., Overall, C. M. & Dufour, A. Matrix metalloproteinases in the CNS: interferons get nervous. *Cell. Mol. Life Sci.* **76**, 3083–3095 (2019).

157. Groves, M. D. *et al.* Phase II trial of temozolomide plus marimastat for recurrent anaplastic gliomas: A relationship among efficacy, joint toxicity and anticonvulsant status. *J. Neurooncol.* **80**, 83–90 (2006).

158. Xie, Y. *et al.* Nuclear matrix metalloproteinases: functions resemble the evolution from the intracellular to the extracellular compartment. *Cell Death Discov.* **3**, 17036 (2017).

159. Golubkov, V. S., Chekanov, A. V., Doxsey, S. J. & Strongin, A. Y. Centrosomal Pericentrin Is a Direct Cleavage Target of Membrane Type-1 Matrix Metalloproteinase in Humans but Not in Mice. *J. Biol. Chem.* **280**, 42237–42241 (2005).

160. Urbanavičiūtė, R., Skauminas, K. & Skiriutė, D. The Evaluation of AREG, MMP-2, CHI3L1, GFAP, and OPN Serum Combined Value in Astrocytic Glioma Patients' Diagnosis and Prognosis. *Brain Sci.* **10**, 872 (2020).

161. Xing, S. *et al.* Development and Validation of a Serum Biomarker Panel for the Detection of Esophageal Squamous Cell Carcinoma through RNA Transcriptome Sequencing. *J. Cancer* **8**, 2346–2355 (2017).

162. Adegunsoye, A. *et al.* Circulating Plasma Biomarkers of Survival in Antifibrotic-Treated Patients With Idiopathic Pulmonary Fibrosis. *Chest* **158**, 1526–1534 (2020).

163. Urakami, S. *et al.* Biological and clinical significance of the YKL -40/osteopontin–integrin ʙ4–ᴘ70S6K axis induced by macrophages in early oesophageal squamous cell carcinoma. *J. Pathol.* path.6148 (2023) doi:10.1002/path.6148.

164. Faibish, M., Francescone, R., Bentley, B., Yan, W. & Shao, R. A YKL-40–Neutralizing Antibody Blocks Tumor Angiogenesis and Progression: A Potential Therapeutic Agent in Cancers. *Mol. Cancer Ther.* **10**, 742–751 (2011).

165. Lan, Y., Wang, H., Chen, A. & Zhang, J. Update on the current knowledge of lymphatic drainage system and its emerging roles in glioma management. *Immunology* **168**, 233–247 (2023).

166. Salman, M. M. *et al.* Emerging roles for dynamic aquaporin-4 subcellular relocalization in CNS water homeostasis. *Brain* **145**, 64–75 (2022).

167. Saadoun, S. Aquaporin-4 expression is increased in oedematous human brain tumours. *J. Neurol. Neurosurg. Psychiatry* **72**, 262–265 (2002).

8. The Bioethical Committee approval

Mouse experiments presented in the study were approved by the 1st Local Bioethical Committee in Warsaw, Poland, the reference number: 1123/2020.